MASTERARBEIT / MASTER'S THESIS

Titel der Masterarbeit / Title of the Master's Thesis

„Impact of growing planets on the long-term evolution of protoplanetary disks“

verfasst von / submitted by

Ines Ringseis, BSc BSc

angestrebter akademischer Grad / in partial fulfilment of the requirements for the degree of

Master of Science (MSc)

Wien, 2023 / Vienna, 2023

Studienkennzahl lt. Studienblatt / degree programme code as it appears on the student record sheet:	UA 066 861
Studienrichtung lt. Studienblatt / degree programme as it appears on the student record sheet:	Masterstudium Astronomie UG2002
Betreut von / Supervisor:	Univ. Prof.- Dipl. Phys. Dr. Manuel Güdel

Danksagung

Bedanken möchte ich mich als erstes beim leider bereits verstorbenen ao. Univ.-Prof. Dr. Ernst Dorfi. Er hat mich bereits im ersten Semester meines Studiums mit seinen Vorlesungen fesseln können und hat damit mein Interesse für Astrophysik weiter geschürt. Über die Jahre hinweg habe ich ihn als Lehrenden immer mehr schätzen gelernt und nach der Aufnahme in seiner Arbeitsgruppe auch zu meinem Freundeskreis zählen dürfen. Durch viele inspirierende Gespräche fachlicher und persönlicher Natur wurde das Thema meiner Masterarbeit definierter.
Weiters möchte ich mich bei Univ.-Prof. Dipl.-Phys. Dr. Manuel Güdel bedanken, der nach dem Ableben von Ernst Dorfi die Betreuung meiner Masterarbeit übernommen hat. Auch er hat mich durch Gespräche und Diskussionen über meine Ergebnisse fachlich unterstützt und weiter gebracht.
Ich möchte allen Mitgliedern der Dorfi-Gruppe danken, die mich ebenfalls durch vielerlei Gesprächsrunden unterstützt haben. Insbesondere möchte ich hier meinem Co-Supervisor Daniel Steiner, Bakk. MSc danken, der mich in die Tiefen des *TAPIR*-Codes eingeführt und mir bei allen Programmier- und Computerschwierigkeiten geholfen hat.
Ebenfalls möchte ich all meinen Freunden danken, die mich in der anstrengenden, aber auch sehr schönen und spannendsten Zeit während meines Studiums unterstützt haben. Auch meinen Eltern, die mich immer tatkräftig unterstützt und mein Interesse zur Astronomie und Physik schon in den Kinderschuhen geweckt haben, möchte ich danken.

Abstract

Context: To understand the formation and evolution of planetary systems the physical processes in protoplanetary disks (PPD) and their ability to form planets must be studied. The existence of gaps in such disks has been observed as well as the presence of growing planets within them. Theories suggest that without limitations planets with a high enough mass accretion rate can trigger the occurrence of such gaps. This work simulates the impact of growing planets on the long-term evolution of protoplanetary disks.
Aims: This thesis' aim is to reproduce already observed and simulated effects on the evolution of PPDs induced by a growing planet to verify the correctness of our unique code. Another aim is to potentially find new results, like e.g. the impact of a developing gap on episodic accretion events which only occur in the theory of layered-disk models.
Methods: The calculations were made with the axisymmetric implicit 1+1D radiation hydrodynamics code *TAPIR*. It allows to simulate the long-term evolution of PPDs using a layered-viscosity model. It also enables a self-consistent treatment of the innermost disk region. The planet is modelled as a time-depended sink term which accretes material in the Bondi-regime. This sink term can react to the properties provided by the PPD.
Results: A planet with a mass accretion rate exceeding the mass flux in the disk at the planet's position is able to trigger gap formation, which influences the evolution of the embedding disk. The total disk mass and therefore also the star's mass accretion rate decreases rapidly. After the formation of a gap the inner disk empties unopposed, whereas the outer disk persists for a considerably longer time. This leads to an earlier disappearance of an out-bursting behaviour of the disk. Planets which evolve in a disk with a high burst frequency are able to gain mass much faster which leads to a different evolutionary track than for planets embedded in quiescent disks.
Conclusion: The results show that many observational effects and models done with other simulations can be reproduced by this code. Some results of this thesis differ from results of other works, which can be caused by numerical limitations and the usage of simple sink term properties approximations. But most results coincide with results from other published works and are partly more detailed due to the used method. The results of this work yield new insights to this topic.

Kurzfassung

Kontext: Um die Entstehung und Entwicklung von Planetensystemen zu verstehen, muss man die physikalischen Prozesse in protoplanetaren Scheiben und deren Fähigkeit, Planeten zu formen, untersuchen und verstehen. Die Existenz solcher Scheiben und die Präsenz von Lücken in ihnen und darin wachsenden Planeten wurde bereits beobachtet. Theorien besagen, dass, unter anderem, Planeten, die groß genug sind und daher viel Masse akkretieren, Verursacher solcher Lücken sind. Diese Arbeit simuliert den Effekt von wachsenden Planeten auf die Langzeit-Entwicklung der protoplanetaren Scheibe.
Ziele: Das Ziel dieser Arbeit ist es, bereits beobachtete und simulierte Phänomene in protoplanetaren Scheiben, hervorgerufen durch akkretierende Planeten, zu reproduzieren um die Richtigkeit unserer einzigartigen Methode zu verifizieren. Ebenso sollen neue Erkenntnisse, wie z.B. der Einfluss von entstehenden Gaps auf, nur in Modellen mit geschichteter Viskosität auftretende, episodische Akkretionsereignisse gewonnen werden.
Methoden: Die Berechnungen werden mit dem achsensymmetrischen impliziten 1+1D Strahlungs-hydrodynamik-Code *TAPIR* durchgeführt. Mit diesem können Langzeitentwicklungen von Scheiben mit geschichteter Viskosität modelliert werden. Besonders gut können die Prozesse am Innenrand der Scheibe berechnet werden. Der Planet ist modelliert als Sinkterm, welcher im Bondi-Regime Masse aus der Scheibe akkretiert. Der Sinkterm kann auf die Bedienungen in der Scheibe reagieren und seine Akkretionsrate dazu anpassen.
Resultate: Ein Planet, dessen Akkretionsrate den Massenfluss durch die Scheibe an dieser Stelle übersteigt, kann eine Lücke in der Gasscheibe öffnen. Dies beeinflusst die Entwicklung von der protoplanetaren Scheibe. Deren Gesamtmasse und die Akkretionsrate auf den Stern verringert sich dadurch rasch. Nach der Entstehung der Lücke entleert sich die innere Scheibe unbeeinflusst, während die äußere weiter besteht. Dies führt zu einem früheren Stopp von Bursts wenn sich ein Gap in der Scheibe öffnet. Planeten, die in einer burstenden Scheibe wachsen, können schneller an Masse zunehmen als jene die sich in nicht-burstenden Scheiben entwickeln.
Fazit: Die Ergebnisse zeigen, dass viele, durch Beobachtungen und andere Simulationen gefundene Phänomene, mit diesen Methoden nachproduziert werden können. Mögliche

Abweichungen von bisherigen Erkenntnissen aus anderen Studien können von numerischen Limitierungen und einfachen Approximationen des implementierten Sinkterms kommen. Jedoch stimmen die meisten Ergebnisse recht gut mit bisherigen publizierten Arbeiten überein und einige Ergebnisse sind noch präziser und umfangreicher als andere bisherige Simulationen. Die Ergebnisse bringen neue Einblicke in diese Thematik.

Contents

Danksagung i

Abstract iii

Kurzfassung v

1 Introduction 1

2 Physical description 3

2.1 Protoplanetary Disks . . . 3
2.1.1 Formation of a protoplanetary disk . . . 3
2.1.2 Structure of a protoplanetary disk . . . 4
2.1.3 Evolution of a protoplanetary disk . . . 6
2.1.4 Layered disk . . . 9
2.1.5 FU Orionis outbursts . . . 10
2.2 Planets . . . 11
2.2.1 Formation of planets . . . 11
2.2.2 Hill radius . . . 13
2.2.3 Bondi accretion . . . 13
2.3 Interaction of the PPD and planets . . . 18
2.3.1 Formation of gaps . . . 18
2.3.2 Migration of planets . . . 21

3 Physical equations 25

3.1 Equations of RHD . . . 25
3.2 Adaption of the RHD equations . . . 26

4 Numerical method 29

4.1 Discretized set of equations . . . 32
4.2 Numerical implementation of the sink term . . . 33
4.2.1 Formalism of the sink term . . . 33

4.2.2 Viscosity 36
4.2.3 Time dependency of planetary properties 36
4.2.4 Assumptions and numerical impact on the disk 37
4.3 Evolution of a PPD without a sink term 38

5 Results **43**
5.1 Constant accretion rate (fiducial model) 43
5.2 Parameter variation 45
5.2.1 Variation of constant mass accretion rate and orbital distance . . . 45
5.2.2 Time dependent accretion scheme - Bondi accretion 52
5.3 Layered viscosity 59
5.3.1 Impact of gap formation on the outburst behaviour 59
5.3.2 Impact of bursts on gap formation 61
5.3.3 Effect of bursts on the planet's mass accretion rate 63
5.4 Comparison of burst and non-burst models 64

6 Discussion **69**
6.1 Limitations to the model 77

7 Conclusion and further work **79**
7.1 Further Outlook 80

Bibliography **83**

1 Introduction

The exact formation and evolution of our solar system, our home planet Earth and consequently the existence of life is still a big question mark in the scientific community. Since the discovery of the first exoplanet 51 Pegasi b 1995 (Mayor and Queloz, 1995) the craving for understanding the formation process has grown strongly. A fundamental part for understanding the planetary evolution is to study the processes, dynamics, structures and evolution of protoplanetary disks, the birth places of planets.
The first observational discovery of such a structure was done by Smith and Terrile (1984). This led to the search for more comparable systems around newly born stars. A few years later with strongly improved technology a new mission was started with the Hubble space telescope in 1990. One of the first detailed imaged observation of such a protoplanetary disk was done with this famous space telescope by Weinberger (2004) around the pre-main-sequence star TW Hydrae. This imaged disk showed substructures which could not have been resolved until then. These structures show concentric rings in the gas/dust disk, which leads to the assumption of a growing and evolving giant planet being present in the disk. Since evolving planets are deeply embedded in their surrounding gas and dust disk it is hard to image them directly. Therefore the formation process is still very poorly unknown. The first direct imaging of a planet present in a gap of a protoplanetary disk was done by Keppler et al. (2018). This shows that the gap formation process and the evolution of a planet are, amongst others, linked to each other.
To understand this formation process many theoretical studies have been made in the last decades. One of the first simulation work for such a problem was done by Cameron (1979) which is based on the code of Lin and Pringle (1976), which simulates the movement of particles in a binary system by solving the 2 dimensional equations of motion for test particles, including a simple viscosity model and dissipation. Since then many simulations have been made with different codes and various approaches. The computing power has increased dramatically in recent years, so more accurate calculations and models could be produced, e.g. Jin et al. (2016),Vorobyov and Elbakyan (2019) or Kuwahara et al. (2022). All these codes have one thing in common. They are explicit time-evolution codes, therefore they are restricted by the Courant–Friedrichs–Lewy condition (CFL-condition).

Due to this or similar time step-limiting criteria the call after long-term evolution models got louder. This led to the development of the 1+1D implicit radiation hydrodynamics *TAPIR* code which is applied for the finding of results for this work. It is especially well suited for the simulation of the inner disk as discussed by Steiner et al. (2021). The code is still under development to increase the scope of application.
The aim of this work is to find new results on the impact of a growing planet on the long-term evolution of accretion disks. The planet is modelled as a sink term, which accretes in the Bondi-regime. This represents the accretion properties of a gas giant. Hence, the behaviour of the simulated protoplanetary disk reacting to the planet's mass extraction can be investigated. The results could bring us one step closer to understanding the formation of our solar system and furthermore to understand the origin of life.

2 Physical description

2.1 Protoplanetary Disks

Rotating disk-like structures can be observed around newly formed stars. Observations made with the Atacama Large Millimeter Array (ALMA) (e.g in Brogan et al. (2015)) have shown us such formations. These structures are circumstellar accretion disks (Hartmann, Herczeg and Calvet, 2016) surrounding their host star. They are commonly known as protostellar disks as long they are deeply embedded in their parent cloud. When the star gets visible such objects are called protoplanetary disk. [1] These disks are flattened rotating objects consisting out of two components, gas and dust.

Protoplanetary disks evolve over time and are believed to disappear a few million years after their formation due to accretion processes, photoevaporation and condensing into clumps which will form future planets of a planetary system (Andrews and Williams, 2005).

2.1.1 Formation of a protoplanetary disk

As a dense region in a molecular cloud collapses and a new star forms, material in its gravitationally bound surrounding starts to fall towards the forming protostar. Each particle in the parent cloud has an intrinsic angular momentum due to random gas motions caused by turbulence in the initial molecular cloud. These motions are randomly distributed which can lead to high velocities of individual particles and therefore also a wide range angular momentum distribution. These quite randomly oriented momenta of the particles get cancelled out in the favour of the cloud's net angular momentum during the disk formation process. Hence, only the spin direction of the cloud's original net angular momentum remains which causes the formation and rotation of the PPD (Pringle, 1981). Due to the high kinetic energy and angular momentum of the particles they do not fall onto the star. They form a flattened rotating disk around their host star. The disk-like shape occurs because of the centrifugal force, caused by the particle's intrinsic angular momentum. This force works against the gravitational force (which is

[1] This work will use this afore described definition of protostellar and protoplanetary disk.

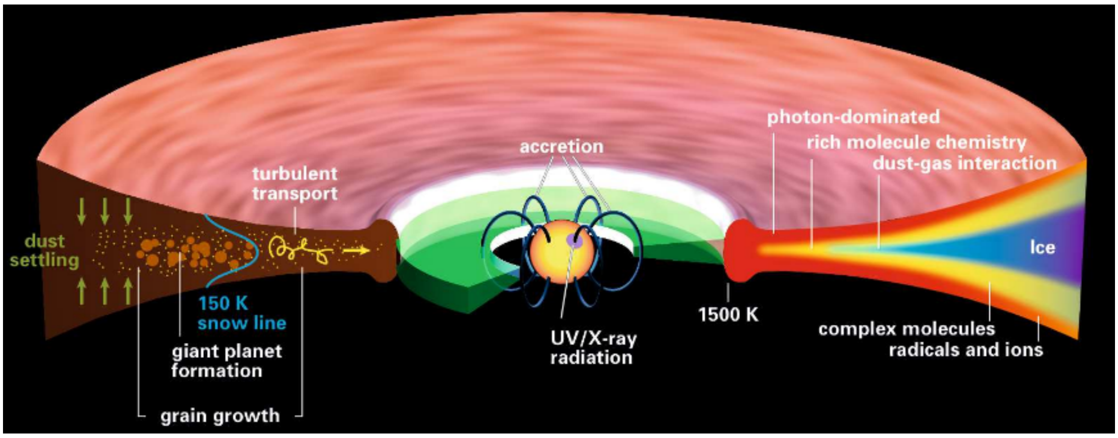

Figure 2.1: Structure of a protoplanetary disk (Henning and Semenov, 2013)

generated by the star and the disk itself) only in the radial direction. In the vertical direction the cloud is still able to fall freely towards the the mid plane. Angular momentum conservation states that material gets accelerated with decreasing distance to the star. After this disk formation process the disk stays in a quasi static equilibrium for the most part of its lifetime. Thus timescales on which the structure of the disk changes are much longer than the orbital period of gas and dust (Armitage, 2010).

2.1.2 Structure of a protoplanetary disk

A protoplanetary disk is quite a complex structure. There are many different physical processes occurring simultaneously which influence the structure and the appearance of such a disk. The PPD can reach an extent of a few 100 AU (Henning and Semenov, 2013). In Fig. 2.1 you can see an illustration of a protoplanetary disk around a newly formed star. The protostar, which is located in the system centre, radiates especially UV- and X-ray photons which heats the disk's surface layers and its inner parts. Such disks mainly consist of gas and dust particles. The gas component represents about 99% of the disk mass, whereas the dust component constitutes the remaining 1% (Andrews, 2020).
The extension of a disk is limited by the surrounding ISM. The inner edge is defined by the so-called magnetic truncation radius where the force of the star's magnetic field outmatches the forces preserving the disk-like structure (Hartmann, Herczeg and Calvet, 2016).
Different effects are sustaining a hydrostatic equilibrium state in vertical and radial direction. For getting a solution for the hydrodynamical equations and the Poisson equation for the gravitational potential two main assumptions must be made (Armitage, 2010):

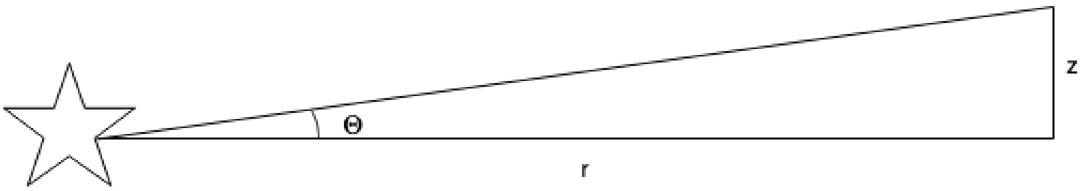

Figure 2.2: Vertical structure of a protoplanetary disk

- **Axisymmetry and low mass ($\boldsymbol{M_* \gg M_{\text{disk}}}$)**: this assumption allows to neglect the gravitational potential of the disk itself, since the high gravitational potential of the star out-rules any possibly occurring gravitational instabilities in the disk. This approach is sufficient for disks with masses of $M_{\text{disk}} \approx 0.01 M_*$ (for masses similar to that of the minimum mass Solar Nebula) up to disk masses of $M_{\text{disk}} \approx 0.1\mathrm{M}_*$ (Armitage, 2010). Thus the approximation of an axisymmetric disk is maintainable for the most part of the it's lifetime. More massive disks have non-neglectable self-gravitation and therefore cannot maintain a steady-state.

- **Thin disk approximation $\boldsymbol{\left(\frac{h}{r} \ll 1\right)}$**: the approximation of a thin disk, where the scale height h is much smaller then the radial extension r, can be made because a disk has a large surface area, which allows effective radiation cooling. Therefore it possesses a low temperature, thus gravitation dominates gas pressure in vertical direction.

Radial force balance

To get a force balance in the vertical direction z, the vertical gas pressure must be equal the acceleration towards the mid-plane provoked by the vertical component of the star's gravitational force. By assuming an isothermal equation of state (EOS) the resulting differential equation leads to the solution for the density ρ of

$$\rho(z) = \rho_0 \cdot e^{\frac{-z^2}{2h^2}}, \tag{2.1.2.1}$$

where ρ_0 is the mid-plane density defined by the surface density Σ

$$\rho_0 = \frac{1}{\sqrt{2\pi}} \frac{\Sigma}{h}, \tag{2.1.2.2}$$

and h is the scale-height of the disk which is defined by the relation of the speed of sound

c_s to the angular velocity Ω

$$h = \frac{c_\mathrm{s}}{\Omega}. \tag{2.1.2.3}$$

Radial hydrostatic structure

As shown by Armitage (2010) the gas component of the disk experiences three different forces in the radial direction. A particle experiences the outward directed centrifugal force induced by the rotational velocity $v_{\Phi,\mathrm{g}}$, the gas pressure and the inward directed gravitational acceleration due to the gravitational potential of the central star. For a stable orbit the radial force balance must be found by the following equation

$$\underbrace{\frac{GM_*}{r^2}}_{\substack{\text{gravitational}\\ \text{acceleration}}} = \underbrace{\frac{v_{\Phi,\mathrm{g}}^2}{r}}_{\substack{\text{centrifugal}\\ \text{acceleration}}} - \frac{1}{\rho} \underbrace{\frac{dP}{dr}}_{\substack{\text{pressure}\\ \text{gradient}}} . \tag{2.1.2.4}$$

The last term of Eq. 2.1.2.4 represents a pressure force F_pres

$$F_\mathrm{pres} = -\frac{dP}{dr}, \tag{2.1.2.5}$$

which counteracts the gravitational acceleration and therefore leads to a smaller orbital velocity for the gas compared with the Keplerian velocity $v_\mathrm{K} = \sqrt{GM_*/r}$. Relating these two velocities and inserting solar-like values one can see that the velocity of the gas is quite a bit smaller than the Keplerian velocity:

$$\frac{v_{\Phi,\mathrm{g}}}{v_\mathrm{K}} = 0.996. \tag{2.1.2.6}$$

If one only considers the motion of the gas, this small difference to the Keplerian velocity is negligible. But as we see in Sec. 2.2 this disparity is significant for the formation of planetesimals.

2.1.3 Evolution of a protoplanetary disk

A protoplanetary disk is not a static structure. It evolves over its whole lifetime (a few million years) and undergoes different processes which regulate the transport of matter inwards and the related angular momentum transport within the disk (Henning and Semenov, 2013). The evolution is subdivided into four stages (see Fig. 2.3) as described in Yorke, Bodenheimer and Laughlin (1995). The first stage a) Class 0: is right after the formation of the star and its disk. The gas and the dust are compound. The star

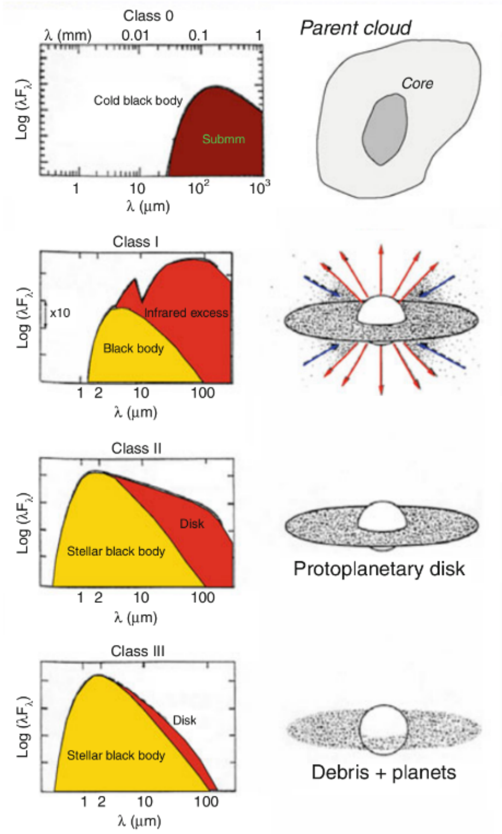

Figure 2.3: Different stages of the evolution of a protoplanetary disk (Yorke, Bodenheimer and Laughlin, 1995). a) Embedded protostar: right after formation of the star. b) accreting envelope: star and disk are still in the envelope and they accrete material from it . c) Accretion disk: the envelope has vanished. d) Debris disk: the gas has been evaporated, only planetesimal remain left. (Figure from (Mulders, 2013))

just formed in its parenting molecular cloud. b) Class I: A protostellar disk has formed around the newly born star. The disk and the star are still surrounded by an accreting envelope. Eventually, with time the dust-grains are growing and begin to settle and the first pebbles are forming. c) Class II: The envelope has vanished and the accretion disk is present, feeding the star with material. d) Class III: due to accretion, planet formation and photoevaporation the gas disk has almost vanished and a debris disk is left (Alexander et al., 2014).

To understand the evolution of a protoplanetary disk and planet formation it is necessary to know how the physical processes work in such disks, like viscous accretion, dust settling, dynamical interactions of particles in the disk and photoevaporation.

Viscosity and Accretion

A protoplanetary disk is an accretion disk. Mass flows inward due to angular momentum transport (Lynden-Bell and Pringle, 1974; Bertout and Bouvier, 1989). This transport process is induced by molecular viscosity, shear instability (Urpin and Brandenburg, 1998), magnetorotational instability (MRI) (Balbus and Hawley, 1991) or magnetically driven winds (Bai and Stone, 2013). All these different viscous effects combined add up to the effective viscosity ν

$$\nu = \alpha c_{\mathrm{s}} H_{\mathrm{P}}, \tag{2.1.3.1}$$

introduced by Shakura and Sunyaev (1973), where c_{s} is the speed of sound and H_{P} is the scale height. The viscous α-parameter depicts the mentioned viscous mechanisms. The effective viscosity allows most particles to decrease their angular momentum, therefore spiral inward and accrete onto the star. The accretion rate can span from $10^{-6} M_{\odot}/\mathrm{yr}$ for very young stars to $10^{-9} M_{\odot}/\mathrm{yr}$ (Hartmann et al., 1998). Since angular momentum must be conserved, the lost angular momentum of a particle must be transferred to an other particle. The particles which receive angular momentum move radially outwards.

This radial redistribution of angular momentum has a large impact on the structure and evolution of the disk. If the specific angular momentum l increases with radius this flow is stable to axisymmetric perturbations. The Keplerian disks which are used in this work possess an increasing l with increasing radius, thus there is no indication for hydrodynamic turbulence activating the turbulent viscosity which is strong enough to drive accretion.

Different works, e.g. Armitage (2010) or Ratschiner (2020), provide a good explanation and summery of the viscosity's functionality and properties. As explained, molecular viscosity ν_{m} is not an important part of the transport mechanism of angular momentum because

$$\nu_{\mathrm{m}} \sim \frac{1}{n\sigma_{\mathrm{mol}}} c_{\mathrm{s}} \tag{2.1.3.2}$$

(σ_{mol} is the cross section and n is the number density of the particles) leads to a far too long viscous time scale of about $t_{\nu} \simeq \frac{r^2}{\nu_m} = 3 \cdot 10^{13}$ yr which is about 10^7 times longer than the observed lifetime of a protoplanetary disk. Hence, the molecular viscosity is not the main mechanism of angular momentum transport.

But there is another effect sustaining instabilities, namely magnetic fields. Ionised particles couple to the magnetic field lines, which can lead to instabilities for differential rotating disks (e.g. Keplerian accretion disks). These instabilities are called *magnetorotational instability (MRI)* (For detailed information see the work of Balbus and Hawley (1991)).

If a weak vertical magnetic field penetrates a circumstellar disk its field lines connect to the charged particles in the PPD. In this differential rotating system two particles at neighbouring radii which are coupled together by a magnetic field line will be separated due to the differential rotation. The field line gets stretched and twisted and works against this alteration (magnetic tension). Therefore the inner particle will be decelerated and the outer one gets accelerated. This transfer of angular momentum increases the separation of the particles, hence the instability gets more exited. MRI is a big contributor for mass accretion and they have a big impact on the angular momentum transport (Kretke et al., 2009).
Angular momentum can also be lost due to the effect of non-ideal MHD where the magnetic field lines are open. These open field lines are able to transport mass and therefore J out of the system by disk winds (For more information see Shu et al. (2007)). For the non-ideal MHD there are three important effects which manipulate the dynamics and structure of a protoplanetary disk. These are the *Hall-effect*, the *Ohmic dissipation*, and the *ambipolar diffusion*. For the concept of a layered disk (see chapter 2.1.4) each magnetic effect is dominant in an other part of the disk as explained by Sano and Stone (2002).

2.1.4 Layered disk

As described by Gammie (1996) the material of layered disk is not homogeneously ionised. This is due to the fact that the ionising photon flux coming from the central star is limited. A protostar emits a certain amount of UV- and X-ray photons which are able to ionise the inner part of the disk and its upper layers. They are not able to penetrate deeply enough to reach the dense parts since the disk is optically thick. In the outer regions cosmic rays are able to ionise the disk's outer parts. In regions where no energetic photons reach the neutral material the particles decouple from the magnetic field. Hence, in regions with comparatively low gas ionisation MRI cannot operate efficiently and radial mass transport through the disk is largely reduced. Such a layer is commonly denoted as a *dead zone* (Gammie, 1995). In this region MRI gets suppressed mainly by Ohmic dissipation (Armitage, 2010). In less dens regions the Hall effect and ambipolar diffusion are working against MRI development. The Hall effect dominates in regions where the temperature is below a few thousand Kelvin and the density is between $10^7 - 10^{11}$ cm^{-3} (Sano and Stone, 2002). These conditions are given at about 10-100AU. In the outer part where the disk is less dense ambipolar diffusion is the prevailing non-ideal MHD effect (Simon et al., 2018). These different areas can be seen depicted as layers in Fig. 2.4.

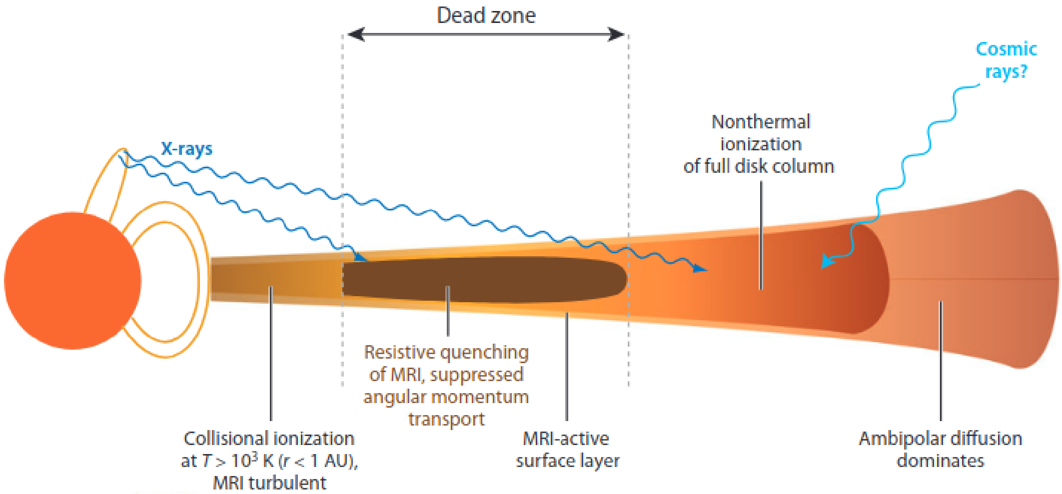

Figure 2.4: Illustration of the cross section of a PPD. On the left hand side the star with its magnetic filed lines is illustrated. This star radiates X- and UV-radiation. The disk consists of different layers differing in temperature, surface density, ionisation and viscosity. In the various layers different physical processes are dominant, e.g. MRI, ambipolar diffusion,... Fig. adapted from Armitage (2011)

2.1.5 FU Orionis outbursts

Episodic accretion events can be observed in young, FU-Orionis like stars. These events can be caused by e.g. thermal instabilities (TI) in the disk (Bell and Lin, 1994), gravitational instabilities (GI) (Vorobyov and Basu, 2005) or interchange instabilities nearby funnel flows (Gammie (1999); Balbus and Hawley (1991)). As discussed by e.g. Armitage, Livio and Pringle (2001) the thermal instability can be induced by gravitational instabilities in the outer disk which transports too much mass for ensuring a steady material flow throughout the disk. Hence, this material gets piled up in the inner disk parts. There the more effective viscous heating leads to a higher temperature which leads to a sudden change in the opacity due to ionisation. This increases the viscosity and the temperature in the adjacent disk regions. As described by Steiner et al. (2021) this higher ν leads to a in- and outward moving density redistribution which also triggers TI. Therefore, ionisation fronts evolve and move in- and outwards, which is heating the disk additionally. The higher gas temperature triggers MRI instabilities when a certain gas temperature T_{active} is reached. At the time when the inner wave reaches the inner boundary of the disk, the mass cannot be redistributed anymore which triggers an outburst and leads to a distinct higher accretion rate. This higher $\dot{M}$ causes also a higher accretion luminosity, thus the irradiation in the disk surface intensifies. After some time the strongly increased viscosity leads to a gas temperature drop and a cooling wave starts to move inward. This reduces the optical depth, which leads to the suppression of TI, since the material cannot be ionised anymore. Consequently, $\dot{M}$ decreases (a more detailed description of a burst can be found in Steiner et al. (2021)).

2.2 Planets

Historically, planets are subdivided in two types, terrestrial planets, like Earth, and giant planets, like Jupiter. Planet formation is not fully understood yet, since many evolutionary phases cannot be observed because the evolving bodies are deeply embedded in their surrounding PPD. There are many different physical effects influencing this formation (Ida, Lin and Nagasawa, 2013). This section will give a short overview on the topic on planet formation.

2.2.1 Formation of planets

During the formation of a planet it changes its size over a huge range of magnitudes. It starts with the sub-micron sized dust ($\sim 10^{-6}$ m). The radius of a dust grain can grow 13 orders of magnitude in size over time to form a planet like our Earth ($\sim 10^{7}$m) (Armitage, 2010). We distinguish between three main phases during the planet formation. The first two are the same for terrestrial and giant planets. In the third phase the properties of the embryo's surrounding determines its evolution to Earth-like or Jovian planets:

1. **Coagulation from dust to planetesimales:** in this phase the bodies have a size from μm to 10km and a mass of $M \leq 10^{18}$g. Because of their size and mass their motions are determined by the theory of aerodynamics, the interplay of the dust particles caused by the van der Waals force and Brownian motions (Dullemond and Dominik, 2005), chemical interactions, magnetic properties and gravitational instabilities (Goldreich and Ward, 1973). This process takes place in the denser regions of the disk. In the first phase at small sizes the dust particles are coupled to the gas. They are moving with the gas velocity and are growing due to electrostatic forces between neighbouring particles. If dust-grains reach an extent of a few cm they start to decouple from the gas and begin to orbit the central star with Keplerian velocity instead of sub-keplerian velocity of the gas as mentioned in

Sec. 2.1.2. These decoupled grains are not supported by the gas pressure anymore. (Weidenschilling, 1977)

2. **Planetesimals to embryos:** their size range spans from 10km to 1000km and the mass range is $M = 10^{18} - 10^{25}$g. If a planetesimal grows bigger than approximately 10km the gravitational forces start to operate since the body has gained enough mass so gravitational interactions can dominate the ongoing evolution. Also collisions are taking place, as well as mutual distruction (fragmentation), which can cause the growth of planetesimals.

3. **Planets**

   Terrestrial planets

   After the formation of the first planetesimals their further evolution is determined by their gravitational interactions. The gas disk has no large impact on the growth of terrestrial planets. Thus to calculate their dynamical evolution a N-body simulation must be made. Effects which should be included are collisions, including e.g. gravitational focusing, shear and dispersion, accretion, scattering and dispersion, statistical models (e.g. for shear, dispersion or isolation mass) and velocity dispersion of the planetesimals via viscous stirring, dynamical friction, gas drag. For further information see Armitage (2010).

   Giant planets

   The formation of a gas giant has four main evolutionary stages (Armitage, 2010):

   a) *Core formation:* a protoplanet (the core of the emerging giant) grows due to two-body collisions until its core reaches a certain mass, where it is massive enough to accumulate a considerable atmosphere. This phase is similar to the growth of terrestrial planets.

   b) *Hydrostatic growth:* The gaseous envelope encompassing the core is initially in a hydrostatic equilibrium. Energy from impacting small solid bodies and heat produced by friction are transported through this atmosphere by diffuse radiation or convection. This equilibrium is maintained until the core reaches a critical mass defined by the atmospheric gas opacity and the planetesimal accretion rate.

   c) *Runaway growth:* The gas accretion rate is not longer regulated by the hydrostatic condition of the atmosphere but by the interaction of the disk with the planet. During this stage the planet accumulates the lion's share of its gaseous atmosphere. In this phase the accretion rate can be approximated by *Bondi accretion* (see Sec. 2.2.3). A rough estimate for the onset of the runaway is the point in time when the atmosphere mass roughly equals the core mass (Bodenheimer and Pollack (1986), Stökl et al. (2016).)

d) *Completion of accretion:* The runaway growth ends when there is no material left to accrete. This can be caused either by a disappearing disk due to accretion and photoevaporation or gap opening in the planet's environment due to interactions with the disk (see Sec. 2.3.1).

The evolutionary stage focused on in this work is the period where the protoplanets already have a radius of a few thousand km (order of Mercury's radius), i.e. the third main phase (see Sec. 2.2.1). This stage has been chosen for this study, since smaller objects with a small gravitational potential do not have a significant impact on the evolution of the protoplanetary disk and therefore will not be discussed in this work.
The impact of planets in their third evolutionary stage will be discussed in Sec. 5.

2.2.2 Hill radius

The Hill radius is a concept for the gravitational impact radius of a body in a 3-body problem. It is defined by

$$r_H = a\sqrt[3]{\frac{M_\mathrm{p}}{3M_*}}, \tag{2.2.2.1}$$

where a is the distance of the planet to the star, m_p is the mass of the planet and M_* is the mass of the star.
Let's assume a star orbited by a planet. If the planet is located near to the star the gravitational force of the star dominates the total gravitational potential of the star-planet system, thus the Hill-sphere is quite small compared to a planet with larger separation.

2.2.3 Bondi accretion

The *Bondi accretion* (Bondi, 1952) is the spherical accretion of material onto a compact body, e.g. black holes, stars and planets, traveling through a homogeneous medium. The accretion rate $\dot{M}$ is defined as

$$\dot{M} = \frac{\partial M}{\partial t} = 4\pi\lambda\rho_\infty\frac{(GM)^2}{c_{\mathrm{s},\infty}^3}, \tag{2.2.3.1}$$

where λ is a constant equaling 1.12 for a spherical stationary isothermal system, defined by the accretion rate at the Bondi radius (see below), ρ_∞ is the density of the surrounding medium at infinity, G is the gravitational constant, M is the mass of the accreting object and $c_{\mathrm{s},\infty}$ is the speed of sound in the medium at infinity.
To derive this correlation one should make following assumptions (strictly following Bondi (1952)). The density ρ_∞ and the pressure p_∞ of the medium around the object are connected by the equation of state (EOS)

$$\frac{p}{p_\infty} = \left(\frac{\rho}{\rho_\infty}\right)^\gamma, \tag{2.2.3.2}$$

where γ has a value between $1 \leq \gamma \leq \frac{5}{3}$.
With a static equation of continuity

$$\vec{\nabla} \cdot (\rho \vec{u}) = 0, \tag{2.2.3.3}$$

one can find the constant accretion rate by integrating Eq. 2.2.3.3 (depending on the radius r and velocity v) and multiply it by 4π, hence

$$4\pi r^2 \rho v = \text{constant}. \tag{2.2.3.4}$$

The Bernoulli equation gives

$$\frac{v^2}{2} + \int_{p_\infty}^{p} \frac{dp}{\rho} - \frac{GM}{r} = \text{constant}, \tag{2.2.3.5}$$

and the constant equals 0 due to the boundary conditions at infinity. By including the isothermal EOS, Eq. 2.2.3.5 can also be written as

$$\frac{v^2}{2} + c_\mathrm{s}^2 \ln \rho - \frac{GM}{r} = 0. \tag{2.2.3.6}$$

With the dimension-less variables x, u, g for r, v, ρ

$$x = \frac{r}{r_\mathrm{B}}, \tag{2.2.3.7}$$

$$u = \frac{v}{c}, \tag{2.2.3.8}$$

$$g = \frac{\rho}{\rho_\infty}, \tag{2.2.3.9}$$

where $r_{\mathrm{B}} = GM/c_{\mathrm{s}}^2$ is the Bondi radius, one can get the non-dimensional form for the equation of mass accretion 2.2.3.4 and equation of motion

$$x^2 ug = \lambda, \tag{2.2.3.10}$$

and

$$\frac{u^2}{2} + \ln g - \frac{1}{x} = 0. \tag{2.2.3.11}$$

Hereby λ is defined as in Eq. 2.2.3.1.
Deriving Eq. 2.2.3.11 with respect to x leads to

$$u\frac{du}{dx} + \frac{1}{g}\frac{dg}{dx} + \frac{1}{x^2} = 0. \tag{2.2.3.12}$$

The usage of the derivation of g, $\frac{dg}{dx} = g\left(-\frac{2}{x} - \frac{1}{u}\frac{du}{dx}\right)$ leads to the non-dimensional wind equation

$$\left(u - \frac{1}{u}\right) du = \left(\frac{2}{x} - \frac{1}{x^2}\right) dx. \tag{2.2.3.13}$$

It is simple to see that if the velocity v equals the speed of sound c_{s} the LHS gets 0, thus there exists a critical point. Therefore the RHS also has to be 0, hence

$$\begin{aligned} \frac{2}{x} - \frac{1}{x^2} &= 0, \\ \Leftrightarrow x &= \frac{1}{2}. \end{aligned} \tag{2.2.3.14}$$

Entering this solution in Eq. 2.2.3.6 the critical value for g is $e^{\frac{3}{2}}$. By entering this in Eq. 2.2.3.10 this leads to the critical value for $\lambda_{\mathrm{c}} = 1.12$.
A plot of the solution for Eq. 2.2.3.13 can be seen in Fig. 2.5. It shows the mass accretion rate in non-dimensional variables x and v. The bold line passes through the critical point at $x = 1/2$ and $v = 1$.
The Bondi accretion can be used as an approximation for the mass accretion of a growing planet and its accumulation of mass during the run-away phase (Lambrechts and Johansen, 2012). Hence, this accretion rate will be used in this work to determine the magnitude of the sink term which is used to simulate a protoplanet in the disk.
The growth of a giant planet is well described by the Bondi accretion regime as discussed by Johansen and Lambrechts (2017). They claim that during the growth of the planet its gravitational radius changes from the Bondi radius r_{B} (applicable for $M_{\mathrm{p}} < 10^{-3}\ \mathrm{M}_{\oplus}$) to

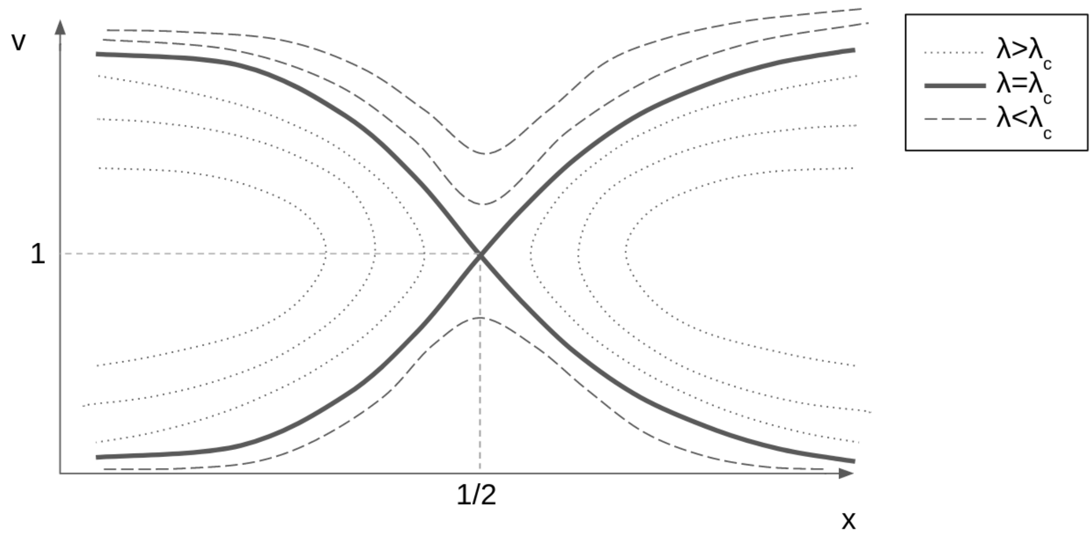

Figure 2.5: Solution of equation 2.2.3.13 which describes the spherical mass accretion onto a compact object. The bold line shows the accretion at the critical value λ_c, the dotted line is an accretion rate higher than λ_c (no physical solution) and the dashed lines shows the case $\lambda \leq \lambda_c$. The material falling onto the object undergoes a supersonic-subsonic transition.

the Hill radius r_H ($M_p > 10^{-3}$ M$_\oplus$). To identify the applicability of the Bondi accretion acting in the extent of the Hill radius to the growth of a planet, one should compare the Bondi radius to the Hill radius

$$\xi = \frac{r_H}{r_B} = \frac{a\left(\frac{M_p}{3M_*}\right)^{1/3}}{\frac{GM_p}{c_s^2}} \tag{2.2.3.15}$$

where M_p is the mass of the planet. This relation ξ is always larger than 1 which means that the Bondi radius is always smaller than the Hill radius which coincides with the results of Johansen and Lambrechts (2017), who state that, as soon as $r_H > r_B$ the planet is big enough to reach the run-away phase potentially. Since the planets used in this thesis, are all big enough to have the ability for fulfilling the run-away-criterion, the application of the Bondi accretion using r_H as a gravitational radius for this work is plausible. This accretion rate gives an upper limit for the accretion rate of the protoplanet.
The Bondi radius is only applicable for bodies with masses smaller than the transition mass $M_t \approx 10^{-3} M_\oplus$ (Lambrechts and Johansen, 2012). At this transition mass the Bondi radius gets comparable with the Hill radius. Since in this work only planets with masses higher than M_t are used, r_H is used as the planet's gravitational impact radius.

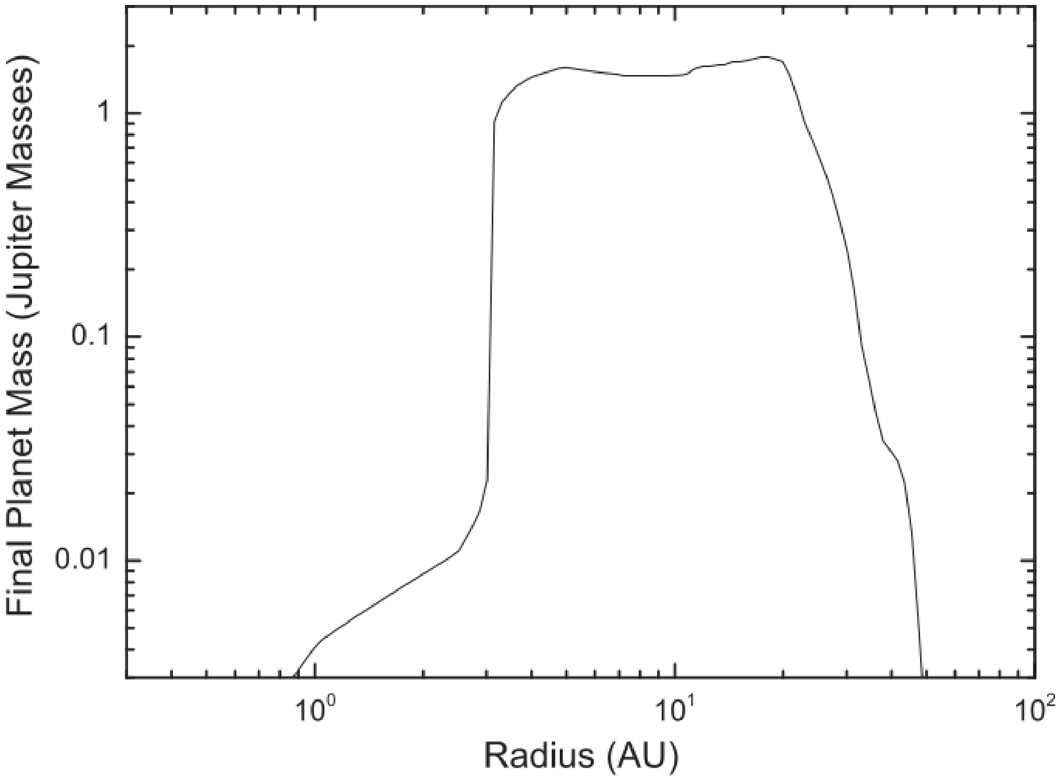

Figure 2.6: Dependency of the planetary final mass on its orbital distance (Xiao and Jin, 2015).

Applying the Bondi accretion law on growing planets in protoplanetary disks leads to a good sink term approximation if the planet is already in the runaway phase (Johansen and Lambrechts, 2017; Edgar, 2004). In comparison to other works, e.g. Stoekl et al. (2016), for the phase prior to the runaway the Bondi accretion is way to high as it will be discussed in Sec. 5. The dependency of the planetary location in the disk on the planet's final mass is shown e.g. by Xiao and Jin (2015), who claims that the final mass of a planet strongly depends on its distance to the central star as can be seen in Fig. 2.6. This distance dependency strongly correlates to the surface density on the planet's location, which has a significant impact on its growth.

2.3 Interaction of the PPD and planets

2.3.1 Formation of gaps

The disk is the birthplace of planets and therefore is likely to influence the formation and early evolution of protoplanets. Likewise, a planet is able to influence the processes in its surrounding PPD, e.g. if the planet is sufficiently large, it may open a gap in the disk, which can lead to significant changes in the structure of the PPD (Zhang et al., 2018). When a planet gets massive enough (the exact value depends on different disk properties like surface density, viscosity or turbulence), mostly about a few $10M_{\oplus}$, it is able to clear out an annulus which is then visible as a very low-density ring. Lin and Papaloizou (1993) found a criterion for gap opening conditions following

$$\frac{M_{\mathrm{p}}}{M_*} > \frac{81\pi\nu}{8a^2\Omega}, \tag{2.3.1.1}$$

where ν is the kinematic viscosity, a is the orbital distance of the planet and Ω characterises it's angular frequency. This ratio is approximately $\frac{M_{\mathrm{p}}}{M_*} \sim 10^{-2}$ in their calculations. They also propose that there exist two gap forming conditions.

- The planet's Roche radius[2] becomes comparable (or even larger) to the disk's scale height
$$\frac{R_{\mathrm{H}}}{H_{\mathrm{p}}} \geq 1. \tag{2.3.1.2}$$
- The viscous effects of the disk are outmatched by the rate of angular momentum transfer between disk and planet.

Lin and Papaloizou (1993) and Takeuchi, Miyama and Lin (1996) showed that the tidal interaction of the forming planet with the disk induces perturbations due to resonances (mainly Lindblad resonances). These resonances appear as density waves, which move throughout the PPD. They can alter the disk structure due to their propagation and dissipation and are able to open a gap in the disk. When a gap has formed, material is no longer able to flow through these low density regions and therefore has an impact on the planet's accretion rate, since there is no material in its vicinity left which can be accreted. Goldreich and Tremaine (1980) claim that gaps can form due to high accretion rates and an inefficient transport of material due to low viscosity. The viscous transfer of angular momentum causes torques, which contribute to the formation of a gap. Additionally

[2]The Roche radius defines the region in which a companion of a massive central object cannot counteract the tidal forces generated by the central mass using its own gravitational self-attraction. Hence, the companion gets disrupted by these tidal forces.

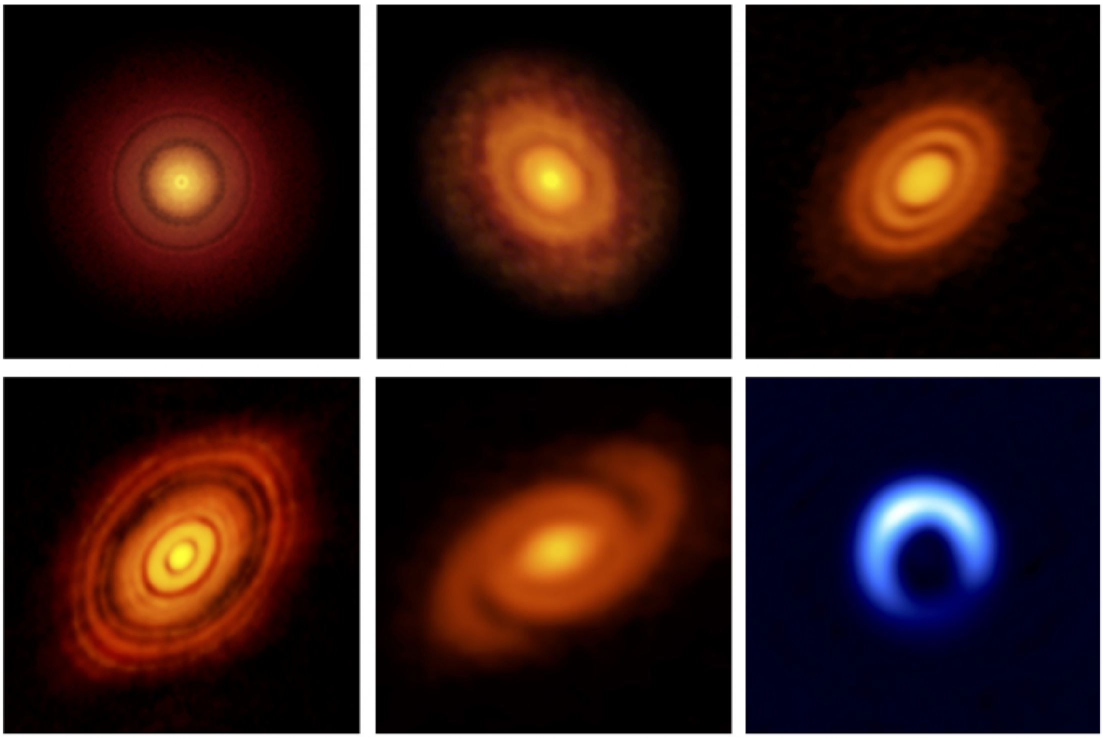

Figure 2.7: Different images of protoplanetary disks with gaps and spirals. Images taken by ALMA. Credits: S. Andrews, L. Cieza, A. Isella, A. Kataoka, B. Saxton (NRAO/AUI/NSF), and ALMA (ESO/NAOJ/NRAO).

the planet induces perturbations due to the gravitational interactions with the disk. Eccentricity of the planet is a main generator of torques at corotation resonance and Lindblad resonances. The different resonances occurring in the disk can lead to a constructive interference, which supports the opening of a gap. This excitement stimulates angular momentum transfer and the formation of tidal arms. If the planet is massive enough the material at inner radii still accretes towards the star and mass at outer radii gets piled up and a gap can open. The PPD is not able to efficiently transport the gas and dust in its interior anymore and it is not capable of compensating the perturbations induced by the evolving planet (Armitage, 2010). These effects result in a very low disk gas density at the planets radial location. Figure 2.7 shows some examples of PPD with gaps and induced spirals observed by ALMA.

Paardekooper and Mellema (2006) published that planets with masses $M_{\mathrm{p}} > 0.05\ \mathrm{M_J}$ are able to add additional density gradients at at radii inside and outside the planet's orbital radius. This can be seen in Fig. 2.8. In an observational survey this effect could

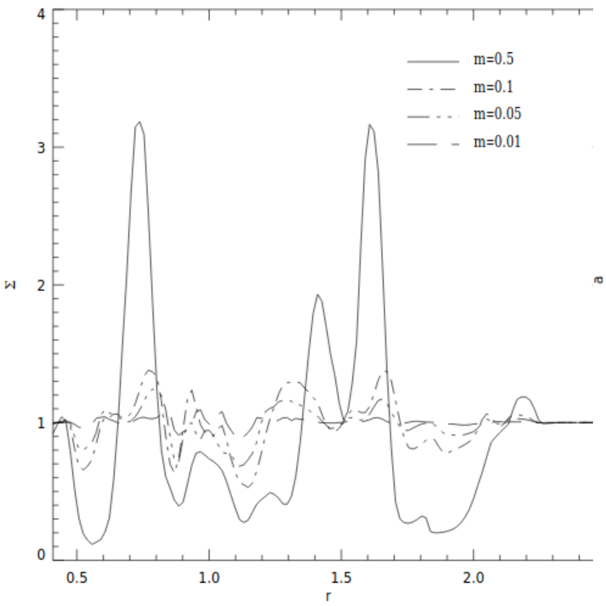

Figure 2.8: Distribution of surface density Σ over the disks extend. An immanent planet with mass m in $M_\oplus$ at $r = 1$ induces additional low density regions at $r = 0.55$ and $r = 1.8$ due to the occurrence of resonances induced by the tidal interaction of the planet with the disk. (Paardekooper and Mellema, 2006)

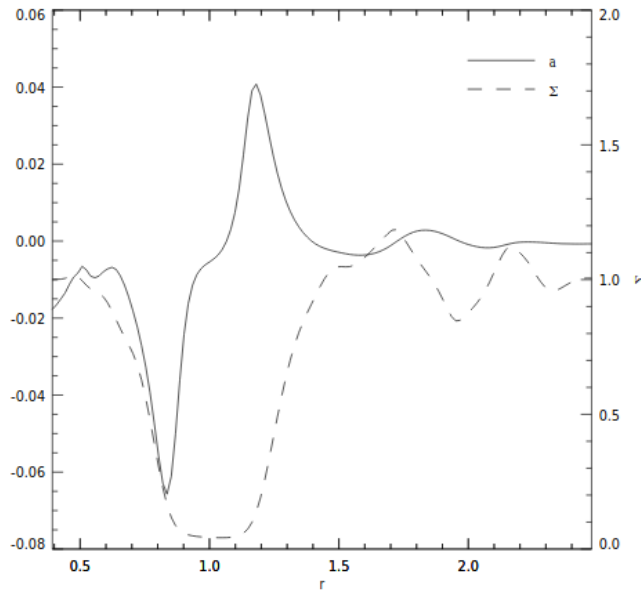

Figure 2.9: Radial plot of the acceleration a (solid line) and gas surface density (dashed line). At the inner gap boundary a is negative and at the outer boundary it is positive. This leads to a mass flow away from the planet towards the gap boundaries. (Paardekooper and Mellema, 2006)

be a problem by differing between a single and multiple planetary system. The authors also propose that a planet present in the disk influences the radial direction of the mass flow within the disk. At the inner and outer regions of a forming gap the gas pressure gradient pushes material towards the gap boundaries, yielding a mass pile-up just inside and outside the gap, which can be seen in Fig. 2.9. Paardekooper and Mellema (2006) conclude that the formation of a gap in the dust disk only need a small dip in the gas disk which can be created by relatively small planets ($M_\mathrm{p} = 0.05 M_\oplus$).
Crida, Morbidelli and Masset (2006) calculated another gap opening criterion, based on the pressure forces acting in the disk due to a present planet. This pressure criterion is

$$\frac{3H_\mathrm{p}}{4R_\mathrm{H}} + \frac{40M_\mathrm{p}}{M_\star \mathcal{R}} < 1, \tag{2.3.1.3}$$

where H_p, R_H, M_p and $M_\star$ are, again, the pressure scale height, the Hill-radius, the mass of the planet and the mass of the star, respectively. $\mathcal{R}$ is the Reynolds-number which can also be written as $\Omega_\mathrm{p} a^2/\nu_\mathrm{p}$, where Ω_p, a^2 and ν_p are the Keplerian angular frequency, the orbital distance and the kinematic viscosity, respectively.
The formation of a gap can be seen in the azimuthal velocity u_φ, as claimed by Teague et al. (2018) and Pinte et al. (2018), who discovered that it is possible to determine the angular velocity of gas annuli of PPDs by analysing molecular lines with ALMA. Teague et al. (2018) also states that a planet present in a disk induces local pressure gradient perturbations, which leads to perturbations in u_φ and can be seen in Fig. 2.10, which is a result of the theoretical work of Zhang et al. (2018).

What should be noted is another possible gap formation scenario as discussed by Morishima (2012). They propose that a gap in a PPD with a dead zone can open behind the outer edge of the dead zone. This is because at this point the photoevaporative mass loss rate at the planet's orbital distance is higher than the radial mass accretion rate. This leads to a mass flow suppression as a consequence of a low viscosity in the dead zone region.
Many of the mentioned processes, like spiral arms and waves induced by resonances, are no axisymmetric 1D-problems an therefore cannot be considered in this work.

2.3.2 Migration of planets

As mentioned above the transfer of angular momentum is due to a torque which acts on the inner and the outer boundaries of the planet. The net torque, arising from different torques acting on the inner and outer radial planetary gap boundaries, causes the planet to migrate inwards (Goldreich and Tremaine, 1980). Migration is the most likely explanation

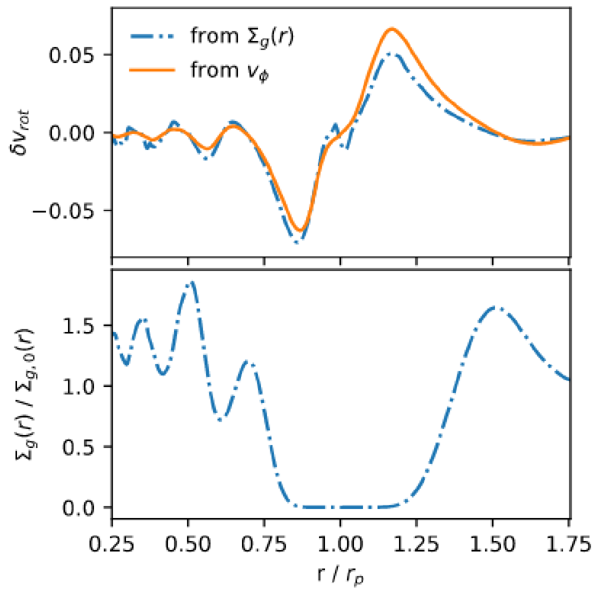

Figure 2.10: The impact of gap formation on the angular velocity δv_{rot} (upper panel) and the surface density in units of the initial surface density $\Sigma_{\mathrm{g}}/\Sigma_{\mathrm{g},0}$ (lower panel) (Zhang et al., 2018).

for the existence of hot Jupiters [3] (Dawson and Johnson, 2018).
There exists two main types of migration (Lubow and Ida, 2010):

- **Type I migration:**
  Type I migration happens to low-mass planets while they are forming in a PPD. In this case the disk is able to compensate the perturbations induced by the protoplanet. The PPD is able to efficiently redistribute the material and its angular momentum, effectively smoothing out perturbations and irregularities in the radial and angular density distribution (Lin and Papaloizou, 1986), i.e. gaps can not form. Hence, the overall disk structure is largely unaffected by the presence of a low-mass planet, i.e. the planet is not able to open a gap.

- **Type II migration:**
  The difference to type I migration is that the perturbation caused by the planet's gravitation outmatches the disk's ability of redistributing material, hence, the disk is not able to flatten the planet's perturbations, eventually leading to the formation of a gap. This is only possible for planets with a mass of $M_{\mathrm{p}} \approx M_{\mathrm{J}}$ (Lin, Bodenheimer

[3] Hot Jupiters are planets with masses comparable to Jupiter (M_{J}) but semi-major axis with an orbital period of a few days (Mayor and Queloz, 1995).

and Richardson, 1996).

The transition from type I to type II migration depends on various properties of the disk and an embedded planet, like planet mass, viscosity, gas properties, temperature, material composition, metallicity, etc. Usually the mass which is needed to open a gap is a considerable fraction of one Jupiter mass (Armitage, 2010).

3 Physical equations

To describe the complex protoplanetary accretion disk system a set of partial differential equations (PDE) is necessary. The equations which describe the occurring physical processes are the equations of continuity, motion, energy and equation of state. In the following section a short introduction to each of the equations will be given. In Sec. 3.1 the equations of radiation hydrodynamics (RHD) will be introduced. For further information see Ragossnig et al. (2020). Sec. 3.2 shows how these equation must be adapted to simulate a growing planet in the PPD.

3.1 Equations of RHD

All of the following equations are written in a conservative way, which defines the conservation of quantities like mass, momentum and energy.

Equation of continuity

$$\frac{\partial \Sigma}{\partial t} + \vec{\nabla} \cdot (\Sigma \vec{u}) = 0, \tag{3.1.0.1}$$

characterises the flow of mass in a system. The change of surface density Σ in a control volume ΔV per unit time t equals the net flow of current density with velocity $\vec{u}$ in and out of ΔV.

Equation of motion

$$\frac{\partial \Sigma \vec{u}}{\partial t} + \vec{\nabla} \cdot (\vec{u} \Sigma \vec{u}) + \vec{\nabla} P + \Sigma \frac{G M_*}{r^2} - \frac{4\pi}{c} \kappa_R \Sigma \vec{H}_0 + \vec{\nabla} \cdot \mathbf{Q} = 0, \tag{3.1.0.2}$$

In this and in the following equations P describes the gas pressure, G is the gravitational constant, M_* is the mass of the central protostar and r is the distance of the annulus to it. κ_i is the opacity which is calculated from tables, c describes the speed of light, H is the radiation flux and $\mathbf{Q}$ is the viscous pressure tensor. The equation of motion describes the conservation of momentum.

Internal energy
The conservation of internal energy is described as

$$\frac{\partial \Sigma e}{\partial t} + \vec{\nabla} \cdot (\vec{u}\Sigma e) + P\vec{\nabla} \cdot \vec{u} - 4\pi\kappa_P \Sigma(J - S) + \mathbf{Q} : \vec{\nabla}\vec{u} + \Delta E_{\mathrm{rad}} = 0, \tag{3.1.0.3}$$

where e describes the specific energy, J is the radiant energy density, S the source function, $\mathbf{Q}$ is the viscous pressure tensor and E_{rad} is the radiative heating/cooling term. The last term characterises the viscous energy generation which is the energy generated by viscous stress.

Equation of state (EOS)

$$P = \rho c_{\mathrm{s}}^2 \tag{3.1.0.4}$$

The equation of state defines the conditions of the system. Here the gas pressure is connected with the density of the disk and the speed of sound in an isothermal way. This equation describes the internal structure of the gas in the protoplanetary disk.

3.2 Adaption of the RHD equations

The PDE system described above represents the structure, evolution and dynamics of a protoplanetary disk over its lifetime. To simulate a planet in this disk the RHD equations must be extended by source and sink terms due to the presence of a planet in the PPD.

Adapted continuity equation
The continuity equation receives an additional sink term $\dot{\tilde{\Sigma}}(r)$ which describes the mass which gets subtracted from the disk's total mass content. This sink term in this work has the properties of the mass accretion rate calculated by Bondi accretion (see Sec.2.2.3). The adapted equation of continuity then takes the form

$$\frac{\partial \Sigma}{\partial t} + \vec{\nabla} \cdot (\Sigma \vec{u}) - \dot{\tilde{\Sigma}}(r) = 0. \tag{3.2.0.1}$$

with the sink term $\dot{\tilde{\Sigma}}(r)$ being the temporal change of the surface density due to the mass accretion rate per unit of volume dV

$$\dot{\widetilde{\Sigma}} = \frac{\partial \widetilde{\Sigma}}{\partial t}, \tag{3.2.0.2}$$

$$\int_V \dot{\widetilde{\Sigma}} dV = \dot{M}_{\mathrm{p}}, \tag{3.2.0.3}$$

where $\dot{M}_{\mathrm{p}}$ equals the Bondi accretion described in Sec. 2.2.3.

Adapted motion equations

The sink term does not only modify the amount of mass in the disk. Removing mass from the system leads to a corresponding flow of momentum from the disk towards the planet. The equation of motion therefore has to be adapted by an additional term

$$\vec{\Lambda}_{\mathrm{sink}} = \dot{\widetilde{\Sigma}} \cdot \vec{u}. \tag{3.2.0.4}$$

The adapted form of the motion equation then reads

$$\frac{\partial \Sigma \vec{u}}{\partial t} + \vec{\nabla} \cdot (\vec{u} \Sigma \vec{u}) + \vec{\nabla} P + \Sigma \frac{G M_*}{r^2} - \frac{4\pi}{c} \kappa_R \Sigma \vec{H}_0 + \vec{\nabla} \cdot \mathbf{Q} + \vec{\Lambda}_{\mathrm{sink}} = 0. \tag{3.2.0.5}$$

Adapted energy equation

The energy equation 3.1.0.3 also must be adapted because the material, which gets accreted by the forming planet transforms its potential energy partly into accretion luminosity L_{acc} (Armitage, 2010)

$$L_{\mathrm{acc}} = -\frac{G M_{\mathrm{p}} \dot{M}_{\mathrm{p}}}{r_{\mathrm{H}} - R_{\mathrm{p}}}. \tag{3.2.0.6}$$

This radiation generates radiation pressure, therefore counteracts accretion, which causes an additional energy term in the equation. Also the contained internal energy of material which is accreted on the planet, i.e. $\dot{\widetilde{\Sigma}} \cdot e$, must be considered since this energy is removed from the system. These two effects lead to the following term of

$$\Theta_{\mathrm{sink}} = \dot{\widetilde{\Sigma}} \cdot e + l_{\mathrm{acc}}, \tag{3.2.0.7}$$

with l_{acc} being the volume specific accretion luminosity, and this term is included in

Eq. 3.1.0.3 in the form of

$$\frac{\partial \Sigma e}{\partial t} + \vec{\nabla} \cdot (\vec{u}\Sigma e) + P\vec{\nabla} \cdot \vec{u} - 4\pi\kappa_P \Sigma (J - S) + \mathbf{Q} : \vec{\nabla}\vec{u} + \Theta_{\mathrm{sink}} = 0. \tag{3.2.0.8}$$

The first term in Eq. 3.2.0.7 represents the energy which is extracted from the disk by removing disk material. The second term describes the energy generated by the accreting material.

4 Numerical method

The code which is used for the simulations in this work is called **TAPIR** (**T**he **A**da**p**tive **I**mplicit **R**adiative Hydrodynamics). A detailed description of the code can be found in Ragossnig et al. (2020). TAPIR is an implicit and adaptive code and is written in Fortran90.
This code solves a system of partial differential equations (PDE) (see Sec. 3) which describes physical structures like protoplanetary disks. To solve this system the equations must be integrated, for this the equations must be discretized. These discretized forms will be presented in the following chapter. This section closely follows Ragossnig et al. (2020) and Steiner et al. (2021).

Implicit method

There are two main methods to compute the solution of a system of time-dependent differential equations. They are called *explicit* and *implicit* method. The main difference between these two schemes is the way of evaluating the new time step.
The explicit method uses the the old values to calculate those of the new time step. An illustration of this method can be seen in Fig. 4.1 on the left side.
An advantage of an explicit method is that it is easier to implement compared to an implicit integration method. However, for the explicit method there exists a strict restriction on the time step. To get a stable solution the time step must satisfy the CFL-condition. This condition contains the maximum time step which can be achieved (for more detailed information see LeVeque (2002)). For the simulation of physical problems like the evolution of protoplanetary disks on the one hand small time steps are needed because some physical processes (like the propagation of perturbations) occur on small spatial and temporal scales. Thus the computational time to simulate the whole lifetime of a disk is unfeasible with an explicit scheme. So, on the other hand large time intervals are necessary to simulate the whole disk lifetime. The CFL-condition does not allow to adjust the time steps fast enough over a wide range of magnitude to describe the physical processes adequately over the whole disk lifetime.

The implicit method is a scheme to calculate the solution of a system of nonlinear

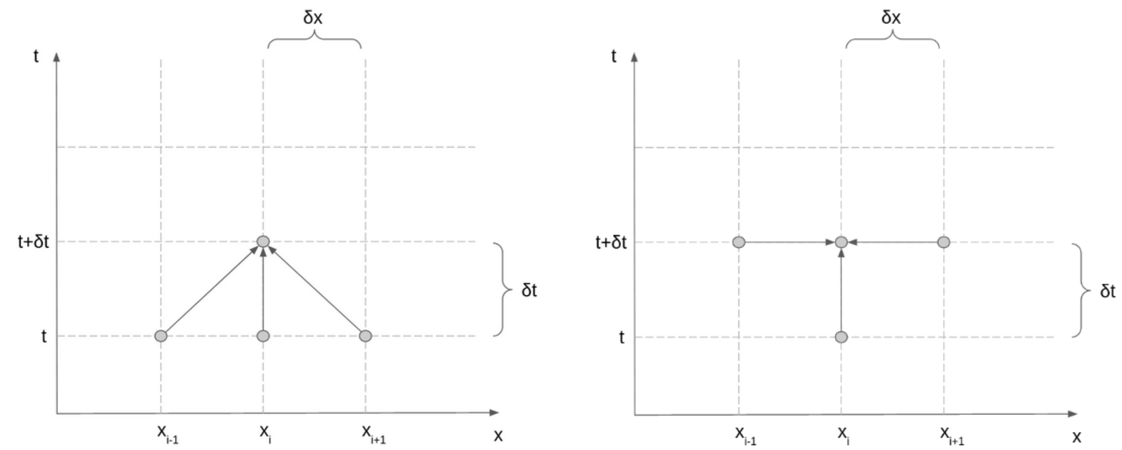

Figure 4.1: *left:* illustration of the explicit method. The value of the variable at the new time step is calculated from the values of the old time step. *right:* illustration of the implicit method. The value of the variable at the new time step is calculated by values of the old and new time step

ordinary and partial differential equations. The viscous timescale for PPDs is much larger than the dynamical timescale. The implicit scheme uses values of the old and new time step to evaluate the value of the variable at the new time step (see right figure of Fig. 4.1). This leads to a nonlinear algebraic system which must be solved at every time step. To solve this system iterative techniques are used. Here the Newton-Raphson iteration is applied to find the root of these equations. Hence, a Jacobi-matrix is needed which must be inverted to find the solution of the PDE system.

The implicit scheme allows to do large time steps with simultaneous high accuracy. Due to these large time steps the implicit method is a proper way to simulate the longterm evolution of physical systems. The time step is determined by the similarity of the new solution to the old one. A more detail description of the implicit method can be found in Steiner (2012).

Boundary conditions

Since boundary conditions (BC) can have a significant impact on the solution of a PDE system, it is important to define appropriate conditions at the boundaries. For an implicit method these conditions enter during the inversion of the Jacobi-matrix. In a physical system like a protoplanetary disk it is challenging to find physically dominated and properly posed terms for the inner and outer boundary because small variations can have large impacts on the solutions (Ragossnig et al., 2020). The inner boundary is hard to define because the disk and the star are a complex interacting structure and therefore not easy to separate. One possible inner BC is the so-called magnetic truncation radius (Hartmann, Herczeg and Calvet, 2016), which is the radius where the angular velocity of the star Ω_* coincides the Keplerian angular velocity of the disk Ω_K. This condition depends on the properties of the star and its magnetic field which interacts intensively with the disk. Alternatively the BC can be characterised by the zero-gradient where two neighbouring cells are set to the same value to satisfy the zero-gradient. An example for this definition of a BC is the pressure-less outflow (LeVeque et al., 1997). The outer BC is characterised by the properties of the ISM which surrounds the PPD. For this work the PPD's outer rim is defined at the point where its surface density is lower than 20 g/cm^2. Important to mention is that in this thesis axisymmetry is assumed during most of the disk's lifetime since the TAPIR is a 1D code. According to different observations it is shown that 80% of the observed PPDs are in an axisymmetric state most of their lifetime (Andrews et al., 2018). To fulfill the axisymmetric criterion the mass of the disk M_d has to be < 0.01 M$_\odot$ to avoid gravitational instabilities (Kóspál et al., 2016; Hillenbrand et al., 2018), as well as the star mass M_* has to be significantly higher than M_d ($M_\mathrm{d} \ll M_*$), since the local gravitational potential of regions in the disk should not overrule the gravitational potential of the star, so no self-gravitating mass blobs can form. This would lead to a non-axisymmetric structure, hence it cannot be calculated by the 1D-code anymore. Additionally the Toomre-parameter must be $\gg 1$.

Initial model

For a problem to be solved by an implicit by an implicit method proper initial values are required, since the root of the equations must be found. If an initial model with values deviating too much from a solution of the system (outside the convergence radius of the Newton-Raphson iteration) it is not possible to find the root through iteration. A detailed description and verification of the initial model used in TAPIR can be found in Ragossnig et al. (2020).

Adaptive grid

Astrophysical problems pose a challenge for hydrodynamic simulations due to the orders of magnitude which have to be covered, both in spatial resolution and in simulation time. A grid with homogeneously distributed grid points corresponding to a certain resolution is not feasible due to limited computational resources. Therefore an adaptive grid is used, which allows to maintain a reasonable resolution in areas of interest while keeping the number of discretization points fairly limited.

The adaptive grid is implemented into TAPIR by using an additional equation, the so-called grid equation, which allows a fully implicit time integration (see Dorfi and Drury (1987) or Steiner (2012)). This allows the grid points to move freely in the computational domain.

4.1 Discretized set of equations

In the following section the discretized equations will be described. For a detailed derivation of these equations see Ragossnig et al. (2020).

Equation of continuity

$$\underbrace{\delta[\rho V_{\mathrm{S}}]}_{\substack{\text{temporal}\\ \text{difference}}} + \underbrace{\sum \tilde{\rho} \Delta \mathrm{Vol}_{\mathrm{S}}}_{\text{advection}} - \underbrace{\mathcal{S}}_{\text{sink/source}} = 0. \tag{4.1.0.1}$$

Here $\delta[x]$ and Δx describes the temporal and the spatial scalar difference of the quantity x, respectively, i.e. $\delta[x] = x - x^{\mathrm{old}}$ and $\Delta x = x_{\mathrm{i+1}} - x_{\mathrm{i}}$. The value of a advected quantity which is advected with the advective flux during the time step δt is marked by $\tilde{x}$. $\Delta \mathrm{Vol}_{\mathrm{S}}$ describes the scalar volume of the grid cell.The sum depicts the summation over all cells.

Equation of motion

The equation of motion is splitted into its radial (r) and angular (φ) components, which are then discretized separately.

r-component:

$$\begin{aligned}
&\underbrace{\delta[\rho v_{\mathrm{r}} V_{\mathrm{V}}] + \sum \widetilde{\bar{\rho} v_{\mathrm{r}}} \Delta \mathrm{Vol}_{\mathrm{V}} - \frac{\bar{\rho} v_{\varphi} v_{\varphi}}{r} V_{\mathrm{V}} \delta t}_{\text{time derivative and advection}} + \underbrace{2\pi r \Delta P \delta t}_{\text{gas pressure}} + \underbrace{\rho \frac{GM_*}{r^2} V_{\mathrm{V}} \delta t}_{\text{gravitation}} \\
&\qquad - \underbrace{\frac{\pi}{r} \Delta \left[\bar{r}^2 \mu_{\mathrm{Q}} \left(\frac{\Delta v_{\mathrm{r}}}{\Delta r} - \frac{\bar{v}_{\mathrm{r}}}{\bar{r}} \right) \right] \delta t}_{\text{viscous force in } r\text{-direction}} - \underbrace{\frac{4\pi}{c} \overline{\kappa_{\mathrm{R}} \rho} H_0 V_{\mathrm{V}} \delta t}_{\text{radiation pressure}} - \underbrace{\mathcal{L}_{\mathrm{sink,r}}}_{\text{sink/source}} = 0.
\end{aligned} \tag{4.1.0.2}$$

φ -component:

$$\underbrace{\delta[r\bar{\rho}v_\varphi V_\mathrm{V}] + \sum \widetilde{r\bar{\rho}v_\varphi}\Delta\mathrm{Vol}_\mathrm{V}}_{\text{time derivative and advection}} - \underbrace{\pi\Delta\left[\bar{r}^2\mu_\mathrm{Q}\left(\frac{\Delta v_\varphi}{r} - \frac{\bar{v}_\varphi}{\bar{r}}\right)\right]\delta t}_{\text{viscous force in } r\text{-direction}} - \underbrace{\mathcal{L}_{\mathrm{sink},\varphi}}_{\text{sink/source}} = 0, \quad (4.1.0.3)$$

where $\Delta\mathrm{Vol}_\mathrm{V}$ is the vectorial volume of a cell, ΔP is the pressure difference, μ_Q is the coefficient of the viscosity, κ_ν is the opacity and H is the radiation flux.

Equation of energy
The equation of energy includes the internal energy, the radiation energy and the radiation flux. The discretized equation takes the form of

$$\begin{aligned} &\delta[\rho e V_S] + \sum \widetilde{\rho} e \Delta\mathrm{Vol}_\mathrm{S} + 2\pi P\Delta(r v_\mathrm{r})\delta t \\ &+8\pi^2\sqrt{2\pi}H_\mathrm{p}\sigma\Delta\left(-\frac{2}{3}\frac{r^2\sigma\Delta(T^4)}{\overline{\kappa_\mathrm{R}\rho_0}V_\mathrm{V}}\right)\delta t + \dot{E}_\mathrm{rad} \\ &-\frac{\mu_\mathrm{Q}}{2}\left\{\left[\frac{\Delta v_\mathrm{r}}{\Delta r} - \frac{\overline{v_\mathrm{r}}}{\bar{r}}\right] + \left[\frac{\Delta v_\varphi}{\Delta r} - \frac{\overline{v_\varphi}}{\bar{r}}\right]^2\right\}V_\mathrm{S}\delta t - \underbrace{\mathcal{T}_\mathrm{sink}}_{\text{sink/source}} = 0. \end{aligned} \quad (4.1.0.4)$$

4.2 Numerical implementation of the sink term

4.2.1 Formalism of the sink term

The calculation of the Bondi accretion rate (Eq. 2.2.3.1), which is then spread over the radial range corresponding to the Hill radius r_H, describes the total mass accretion rate onto the planet. A Gaussian function[1] is used

$$G(\mathrm{i}) = \frac{1}{\sigma\sqrt{2\pi}}\exp\left(-\frac{(r_\mathrm{i} - a)^2}{2\sigma^2}\right), \quad (4.2.1.1)$$

to distribute the calculated accreted mass over r_H. The value of the Gaussian function $G(\mathrm{i})$ can be calculated at each grid point i. The variance σ is defined by the size of r_H, the expected value a is set by the planet's orbital distance and the variable r_i describes the corresponding orbital radius of i.
Since $\dot{M}$ should not be changed by $G(\mathrm{i})$ the Gaussian function must be normalised which

[1] A Gaussian distribution is used as a first simple approximation of the accretion of a sink term.

can be done by integrating the discrete function $G(\mathrm{i})$ using the trapezoidal formula

$$N = \sum_{\mathrm{i}} \frac{1}{2} \frac{G(\mathrm{i}+1) + G(\mathrm{i})}{r_{\mathrm{i}+1} - r_{\mathrm{i}}}. \tag{4.2.1.2}$$

This normalised distribution of $\dot{M}$ leads to a mass accretion rate at each grid point in the form of

$$\dot{M}_{\mathrm{p,i}} = \frac{\mathcal{G}(\mathrm{i})}{N} \dot{M}_{\mathrm{p,i}}, \tag{4.2.1.3}$$

where $\mathcal{G}(\mathrm{i})$ is the integrated value of the Gaussian function at the i-th cell according

$$\mathcal{G}(\mathrm{i}) = \frac{G(\mathrm{i}+1) + G(\mathrm{i})}{2(r_{\mathrm{i}+1} - r_{\mathrm{i}})}. \tag{4.2.1.4}$$

All $\dot{M}_{\mathrm{p,i}}$ add up together to the planet's total mass accretion rate

$$\dot{M}_{\mathrm{p}} = \sum_{\mathrm{i}} \dot{M}_{\mathrm{p,i}}, \tag{4.2.1.5}$$

which proves that the normalisation is done correctly.
In this work it is assumed that a fraction of the Bondi accretion is accreted by the planet since a flow through the gap can occur as Lubow and D'Angelo (2006) have shown. This can be realised by multiplying the accretion rate by a certain efficiency factor ξ where

$$0 \leq \xi \leq 1. \tag{4.2.1.6}$$

With these considerations the discrete sink term in Eg. 4.1.0.1 can be defined as

$$\mathcal{S} = \frac{\mathcal{G}(i)}{N} \dot{M} \cdot \xi \cdot \delta t = \dot{M}_{\mathrm{i}} \delta t. \tag{4.2.1.7}$$

The time step δt in Eq. 4.2.1.7 is needed since the unit of $\dot{M}_{\mathrm{i}}$ is mass per second. The speed of sound c_{S} in the disk at each grid point (which is needed to calculate the accretion rate in Eq. 2.2.3.1) can be calculated by

$$c_{\mathrm{S}}(\mathrm{i}) = \sqrt{\frac{P(\mathrm{i})}{\rho(\mathrm{i})}}, \tag{4.2.1.8}$$

where $P(\mathrm{i})$ and $\rho(\mathrm{i})$ are the gas pressure and the density of the disk respectively.
The accretion rate is physically restricted by the amount of mass in the hill sphere and in the annulus of planetary influence, which is naturally considered in this work, as the

disk and planet are evolving simultaneously. Thus if the mass in an annular cell $m_{\mathrm{cell,i}}$ is smaller than the amount of $\dot{M} \cdot \delta t$ the sink term only extracts the disposable material which is provided by the PPD annulus.

Formalism of the $\mathcal{L}_{\mathrm{sink,r}}$-term

The discrete form of the change of the momentum due to the sink term is defined as

$$\mathcal{L}_{\mathrm{sink,r}} = \dot{M}_{\mathrm{i}} \cdot \delta t \cdot u_{\mathrm{r,i}}, \tag{4.2.1.9}$$

where $u_{\mathrm{r,i}}$ is the radial velocity at grid point i. The term is proportional to the accretion rate of the planet.

Formalism of the $\mathcal{L}_{\mathrm{sink},\varphi}$-term

The angular momentum which is extracted by the sink term is defined by

$$\mathcal{L}_{\mathrm{sink},\varphi} = \dot{M}_{\mathrm{i}} \cdot \delta t \cdot u_{\varphi,\mathrm{i}} \cdot \frac{1}{2}\left(r_{\mathrm{i}} + r_{\mathrm{i+1}}\right). \tag{4.2.1.10}$$

Here $u_{\varphi,\mathrm{i}}$ is the velocity on φ - direction at the i-th cell.

Formalism of the $\mathfrak{T}_{\mathrm{sink}}$-term

As mentioned in Sec. 3.2 the effect of accretion luminosity must also be included since the luminosity radiated during the accretion process is able to heat up the surrounding of the planet. This heating process can influence the mass flow in the disk because the temperature has an impact on the viscosity's efficiency (see e.g. Shakura and Sunyaev (1973), Balbus and Hawley (1991), Sano and Stone (2002) or Demtroder (2017)). The change in temperature can also influence the planet's mass accretion rate as $\dot{M}_{\mathrm{i}}$ also depends indirectly on the temperature because the density ρ and the sound speed depend on T (Bondi, 1952).
Similarly to $\dot{M}_{\mathrm{p}}$ Eq. 3.2.0.6 provides a total accretion luminosity at one point in the disk. By using the expression for the discretized mass accretion rate (Eq. 4.2.1.3) one can get a discretized version of L_{acc}

$$L_{\mathrm{acc,i}} = -\frac{G M_p \dot{M}_{\mathrm{p,i}}}{r_{\mathrm{H}} - R_{\mathrm{p}}}. \tag{4.2.1.11}$$

Inserting this term in Eq. 3.2.0.7 one can get a discretized expression for the energy generated by the planet's accretion process in the form of

$$\mathcal{T}_{\rm sink,i} = \dot{M}_{\rm i} \cdot e_{\rm i} + L_{\rm acc,i}. \tag{4.2.1.12}$$

4.2.2 Viscosity

The kinematic viscosity is, as described by Shakura and Sunyaev (1973),

$$\nu = \alpha c_{\rm s} H_{\rm p}, \tag{4.2.2.1}$$

where α is the viscosity parameter, $c_{\rm s}$ is the the speed of sound and $H_{\rm p}$ denotes the pressure scale height. To simulate a dead zone, a layered-viscosity model is used (Gammie, 1996), where α denotes the effective viscosity and is determined as follows,

$$\alpha = \alpha_{\rm base} + (\alpha_{\rm surf} + \alpha_{\rm deep}) f_{\rm MRI} + \alpha_{\rm grav}, \tag{4.2.2.2}$$

where $\alpha_{\rm base}$, $\alpha_{\rm surf}$, $\alpha_{\rm deep}$ and $\alpha_{\rm grav}$ stand for the base viscosity value, the MRI viscosity in the surface layer, the viscosity for disk parts where the thermal ionisation threshold is exceeded and the GI induced viscosity[2], respectively, whereas $f_{\rm MRI}$ is a flag to adjust the viscosity to low density regions. If Σ is less than 0.1 g/cm^2 the disk is assumed to be not dense enough to develop MRI. So the mentioned flag $f_{\rm MRI}$ is 0, hence α is set to $\alpha_{\rm base}$. For $\Sigma >$ 1.0 g/cm^2+$\Sigma_{\rm sm}$, $f_{\rm MRI}$ is 1, where $\Sigma_{\rm sm}$ defines a smoothing range. For Σ-values in-between, linear smoothing is applied for $f_{\rm MRI}$. For this work $\Sigma_{\rm sm}$ is set to 0.05 g/cm^2. The adjusted α values can be seen in the Tab. 4.1.

$\boldsymbol{\Sigma}$ (g/cm^2)	$\boldsymbol{f_{\rm MRI}}$	$\boldsymbol{\alpha}$
$\Sigma > 0.1 + \Sigma_{\rm sm}$	1	$\alpha_{\rm base} + \alpha_{\rm surf} + \alpha_{\rm deep}$
$0.1 < \Sigma < 0.1 + \Sigma_{\rm sm}$	$(\Sigma - 0.1)/\Sigma_{\rm sm}$	$\alpha_{\rm base} + (\alpha_{\rm surf} + \alpha_{\rm deep}) f_{\rm MRI}$
$\Sigma < 0.1$	0	$\alpha_{\rm base}$

Table 4.1: Table of the MRI-flag scheme.

4.2.3 Time dependency of planetary properties

As mentioned in Sec. 2.2 planets evolve with time, therefore their properties also vary with time. This is also considered in this work.

[2]For all simulations in this work $\alpha_{\rm grav}$=0, since the disk masses are too low for gravitational instabilities.

Each time step the gas accreted by the planet is calculated and consequently the planet mass is increased as follows,

$$M_{\mathrm{p}}(t) = M_{\mathrm{p}}^{\mathrm{old}} + \dot{M} \cdot \delta t, \tag{4.2.3.1}$$

where $M_{\mathrm{p}}^{\mathrm{old}}$ denotes the planet's mass at the old time step. An efficiency factor as described in Sec. 4.2.1 is also included. As the planet accumulates mass the planet also grows in size. Its time-dependent radius R_{p} can be calculated by using the following expression,

$$R_{\mathrm{p}}(t) = \sqrt[3]{\frac{3M_{\mathrm{p}}(t)}{4\pi\rho_{\mathrm{p}}}}, \tag{4.2.3.2}$$

where ρ_{p} characterises the planet's density which is assumed in this work as $\rho_{\mathrm{p}} = 5\ \mathrm{g/cm}^3$. This value has been chosen since it is a mean density of the solar planets [3]. Exact values can be found, e.g. in Unsöld and Baschek (2005).

Since the planet accumulates mass over time the Hill radius also grows proportional to $M_{\mathrm{p}}^{1/3}$, $r_{\mathrm{H}} \propto \sqrt[3]{M_{\mathrm{p}}}$ (see Eq. 2.2.2.1). Therefore, the planet's gravitational impact radius increases, which leads to a wider impact range of the planet on the disk. This is also considered in the Gaussian distribution since the width of the distributed accreted material is defined by r_{H} (see Sec. 4.2.1).

The cumulative planetary mass (Eq. 4.2.3.1) also increases the mass accretion rate as shown in Eq. 2.2.3.1 because $\dot{M}$ depends on M_{p}.

The accretion luminosity is also a time-dependent variable since almost all factors of Eq.4.2.1.11 vary with time in the following way,

$$L_{\mathrm{acc,i}}(t) = -\frac{GM_p(t)\dot{M}_{\mathrm{i}}(t)}{r_H(t) - R_p(t)}. \tag{4.2.3.3}$$

$L_{\mathrm{acc,i}}(t)$ is updated alongside with the disk at every time step, which allows to simultaneously evolve the disk and the planet.

4.2.4 Assumptions and numerical impact on the disk

As mentioned in Sec 2.3 an evolving planet interacts with its enclosing disk. A planet which is embedded in the disk accretes material, which has to be accounted for in the equation of continuity (see Sec. 3.2), since this planetary accretion can alter the surface

[3] density of gas giants: $\approx 1.3\ \mathrm{g/cm}^3$
density of gas giant cores: $\approx 10\ \mathrm{g/cm}^3$
density of earth sized planets: $\approx 5\ \mathrm{g/cm}^3$

density and therefore impacts the evolution of the PPD. The extent of the impact evoked by this perturbation will be discussed in this work later on.
Similar to the removed mass in Eq. 4.1.0.1 there is an additional energy input at each grid point inside the Hill radius r_{H} around the planet's position due to the release of accretion luminosity, which enters the inner energy equation through an extra term.
The PPD is modelled as a 1+1D axisymmetric disk, hence the planet is modelled as a disk ring at the planet's position, which acts as a mass sink. The planet will not exert any gravitational back reaction on the disk. It is assumed that the only gravitational impact of the planet is that it accretes material. The disk is not influenced by any potential gravitationally induced perturbation.
As mentioned in Sec. 4.2.3 the properties of the sink term vary with time which is also implemented in the code.
Migration (see Sec. 2.3.2) of forming planets is not considered in this work. Additionally, due to the assumption of axisymmetry any non-axisymmetric effects of the planet on the disk like tidal arms or resonances are not considered in this work.

4.3 Evolution of a PPD without a sink term

To investigate the impact of an evolving planet on the evolution of a PPD, a model without any sink- or source-term is needed for comparison. Therefore this section discusses the evolution of a PPD during its lifetime without an additional sink term. Other losses, like disk winds or photoevaporation are not included in this work. This section gives a short overview of the PPD evolution, for more detailed information see the work of Steiner et al. (2021). The parameters which have been used for this model can be seen in Tab. 5.1.
By looking at the temporal evolution in Fig. 4.2 one can see the evolution of different disk properties over this time. Panel a) shows the disk's surface density Σ. The inner part of the disk, between $\sim 0.1 - 2$ AU is the densest region. This high density region represents a *dead zone* (see Sec. 2.1.4). Panel (b) shows the material flow $\dot{M}_{\mathrm{flux}}$ throughout the disk. The negative value corresponds to an inward directed flow. The grey dashed line indicates $\dot{M}_{\mathrm{flux}} = 0$. In panel (c) the radial velocity u_{r} of the material in the disk midplane is plotted. The negative value implies the inward movement of particles. The midplane gas temperature $T_{\mathrm{gas},0}$ is shown in panel (d). The scale height in units of the radius H_{p}/R can be seen in panel (e). The dead zone is characterised by a higher H_{p}/R relation in the inner disk part which flattens out over time. This is important for the planet's mass accretion rate and will be discussed in Sec. 5. Panel (f) shows the evolution of the

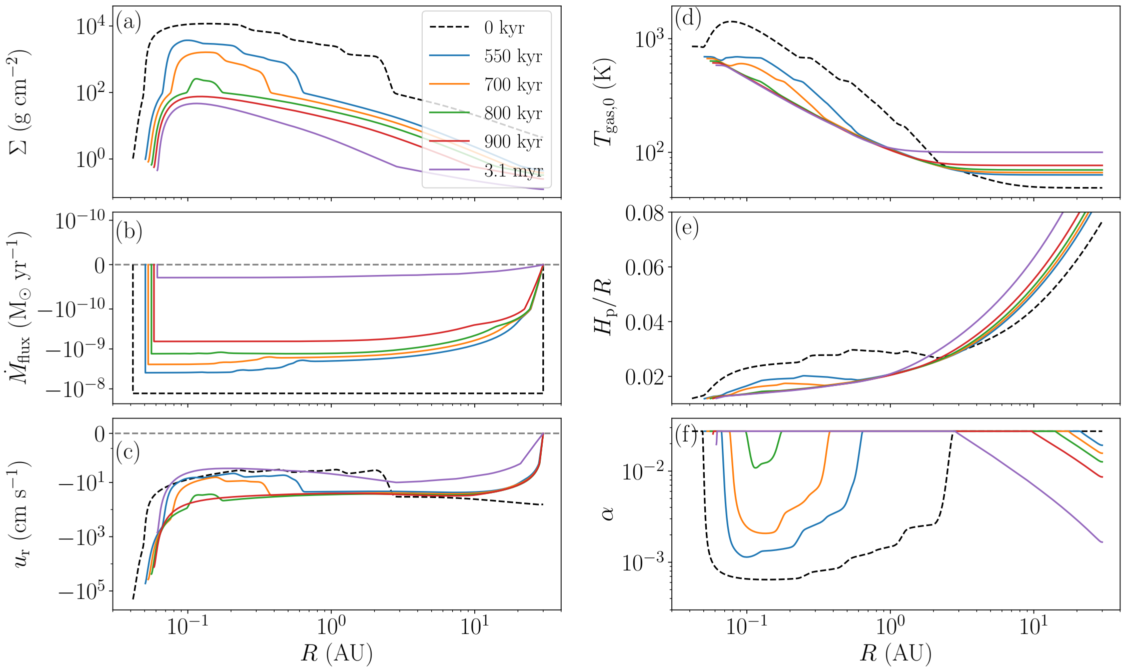

Figure 4.2: Different stages of the evolution of a protoplanetary disk. The panels (a)-(f) show the surface density Σ, the mass flux through the disk $\dot{M}_{\mathrm{flux}}$, the radial velocity u_{r}, the gas temperature at the midplane T_{gas}, the scale height H_{p} in units of the disk radius R and the α-parameter for different times during disk evolution, respectively. The black dashed line is the initial model. The diverse coloured lines correspond to different ages of the disk. The horizontal grey dashed lines in (b) and (c) show $\dot{M}_{\mathrm{flux}} = 0$ and $u_{\mathrm{r}} = 0$ value.

α-parameter. It also indicates the presence and disappearance of the dead zone. The black dashed line (initial model) shows a distinct region in the inner disk part with a considerably smaller α, which also clearly shows the radial extent of the dead zone. The disk becomes less dense due to accretion, hence the UV- and X-ray radiation is able to penetrate deeper into the disk. Thus viscosity increases and the disk becomes optically thin.

The surface density becomes less over time in the whole disk. This mass loss occurs due to accretion processes as discussed in Sec. 2.1.3.

A layered-viscosity model enables the disk to develop periodically occurring short-lived phases characterised by a massive increase in accretion, so-called accretion out-bursts (see Sec. 2.1.5), which affects the whole disk structure and its dynamics. Their effect on the disk structure can be seen in Fig. 4.3 and 4.4. A burst is characterised by a steep increase

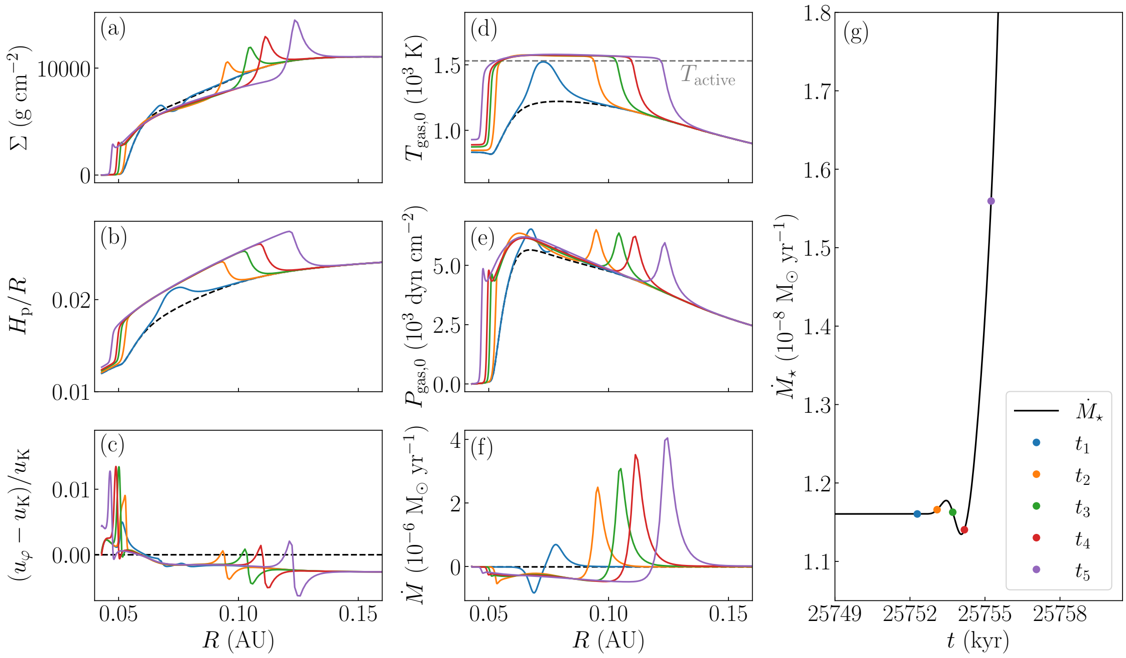

Figure 4.3: Different disk quantities during the onset of an outburst. Panel (a)-(f) show the change in surface density Σ, pressure scale height H_{p}/R, deviation of the angular frequency u_φ from the Keplerian velocity u_{K}, gas temperature $T_{\mathrm{gas},0}$ in the midplane, gas pressure $P_{\mathrm{gas},0}$ and of the rate of the radial mass transport $\dot{M}_{\mathrm{flux}}$, respectively. The different colours of the lines correspond to different times during this onset phase. The dashed black line depicts a quasi static model. In plot (d) the grey dashed line shows the activation temperature T_{active}. Panel (g) shows points in time as colour-coded dots corresponding to their respective colours in (a)-(f) during the onset phase..

of $\dot{M}_\star$ with a duration of a few ~ 10 yr (Reipurth, 1990). A thermal instability (TI) is triggered at ~ 0.075 AU (blue line in Fig. 4.3 (d)) due to a mass pile up in the inner disk region. The temperature there is raised to the value around T_{active} which triggers MRI. The redistribution of the piled up mass can be seen clearly in all of the panels (a)-(f) of Fig. 4.3. The different colours correspond to different moments of the onset (the correlated times can be seen in panel (g)). Thus, the inward and outward moving ionisation fronts are clearly depicted. The dashed black line shows a model during a quiescent phase for comparison. The higher temperature leads to a puffed up inner disk, which can be seen in panel (b) where the disk's scale height is plotted. The deviation from the Keplerian velocity u_{K} (Fig. 4.3 (c)) also shows the in- and outward moving

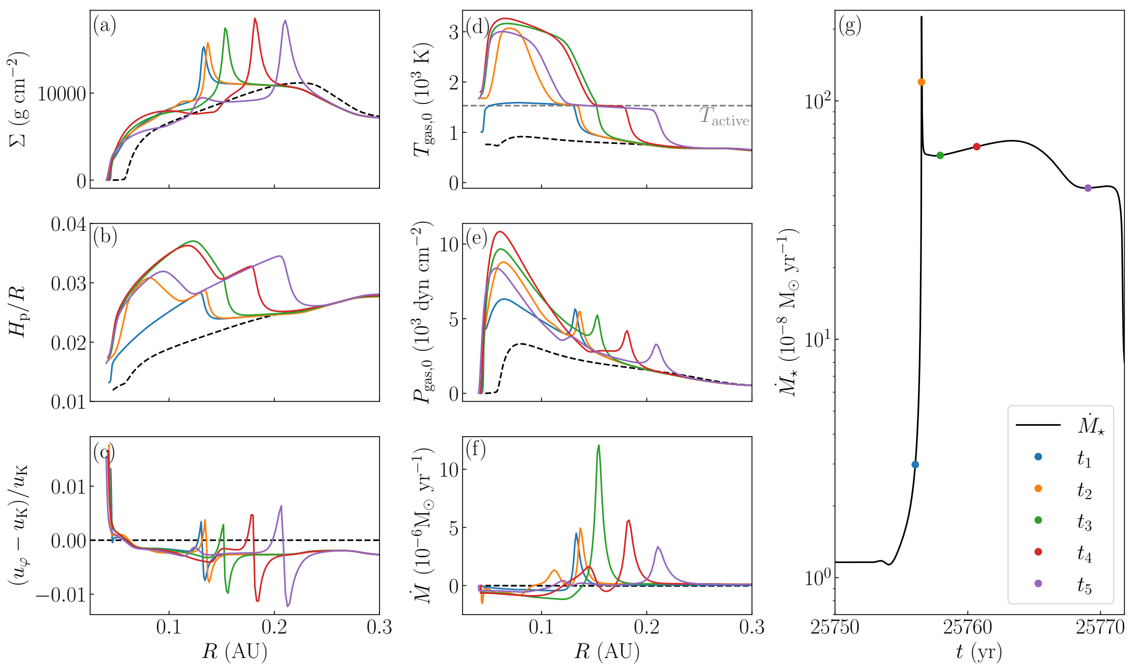

Figure 4.4: The plots show the same disk quantities as in Fig. 4.3, but for the burst phase. Panel (g) again shows the corresponding time slots of each plotted model.

wave and the resulting redistribution of angular momentum. The gas pressure in plot (e) pictures the pressure force acting in the disk. A positive pressure gradient corresponds to a inward directed pressure force. This corresponds to the mass flow plotted in panel (f), where a negative value coincide with an inward directed mass flow and a positive value with an outward one. Here, the movement of the ionisation fronts is clearly depicted. The increased pressure induced by the TI pushes the material in- and outwards, which leads to a more dynamic disk.

As soon as the inward directed ionisation front has reached the inner disk rim the material cannot be redistributed anymore. Thus, the temperature increases again and the outburst phase starts. This is pictured in Fig. 4.4, where each panel shows the same disk quantities as Fig. 4.3. During the outburst the gas in the inner disk is heated considerably, which can be seen in panel (d) of Fig. 4.4.This high temperature consequently yields a larger ionisation degree and therefore a higher magnetic coupling, which further leads to a higher effective α-viscosity. The dead zone heats up due to the high accretion luminosity and eventually leads to an increased effective viscosity in this region. This wave stops around 0.16 AU (green line), where the rearranged material is no longer able to trigger TI. Due

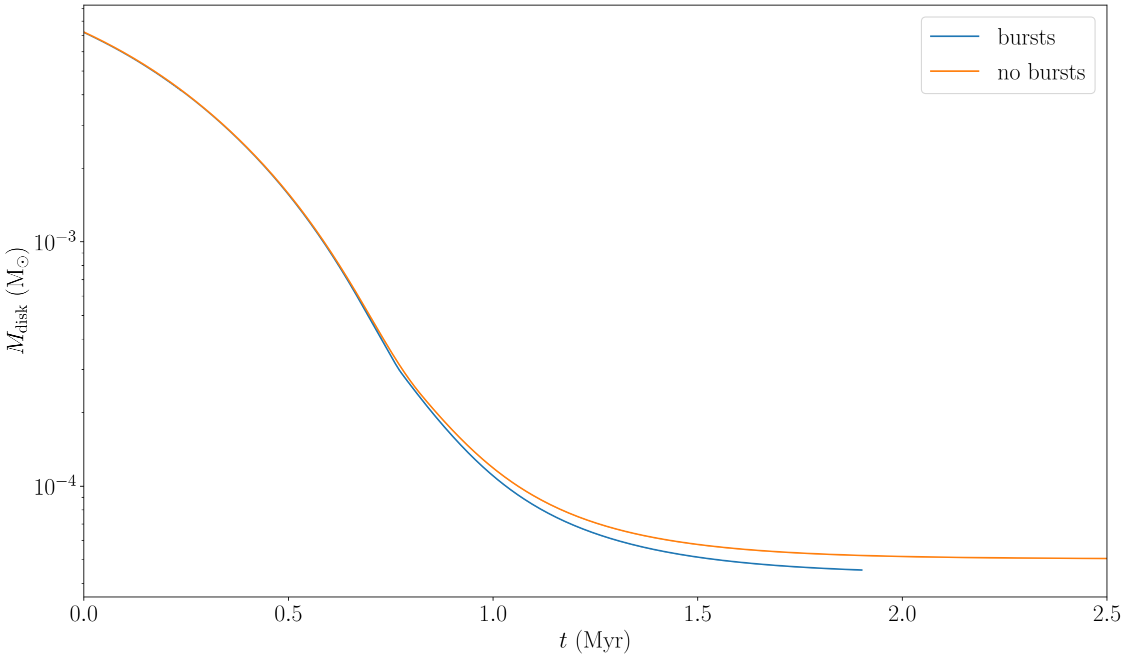

Figure 4.5: Comparison of the total mass evolution of the disk $M_{\rm disk}$ for a disk without episodic accretion events (orange) and a disk with outbursts (blue).

to the higher mass transport rate $\dot{M}$ in the inner disk compared to the outer disk, the inner region starts to deplete. The appearance of bursts stops when the gas drops below the activation temperature which occurs at an age of ~ 250 kyr for this simulation. In the disk's whole lifetime a few dozen bursts can emerge.

For further information about the disk evolution simulated by the TAPIR code see e.g. Ragossnig et al. (2020) or Steiner et al. (2021).

Fig. 4.5 shows the impact of episodic accretion events on the total disk mass $M_{\rm disk}$. The model with outbursts (blue line) shows a deviation for $M_{\rm disk}$ after ~ 500 kyr from the mass evolution of a disk without occurring outbursts, which indicates that the episodic accretion events cause a faster depletion of a PPD. This may have an impact on the accretion rate of a growing embedded planet, as it will be discussed in Sec. 5.4.

5 Results

In this section the simulation results of the impact of a sink term on the evolution of PPDs will be presented. The stellar and disk parameters which are used for these calculations are listed in Tab. 5.1. The impact of a constant sink term on the evolution of a protoplanetary disk will be discussed in Sec. 5.1, which serves as the fiducial model of this work. Sec. 5.2 contains the variation of parameters which includes the gap formation process in the dead zone and beyond it with various constant planetary mass accretion rates (Sec. 5.2.1) and a time-dependent Bondi accretion rate for simulating planetary growth (Sec. 5.2.2). Sec. 5.3 describes the evolution of a disk with episodic accretion events and the impact of an embedded planet on them. The differences in the results of active and quiescent disks will be discussed in Sec. 5.4.

$M_\star$ ($M_\odot$)	$L_\star$ ($L_\odot$)	$R_{\rm in}$ (AU)	$R_{\rm out}$ (AU)	$M_{\rm disk,init}$ ($M_\odot$)	$\dot{M}_{\rm disk,init}$ ($M_\odot {\rm yr}^{-1}$)	$\alpha_{\rm base}$	$\alpha_{\rm MRI}$	$T_{\rm active}$ (K)
1.0	0.5	$5.99{\cdot}10^{-2}$	30	0.007	$1.3{\cdot}10^{-8}$	$4.12{\cdot}10^{-4}$	$2.7{\cdot}10^{-2}$	1530

Table 5.1: The parameters of the disk and the star of the initial PPD model.

5.1 Constant accretion rate (fiducial model)

To investigate the effect of a mass extraction caused by a planet on the long-term evolution of a PPD, a planet with a constant mass accretion rate of $\dot{M}_{\rm p} = 1 \cdot 10^{-3}$ $\mathrm{M}_\oplus$/yr at an orbital distance of $a = 1.0$ AU has been simulated with *TAPIR*. Fig. 5.1 shows the same quantities as Fig. 4.2, but for a PPD with an embedded planet. The impact of constant mass extraction can be seen in the surface density evolution in panel (a), where a gap starts to develop after $\sim$ 570kyr (green line), visible as a low density region. This opening happens after the dead zone has vanished. Panel (b) shows the influence of a sink cell on the radial mass transport rate $\dot{M}_{\rm flux}$ over the whole radial disk extent. This impact is visible earlier (blue line) than the dip in Σ (green line), which can be

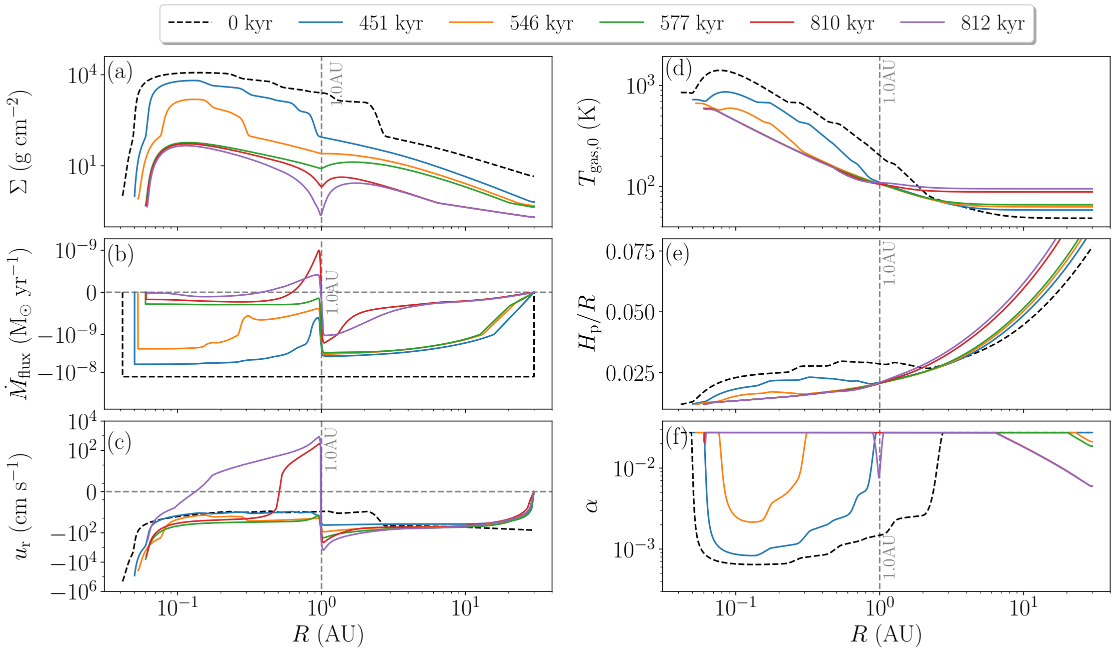

Figure 5.1: The evolution of surface density Σ (panel (a)), mass flux through the disk $\dot{M}_{\rm flux}$ (panel (b)), radial velocity $u_{\rm r}$ (panel (c)), gas temperature at the midplane $T_{\rm gas,0}$ (panel (d)), scale height in units of orbital distance $H_{\rm p}/R$ (panel (e)) and α-parameter (panel (f)) over time with a constant sink term of $\dot{M}_{\rm p}$=$1 \cdot 10^{-3}$ $\mathrm{M}_\oplus$/yr located at an orbital distance of $a = 1.0$ AU. The vertical grey dashed line indicates the position of the planet, and the black dashed line depicts the initial model. The horizontal grey dashed lines in panels (b) and (c) show $\dot{M}_{\rm flux} = 0$ and $u_{\rm r} = 0$ value.

explained by the disturbed angular momentum transport throughout the disk. Before the occurrence of the dip in Σ is noticeable, $\dot{M}_{\rm flux}$ radially inside of the planet becomes smaller until it eventually changes sign and the mass transport for $r < r_{\rm p}$ starts to flow outwards in the vicinity of the planetary location, whereas $\dot{M}_{\rm flux}$ in the outer disk region is almost unchanged. This behaviour is caused by a beginning disconnection of the inner and the outer disk (which will be discussed furthermore in Sec. 5.2) and the correlated disturbed angular momentum transport. As soon as $\dot{M}$ changes sign at the position of the planet (red line at 1.0 AU), a dip evolves in Σ. This sign change of $\dot{M}_{\rm flux}$ is caused by a growing pressure gradient $|dP/dr|$ generated by the planetary mass extraction. Due to steep pressure gradients at the gap boundaries the gas is pushed outwards and inwards at the inner and outer gap boundary, respectively, hence, the pressure gradient

is working against the gap opening[1].Additionally, the exchange of angular momentum between gas particles is less efficient, as one can see by the inward movement of the location of the $\dot{M}_{\mathrm{flux}}$-sign change over time (red and purple line in panel (b)). This is caused by the drain of the inner disk due to accretion and therefore the gap becoming more pronounced in radial direction. This more expanded gap causes a less dense area in this region and the therefore increasing pressure gradient moves inward contemporaneous to the decreasing surface density. This increasing inward moving $|dP/dr|$ pushes material outward at smaller orbital distances over time and the ineffective angular momentum transport in the low density regions leads to the inward moving $\dot{M}_{\mathrm{flux}}$-sign change.
Panel (c) depicts the radial velocity u_{r} of the material. A similar behaviour to $\dot{M}_{\mathrm{flux}}$ is visible, i.e. a perturbation can be seen in u_{r} before a dip in Σ is noticeable. As soon as $\dot{M}_{\mathrm{flux}}$ changes its sign, u_{r} changes its too.
No distinct impact of the gap on the midplane temperature $T_{\mathrm{gas,0}}$ (panel (d)) and therefore the scale height in units of orbital distance H_{p}/R (panel (e)) is noticeable, since the impact of the gap is to small. In later simulations with higher accretion rates impacts on these parameters will be explicitly visible (cf. Sec. 5.2.2).
As soon as a gap has developed a change in the α-parameter can also be seen (panel (f), purple line).

5.2 Parameter variation

This section treats the effect of varying the planetary mass extraction parameters. In Sec. 5.2.1 the impact of various orbital distances and different constant mass accretion rates will be discussed. Sec. 5.2.2 shows the results of a time-depended accretion rate in form of the Bondi accretion.

5.2.1 Variation of constant mass accretion rate and orbital distance

Variation of constant mass accretion rate

The impact of two different constant accretion rates of $\dot{M}_{\mathrm{p}}=5\cdot10^{-3}$ $\mathrm{M}_{\oplus}$/yr and $\dot{M}_{\mathrm{p}}=5\cdot10^{-4}$ $\mathrm{M}_{\oplus}$/yr, induced by a planet, each located at $a = 1.0$ AU can be seen in Fig. 5.2 in panel (a)-(c) and panel (d)-(f), respectively.

Note that the evolution time-spans are different for these two models. The simulation with a higher $\dot{M}_{\mathrm{p}}$ shows impacts at younger disk ages than the simulation with a lower

[1]This will be discussed further on in Sec. 5.2.2

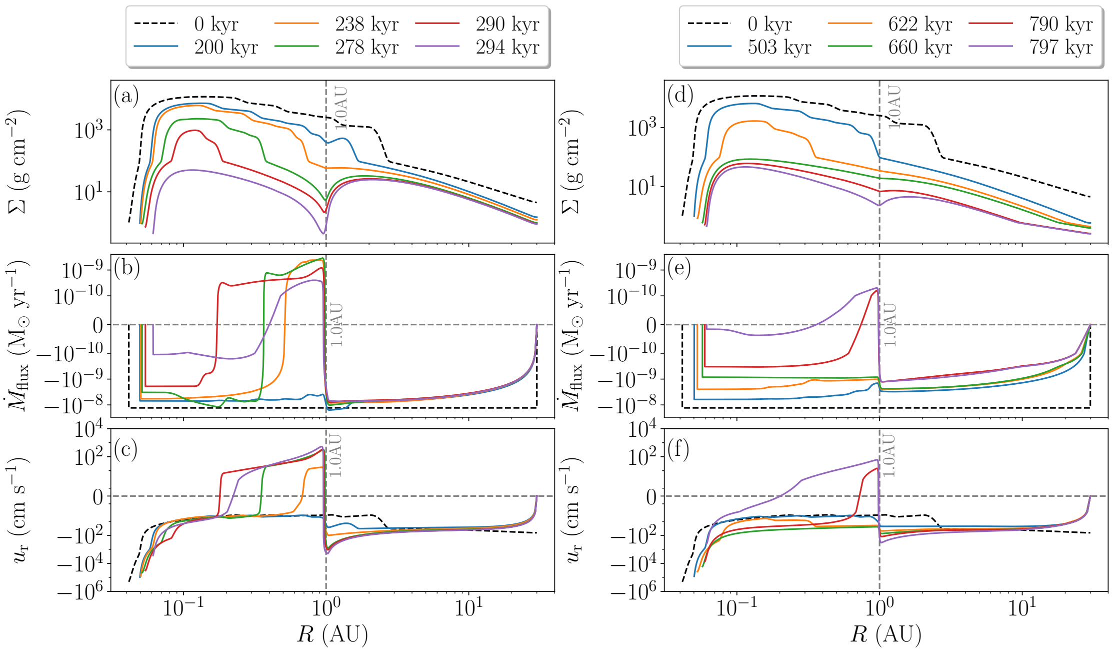

Figure 5.2: The evolution of surface density Σ, mass transport rate $\dot{M}_{\text{flux}}$ and radial velocity u_{r} for the different planetary mass accretion rates of $\dot{M}_{\text{p}}=5 \cdot 10^{-3}\text{M}_{\oplus}/\text{yr}$ (panel (a)-(c)) and $\dot{M}_{\text{p}}=5 \cdot 10^{-4}\text{M}_{\oplus}/\text{yr}$ (panel (d)-(f)), respectively. They are located both at an orbital distance of $a = 1.0$ AU

$\dot{M}_{\text{p}}$, hence a gap forms at earlier stages if $\dot{M}_{\text{p}}$ is higher (see panel (a)). A first dip in Σ is visible at ~ 200 kyr for the higher planetary accretion rate, whereas panel (d) shows a slight perturbation in Σ after over 700 kyr for the lower $\dot{M}_{\text{p,5e}-4}$. This dip is only visible when the disk has nearly been emptied. Only then the surface density is sufficiently low, that the mass transport rate also decreases sufficiently in order for $\dot{M}_{\text{p}} > \dot{M}_{\text{flux}}$, as can be seen in panels (b) and (e). There the plotted mass transport rate shows impacts on the PPD evolution in different orders of magnitude for the simulations. $\dot{M}_{\text{p,5e}-3}$ causes a clearly visible outward directed flow in panel (b) at the inner gap rim. Also visible is that $\dot{M}_{\text{flux}}$ in panel (b) is higher than in panel (e) by a factor of 10 at the inner gap rim. Additionally, the impact on $\dot{M}_{\text{flux}}$ increases for a larger planetary accretion rate, which can be seen e.g. for the red line where the change in sign extends over one order of magnitude in radial direction (panel (b)), whereas panel (e) shows this sign change only for the outermost region of the inner disk.

Panels (c) and (f), which depict the evolution of u_{r}, also show significant differences, especially panel (f) indicates only a small perturbation at 1.0 AU for the first 700 kyr of

the PPD's lifetime, whereas panel (c) depicts the impact on the disk dynamics by a sign change of the radial velocity already in early evolutionary stages (orange line). Similar to $\dot{M}_{\mathrm{flux}}$, panel (c) shows a more radial extended impact region than panel (f).
Comparing these results to the fiducial model one can see that the magnitude of the impact strongly depends on the value of the planetary accretion rate. The higher $\dot{M}_{\mathrm{p}}$, the larger is the effect on the disk evolution. And especially, if the gap formation takes place after the dead zone has vanished, the impact on the disk behaviour and evolution is small compared to a gap formation scenario in the dead zone happening in the earliest disk ages as already implied in Sec. 5.1. This is more distinct in Sec. 5.2.2.

Variation of orbital distance

This section investigates the influence of the position a of the mass extraction in the PPD. Since the surface density and the mass transport rate seem to have an impact on the effects generated by the gap formation (as described above and shown by Stökl et al. (2016)), the impact of a planet located in the high density region (dead zone) will be investigated. Fig. 5.3 shows the evolution of surface density Σ over time with a sink term of $\dot{M}_{\mathrm{p}} = 1 \cdot 10^{-3}$ $\mathrm{M}_{\oplus}/\mathrm{yr}$ located at orbital distances of $a = 0.5$ AU (panel (a)), 1.0 AU (panel (c)), 3.0 AU (panel (b)) and 7.0 AU (panel (d)).
Note that there is no distinct developed gap visible for small a. This different gap depths emerge from the different $\dot{M}_{\mathrm{flux}}$-values at the various orbital distances, because a planet located farther out is able to create a gap earlier, since its constant mass accretion rate can exceed the lower $\dot{M}_{\mathrm{flux}}$-value of the outer disk parts more easy.
Although gap formation eventually disconnects the outer disk from the inner disk, the latter is still able to accrete its material onto the star, but material from beyond the sink cell is not able to replenish the accreted material anymore. The gap prevents the continuing mass support of the sink term and the inner disk, which also leads to a decrease of $\dot{M}_{\mathrm{p}}$. This process splits the disk into two separate disk parts, which can be seen in Fig. 5.3 (b) represented by the gap, and can only become clearly visible for large enough planetary accretion rates (see e.g. Fig. 5.7 (a) and (b)). This separation decouples the inner disk from the outer one, which affects the mass transport and angular momentum transport significantly. This disconnection does not evolve distinctly in the fiducial model since the planetary accretion rate in this simulation is to small to induce this effect. The disk inside the gap of Fig. 5.3 (b) accretes largely unaltered onto the star, whereas the outer disk does not change distinctly, since the outer disk is not able to lose angular momentum due to accretion anymore, which leads to pile-up of mass at the outer rim of

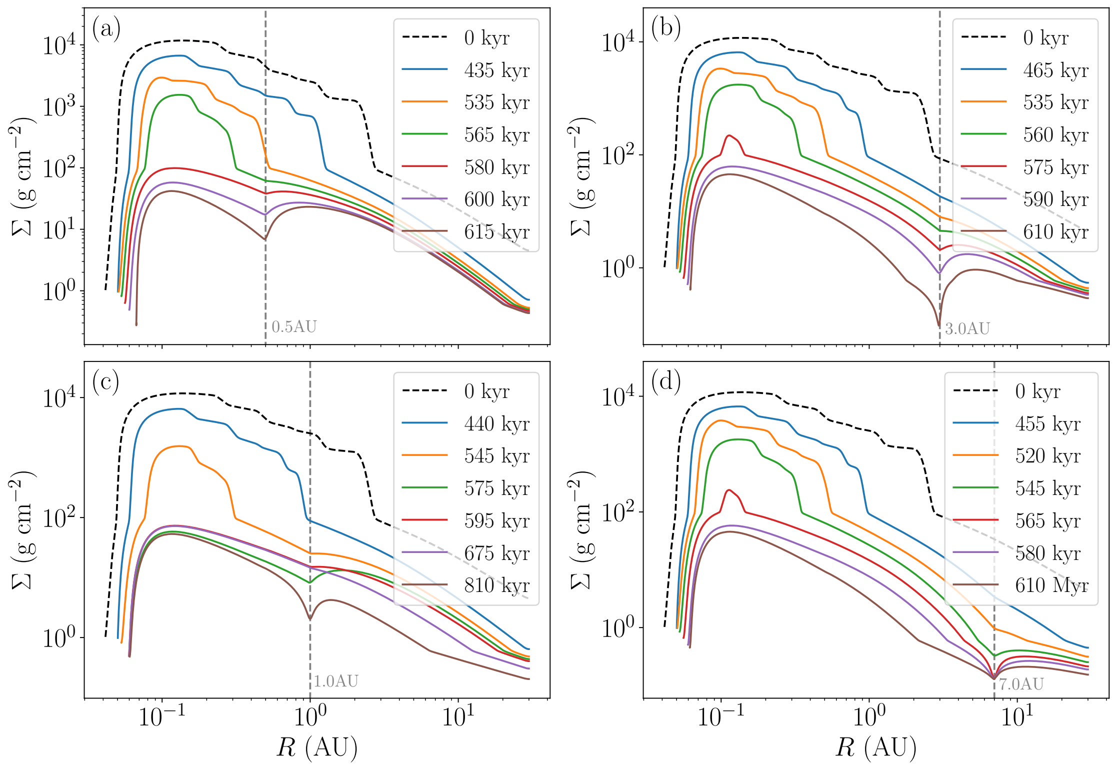

Figure 5.3: The evolution of the surface density Σ over time with constant sink terms of $\dot{M}_{\rm p} = 1 \cdot 10^{-3}$ $M_\oplus$/yr placed at orbital distances a of (a) 0.5 AU, (c) 1.0 AU, (b) 3.0 AU and (d) 7.0 AU. The black dashed line is the initial model and the coloured lines depicts the temporal surface density evolution. The vertical grey dashed line indicates the position of the planet.

the gap. Only on the viscous time scale it is possible for the outer disk to lose material to the gap or the inner disk. This causes the existence of a low $\dot{M}_\star$ combined with a high $M_{\rm disk}$, as it can be seen later in Fig. 5.5.

The effect of a planet being located in the dead zone or beyond it can be seen in Fig.5.4, where a planet with $\dot{M}_{\rm p} = 1 \cdot 10^{-3}$ extracts material at the orbital distance of a =0.5AU (panel (a)-(c)) and $a = 7.0$ AU (panel (d)-(f)). One can see that this planet is only able to open a gap at higher orbital distances, since $\dot{M}_{\rm flux}$ at $a = 7.0$ AU is small enough to be exceeded by $\dot{M}_{\rm p}$ (panel (e) blue line and older). A perturbation in $\dot{M}_{\rm flux}$ is also visible for the planet at a =0.5AU in panel (b) but it is not large enough to change sign and therefore no gap emerges.

Close to the outer gap boundary the mass transport rate has a very small local peak in (e) (red line), which is due to the combined effect of both gas pressure pushing the

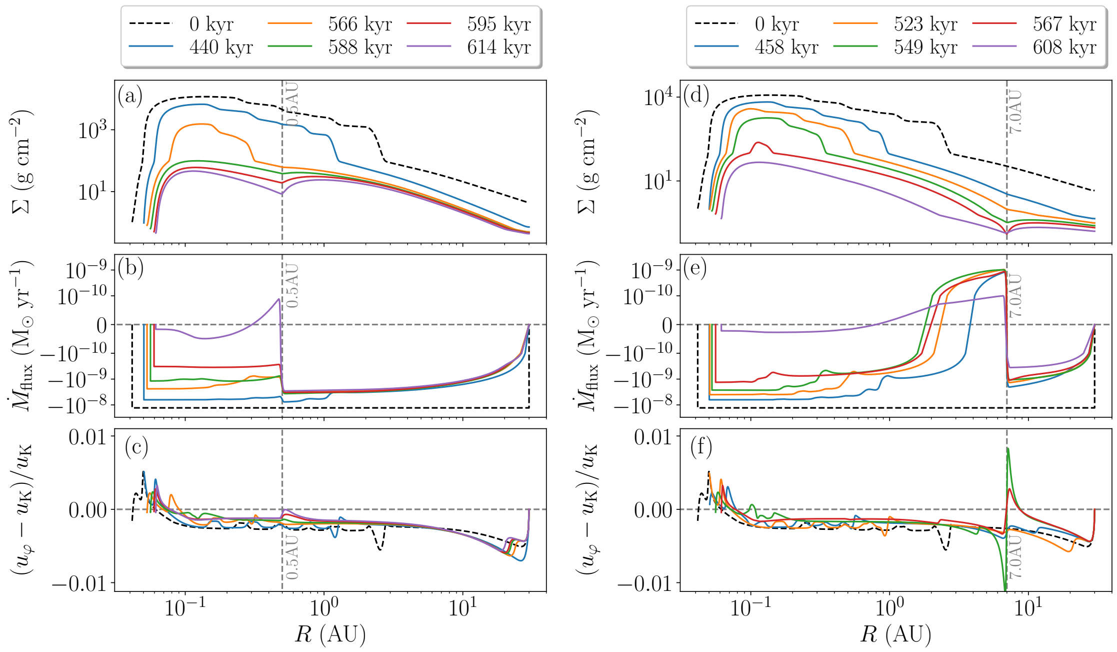

Figure 5.4: Evolution of surface density Σ, mass transport rate $\dot{M}_{\mathrm{flux}}$ and deviation of the angular velocity u_φ from the Keplerian velocity u_K for $\dot{M}_\mathrm{p}{=}1 \cdot 10^{-3}\mathrm{M}_\oplus/\mathrm{yr}$ at orbital distances of $a = 0.5$ AU (panel (a)-(c)) and $a = 7.0$ AU (panel (d)-(f)). Each snapshot in the middle and lower panel corresponds to the same colour in the Σ-profile in the upper panel.

gas inwards and the low column density in the gap, resulting in a net outward-directed angular momentum transport.

As already discussed, the point where $\dot{M}_{\mathrm{flux}}$ gets positive moves inward over time[2], which also applies for this model, which can be seen in panel (e) and Fig. 5.2 (b),(e). This shows again that after a gap has developed, the disk inside the gap accretes onto the star, whereas the outer disk is not able to interact unperturbed with the inner disk.

For the planet at 7.0 AU there is a Sub-Keplerian and Super-Keplerian peak for the inner and outer boundary, respectively, in the vicinity of the gap boundaries, which are due to the conservation of angular momentum J and an increased pressure gradient. Since no distinct gap forms for the planet at $a = 0.5$ AU, the pressure gradient there does not change significantly, hence $(u_\varphi - u_\mathrm{K})/u_\mathrm{K}$ shows only small perturbations.

Again, a perturbation in $\dot{M}_{\mathrm{flux}}$ and $(u_\varphi - u_\mathrm{K})/u_\mathrm{K}$ is visible before a dip in Σ can be seen for both cases in Fig. 5.4.

[2]There also exists cases where this point can move outwards again. This will be discussed in Sec. 5.2.2.

Combining parameter variations

As discussed in Sec. 2.1.4 the dead zone is a region in the disk with high surface density and a low viscosity. As we saw above, these characteristics can have an impact on the formation of a gap. By placing a constant sink term in the dead zone the disk can get perturbed at that location, but the planetary mass accretion rate needs to reach a certain value to create a gap. This value depends on the disk parameters, especially the viscosity combined with the mass transport rate and the surface density. The higher the planetary mass accretion rate the higher the impact on the disk evolution.
Simulations with different constant mass accretion rates at different orbital distances a from the star were made to analyse their impacts on the structure and evolution of the disk.
In Fig. 5.5 the impact of different sink terms on the total disk mass M_{disk} (panel (a)) and the accretion rate onto the star $\dot{M}_\star$ (panel (b)) are shown. In panel (a) the difference between the disk without any sink term and the models with $\dot{M}_{\text{p}} = 1 \cdot 10^{-7}$ $\text{M}_\oplus$/yr is barely visible. This is caused by the small planetary accretion rate. Compared to the total disk mass, this sink term extracts a negligible amount of material from the disk. A difference can only be seen in the inlay plot, where M_{disk} only differs by a maximum factor of 10^{-2} for the different models. A larger disparity is noticeable in panel (b), where the accretion rate on the star starts to diverge from the model without a sink term at around ~ 2 Myr for $\dot{M}_{\text{p}} = 1 \cdot 10^{-7}$ $\text{M}_\oplus$/yr. This deviation is caused by the diminishment of the total disk mass due to the planetary mass extraction, so at the end of the disk's lifetime there is less material available which can be accreted onto the star. Though, the is no distinction between the different positions of this sink term visible in $\dot{M}_\star$. This is due to the fact that the annulus from which the sink cell receives its mass is able to replenish the gap, because $\dot{M}_{\text{flux}} > \dot{M}_{\text{p}}$ for all radial planet positions. This means that the variation of a does not have a visible impact on the disk dynamics for this mass accretion rate. The sink term extracts the same amount of mass at each simulated orbital distance.
The impact of a planet on the evolution of the disk mass becomes visible for planetary accretion rates of $\dot{M}_{\text{p}} = 1 \cdot 10^{-5}$ $\text{M}_\oplus$/yr and higher. Here the mass extraction is big enough to see a difference compared to the model without a sink term. Even a disparity for the different orbital distances can be seen in this plot. This radius-dependent behaviour arises from the higher Σ (and therefore also different $\dot{M}_{\text{flux}}$ and α) in the inner disk, which allows the planet to draw material from the surrounding disk annuli over a more extended period of time. The annulus for sink cells farther out is emptied more quickly,

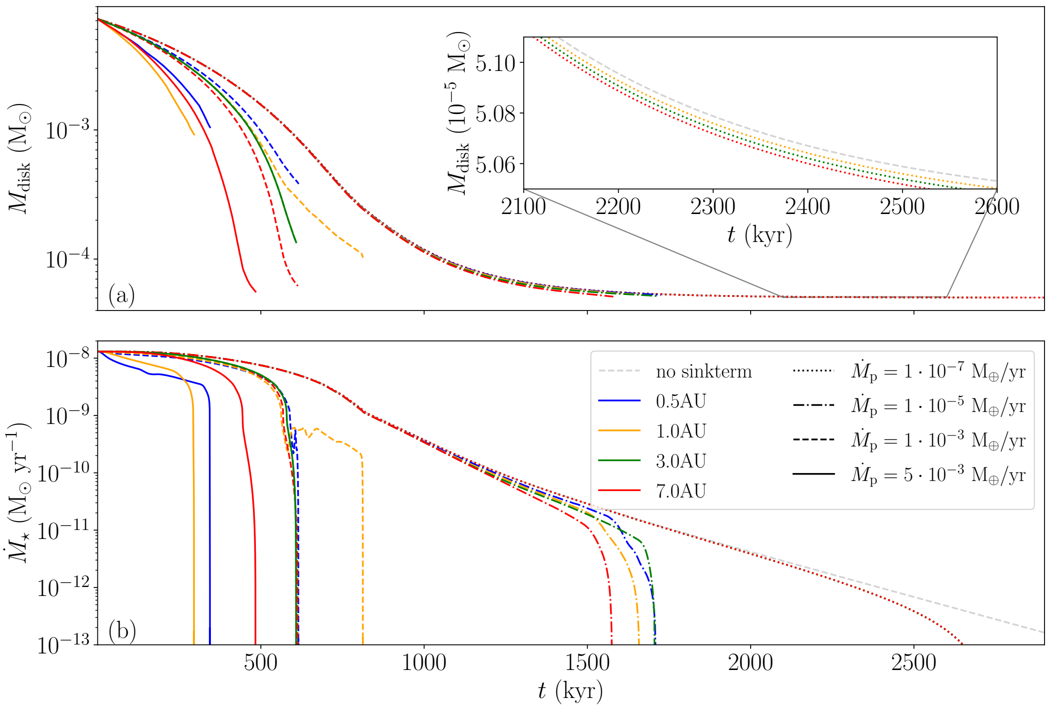

Figure 5.5: Plot (a) shows the evolution of the disk mass $M_{\rm disk}$ over time with different constant sink terms at various orbital distances a of 0.5-7.0 AU. In the lower panel the accretion rate onto the star for the same $\dot{M}_{\rm p}$ and a as in the left panel are plotted. Dotted, dash-dotted, dashed and solid lines describe $\dot{M}_{\rm p} = 1 \cdot 10^{-7}, 1 \cdot 10^{-5}$, $1 \cdot 10^{-3}$ and $5 \cdot 10^{-3}$ $\mathrm{M}_\oplus$/yr, respectively. The colours blue, yellow, green and red correspond to the orbital distance of 0.5, 1.0, 3.0 and 7.0 AU, respectively. For comparison the grey dashed line is the disk evolution without any sink term. The inlay plot shows a zoom-in view of the region between 2.1-2.6 Myr for $M_{\rm disk}$.

since there the lower mass transport rate hinders the replenishment of this area, which then eventually leads to the formation of a gap. In the lower plot of Fig. 5.5 one can see that a sink term of $1 \cdot 10^{-3}$ $\mathrm{M}_\oplus$/yr with smaller orbital distances has larger impacts on $\dot{M}_\star$. It is clearly visible that a sink cell has a large impact if it is located inside the dead zone (yellow and blue dashed line). Thus, this mass extraction has a distinct impact on the disk dynamics. A similar behaviour can be seen for the $5 \cdot 10^{-3}$ $\mathrm{M}_\oplus$/yr sink terms (solid lines in Fig. 5.5). The higher the accretion rate of the sink term, the faster a change in $M_{\rm disk}$ can be seen, since more mass is extracted from the disk in shorter time-spans. The models at 3.0 AU and 7.0 AU, which are lying beyond the dead zone, have a higher accretion rate onto the star than those which are placed inside the dead zone. This significant impact on $\dot{M}_*$ caused by the different $\dot{M}_\mathrm{p}$ depends strongly on the surface density structure. So, as one can see in Fig. 5.5 the smaller $\dot{M}_\mathrm{p}$ gets and the smaller the orbital distance, the smaller is the effect on M_disk and $\dot{M}_\star$ compared to sink terms outside of the dead zone. However, if $\dot{M}_\mathrm{p}$ exceeds a certain upper limit ($\dot{M}_\mathrm{p} = 5 \cdot 10^{-3}$ $\mathrm{M}_\oplus$/yr for these simulations), it is able to form a gap fast, therefore the impact on the disk evolution for planets located inside the dead zone becomes larger than for those in the outer disk region. These high planetary accretion rates at small orbital distances can cause low $\dot{M}_\star$ with high M_disk, since these planets form gaps early during the disk evolution, which separates the disk into two parts at young disk ages. The outer disk, which still contains a large amount of material, is not able to transport its mass to the star anymore due to the disturbed mass transport rate, therefore M_disk remains higher whereas $\dot{M}_\star$ drops abruptly after the inner disk has emptied.

Summarised, the formation process is indeed similar for all $\dot{M}_\mathrm{p}$ but the magnitude of the impact on the PPD evolution differs depending on the properties of the sink term and thereby if it is able to open a gap or not.

In Fig. 5.6 the formation of gaps caused by different constant mass accretion rates of $\dot{M}_\mathrm{p} = 5 \cdot 10^{-4}$ (blue), $1 \cdot 10^{-3}$ (red) and $5 \cdot 10^{-3}$ $\mathrm{M}_\oplus$/yr (yellow) at orbital distances of a =0.5, 1.0, 3.0, 5.0 and 7.0 AU are shown. No gap formation was possible for $\dot{M}_\mathrm{p} = 5 \cdot 10^{-4} \mathrm{M}_\oplus$/yr at a = 0.5, 1.0 and 3.0 AU. Also $\dot{M}_\mathrm{p} = 1 \cdot 10^{-3}$ $\mathrm{M}_\oplus$/yr at a =0.5AU shows no gap formation. One can see that the formation of a gap from the first visible Σ-deviation to a fully developed gap takes a time of a few dozen up to 200 kyr, as shown exemplarily for $5 \cdot 10^{-3}$ $\mathrm{M}_\oplus$/yr at 5.0 AU where the gap development takes about 71 kyr. Those sink terms which are lying within the dead zone ($R < 2.0$ AU) and show gap formation, create gaps earlier than those with a planet sitting in the disk on the far side of the dead zone. Low-mass planetary cores cannot open a gap at every radial distance from the star. In the cases where a gap forms, this formation happens during older disk ages, compared to the cases of larger planetary core masses (see red markers in Fig. 5.6), since under these conditions $\dot{M}_\mathrm{flux}$ is small enough for this planet to be out-ruled. The farther out a sink term lies the easier it can form a gap. The higher Σ and $\dot{M}_\mathrm{flux}$ in the inner disk region prevents the formation of gaps for small $\dot{M}_\mathrm{p}$. Hence, gaps can only form in this region if $\dot{M}_\mathrm{p}$ is high enough.

5.2.2 Time dependent accretion scheme - Bondi accretion

In this section the impact of a planet during the run-away phase will be discussed. The sink term has the form of the Bondi-accretion as discussed in Sec. 4.2.1, which models a

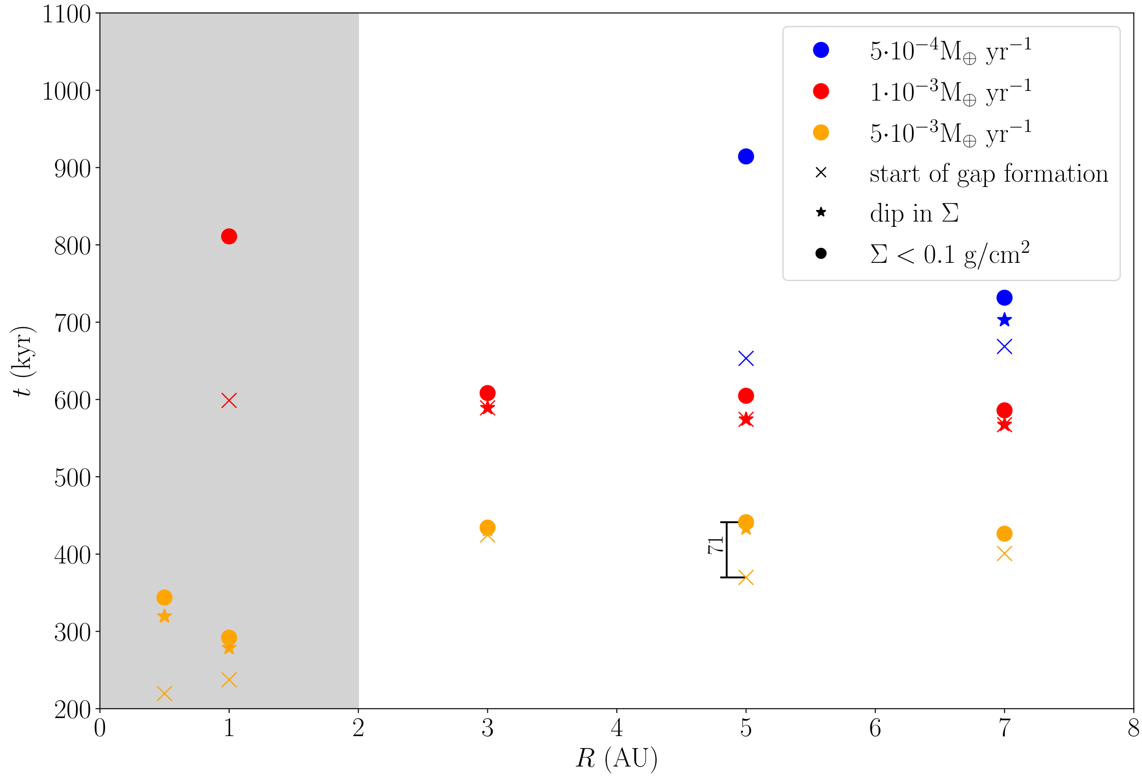

Figure 5.6: Time of the formation of a gap for constant mass accretion rates of $\dot{M}_\mathrm{p} = 5 \cdot 10^{-4}$ (blue), $1 \cdot 10^{-3}$ (red) and $5 \cdot 10^{-3}$ $\mathrm{M}_\oplus$/yr (yellow) at orbital distances of $a = 0.5$, 1.0, 3.0, 5.0 and 7.0 AU. The different markers correspond to a small deviation from the undisturbed Σ-profile ($\times$), a clearly visible dip in Σ ($\star$) and a fully developed gap ($\bullet$). The grey region depicts the dead zone.

giant planet growing through rapid accretion of its surrounding material. The sink term's accretion rate depends on the mass of the planet M_p, the sound speed c_s and the density ρ of the disk at the planet's orbital distance a as can be seen in Eq. 2.2.3.1. Thus, it also depends on the disk properties, which allows $\dot{M}_\mathrm{p}$ to react to the conditions in the PPD. Likewise, $\dot{M}_\mathrm{p}$ also increases due to the planet growth.

As one can see in Fig. 5.7 the evolution of the surface density profile can be quite different depending on the location of the accreting planet, which has an initial mass of $M_\mathrm{p,init} = 0.1$ $\mathrm{M}_\oplus$ in these simulations. The planets at $a = 0.7$ and 1.0 AU (panels (a) and (b)) are embedded in the dead zone, the other sink terms at $a = 3.0$, 5.0 and 7.0 AU are located beyond it. The two outermost planets are not able to form a gap, as shown in panel (e) and (f). The behaviour of the Σ-profile evolution seems to depend strongly

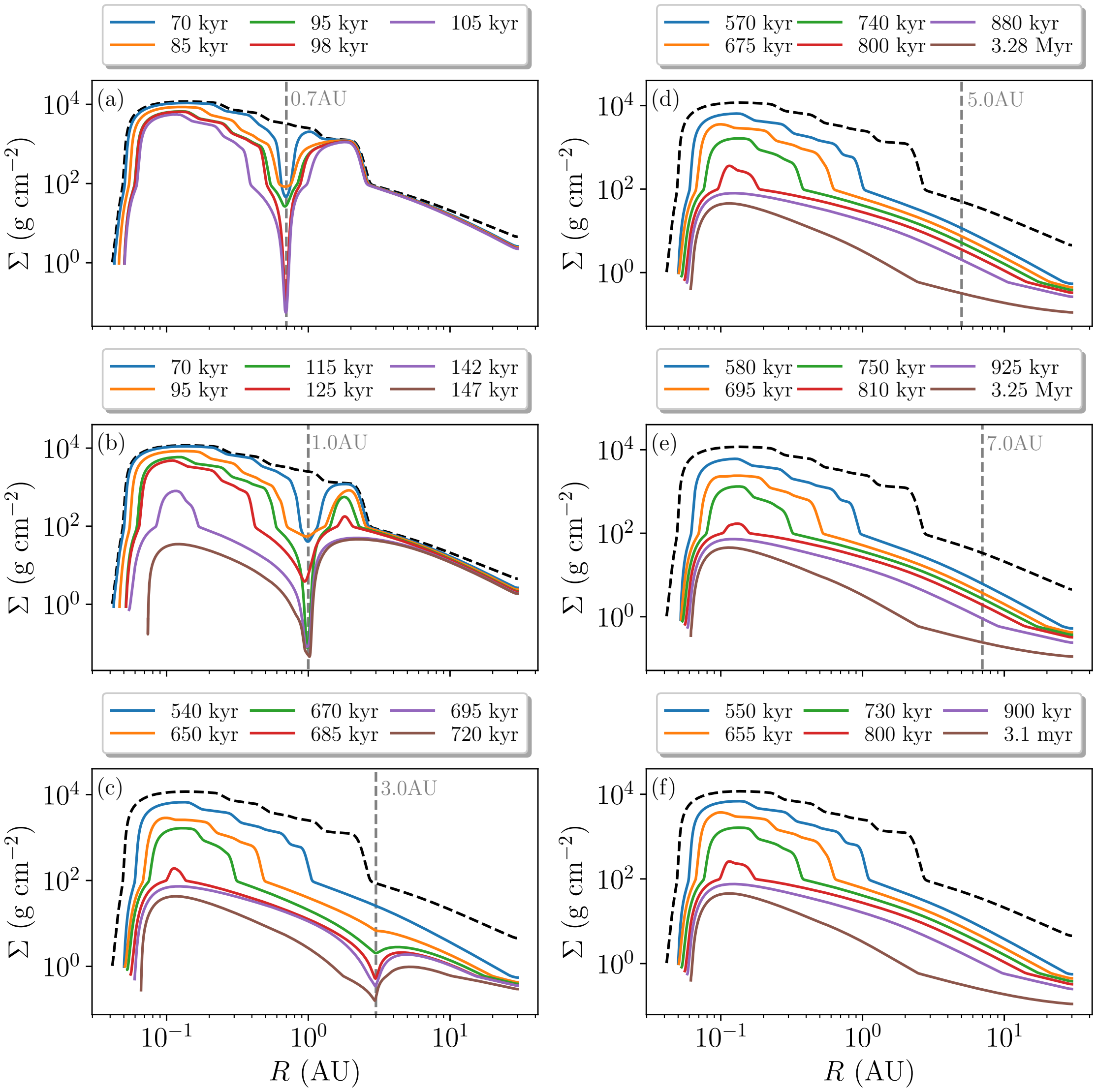

Figure 5.7: Evolution of column density Σ-profile for a PPD with evolving planets with an initial mass of $M_{\mathrm{p,init}} = 0.1\ \mathrm{M}_\oplus$ at $a = 0.7$, 1.0, 3.0, 5.0 and 7.0 AU (panel (a)-(e)). For comparison the evolution of an undisturbed disk is in panel (f). Dashed vertical lines indicate the location of the planet.

on whether the planet is located inside or outside the dead zone. This dependency here seems to be stronger than for the constant accretion rates, which originates from the high density in the inner disk regions and the direct proportionality of $\dot{M}_\mathrm{p}$ to ρ for the Bondi accretion. Due to this higher density the planet can grow fast and therefore also increases

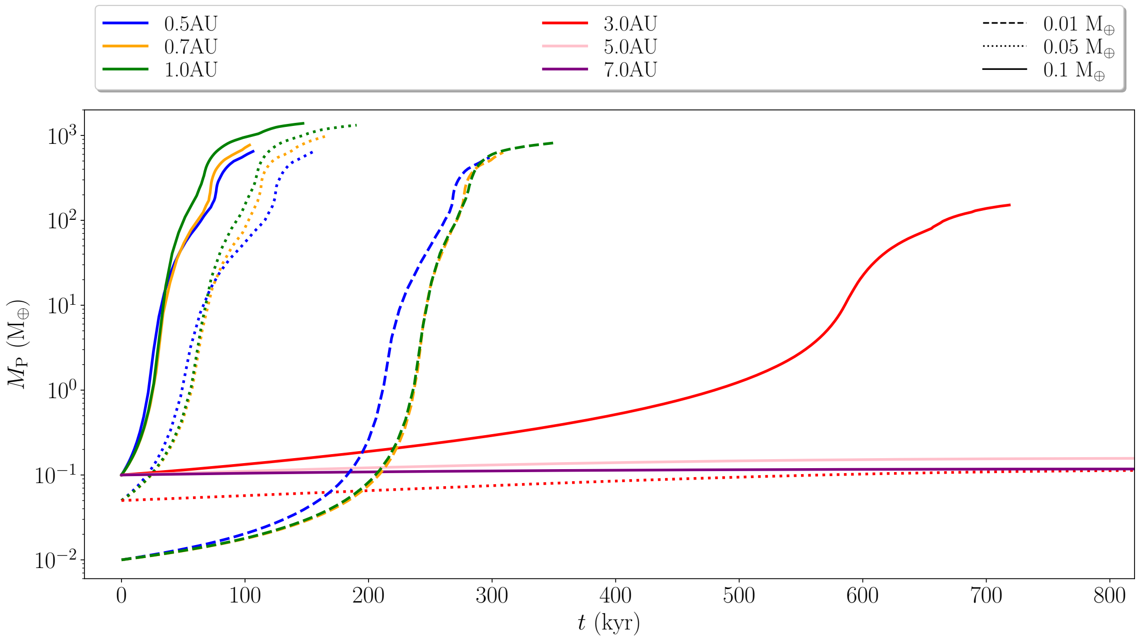

Figure 5.8: Evolution of the planet mass for $M_{\rm p,init} = 0.01$, 0.05 and 0.1 $M_\oplus$, which are pictured by the dashed, dotted and solid lines respectively. They are located at different orbital distance between $a = 0.5$ AU - 7.0 AU. The same colour corresponds to the same a.

its accretion rate quickly. Therefore the formation of a gap is faster and more distinct for planets closer to the star, even for small initial core masses as $M_{\rm p,init} = 0.01$ $\mathrm{M}_\oplus$. Similar to Sec. 5.2, the inner disk decouples from the outer disk after a gap has formed and empties unaffected. This effect occurs earlier in the disk lifetime for time-dependent planets close to the star than for constant sink terms due to the high $\dot{M}_{\rm p}$. No visible impact on the PPD evolution can be seen in this plot for the models without any gap formation.

The corresponding evolution of the planet mass can be found in Fig. 5.8, where the mass growth of planets with different initial masses of $M_{\rm p,init} = 0.01$, 0.05 and 0.1 $\mathrm{M}_\oplus$ (dashed, dotted and solid, respectively) at various orbital distances between $a = 0.5$ - 7.0 AU are shown. The dependency of the position of the planet in the disk can be seen here as an impact on the quantitative accretion behaviour of the planet. Planets which are located in the dead zone reach the run-away state in most cases, even for quite small initial masses of $M_{\rm p,init} = 0.01$ $\mathrm{M}_\oplus$ (dashed). There seems to be no big difference between the cases of $a = 0.5$, 0.7, and 1.0AU. They all have similar evolutionary tracks for all initial masses. The run-away accretion can only be stopped by the planet drawing a high amount of mass from its surroundings and open a gap, which then limits the mass further available in the annulus for planetary accretion. Hence, the run-away growth ends as soon as the disk annuli in the planet's vicinity are vacated, which is indicated by a decreasing slope and an almost constant $M_{\mathrm{p}}(t)$. The farther out a planet is located the smaller is its growing rate. The planet with $M_{\mathrm{p,init}} = 0.1\ \mathrm{M}_{\oplus}$ at 3.0 AU (solid red) is located just behind the dead zone. It grows more slowly than the planetary cores embedded in the high density region, but it is still able to reach the run-away state. The results of Fig. 5.7 together with Fig. 5.8 indicate that planetary cores which experience a run-away growth are able to open a gap in the disk.

No gap formation

The evolution of a PPD with an evolving planet with a low accretion rate and no gap formation is similar to the evolution of an unperturbed disk as panels (d) and (e) in Fig. 5.7 show. Fig.5.9 shows the evolution tracks of planets with different initial masses of $M_{\mathrm{p,init}} = 0.1$ - $5.0\ \mathrm{M}_{\oplus}$ at an orbital distance of $a = 5.0$ AU (panel (a)) and the correlated M_{disk} evolution (panel (b)), whereas panels (c) and (d) depict M_{p} and M_{disk} for $M_{\mathrm{p,init}}$ =0.01-0.2 $\mathrm{M}_{\oplus}$ at an orbital distance of $a = 1.0$ AU, respectively. The total disk mass M_{disk} in panel (b) shows no difference between a disk with embedded small planets ($M_{\mathrm{p,init}}$ =0.1 and 0.2 $\mathrm{M}_{\oplus}$) and a disk without any planet. This result is similar to the results with small constant accretion rates in Sec. 5.2.1 where no gap develops. Even for these higher initial core masses no gap forms, since they do not reach the required $\dot{M}_{\mathrm{p}}$ to disrupt the disk. Therefore this result shows that a planet with an accretion rate below a certain threshold has no visible influence on the long-term evolution of a PPD.

Gap formation

The formation of a gap depends on multiple factors. Both disk and planetary parameters influence the ability of the planet to open a gap and therefore its impact on the long-term evolution of the disk, as shown in Fig. 5.10, where the distinct impact on the evolution of the PPD generated by the gap formation process is shown. Panel (a) again represents the Σ-profile of a disk with a planet with $M_{\mathrm{p,init}} = 0.1\ \mathrm{M}_{\oplus}$ located at 1.0 AU which is chosen in order for the planet to be able to disrupt the density structure of the disk. The impact of the planet is also clearly visible in the profile of the radial velocity u_{r} in panel (c). Compared to the fiducial model in Fig. 5.1, this Bondi-model shows the impact in the radial velocity earlier and the gap develops faster, which is due to the growing planetary

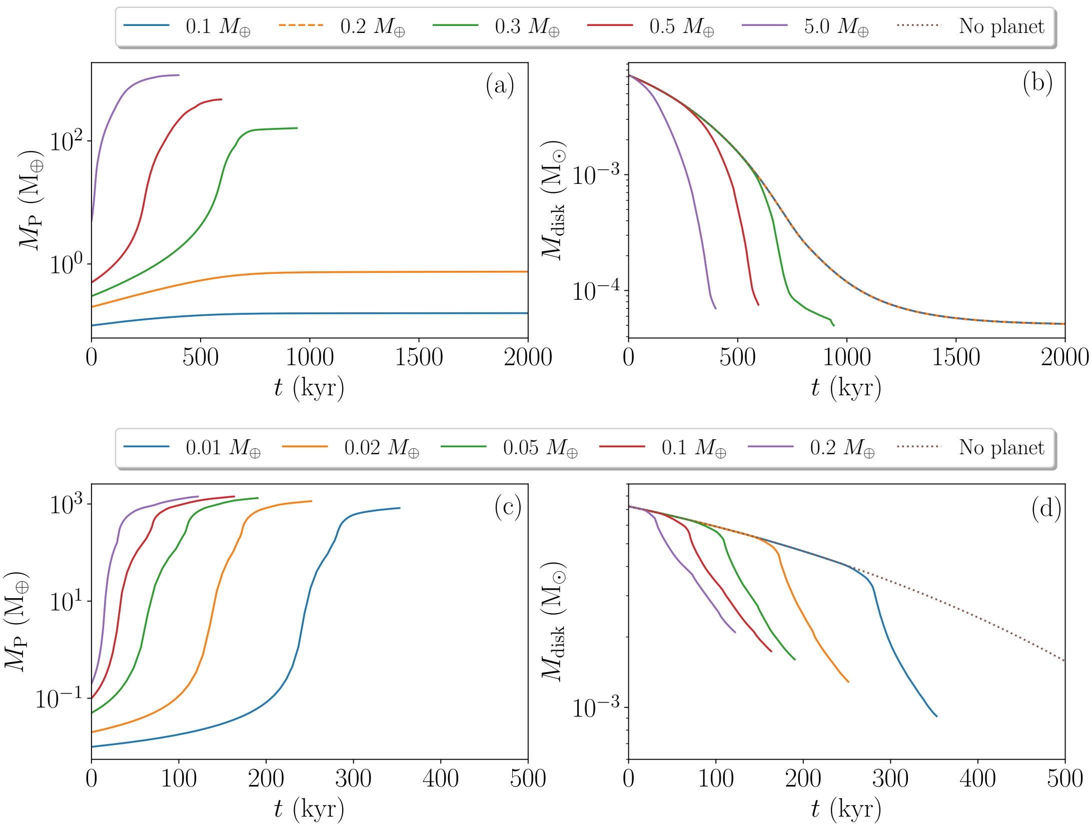

Figure 5.9: Evolutionary tracks of the planet masses with initial masses of $M_{\mathrm{p,init}}$ =0.1-5.0$M_\oplus$ at an orbital distance of 5.0 AU for panel (a) and initial masses of $M_{\mathrm{p,init}}$ = 0.01-0.2 $M_\oplus$ at an orbital distance of 1.0 AU for panel (c). The panels (b) and (d) show the evolution of the total disk mass for the planets located at a = 5.0 AU and a = 1.0 AU, respectively. The dotted purple line is a model without a sink term.

mass core and therefore a fast increasing $\dot{M}_{\mathrm{p}}$ due to the high density at 1.0 AU. Besides the earlier gap formation, the evolution is analogue to Sec. 5.1, but the effects here are more distinct and new effects emerge as will be discussed in the following.
Similar to the fiducial model is, that as soon as the disturbances in u_{r} and $\dot{M}_{\mathrm{flux}}$ start to change sign a gap opens in Σ. These features in u_{r} and $\dot{M}_{\mathrm{flux}}$ become more pronounced for a gap developing further and becoming deeper (cf. panels (a) and (b) in Fig. 5.10). The effectively suppressed angular momentum transport in radial direction and the therefore emerging separation of the inner and outer disk leads to a mass accumulation at the inner and outer gap rim, which can be seen in panels (b) and (c). Therefore, and due to

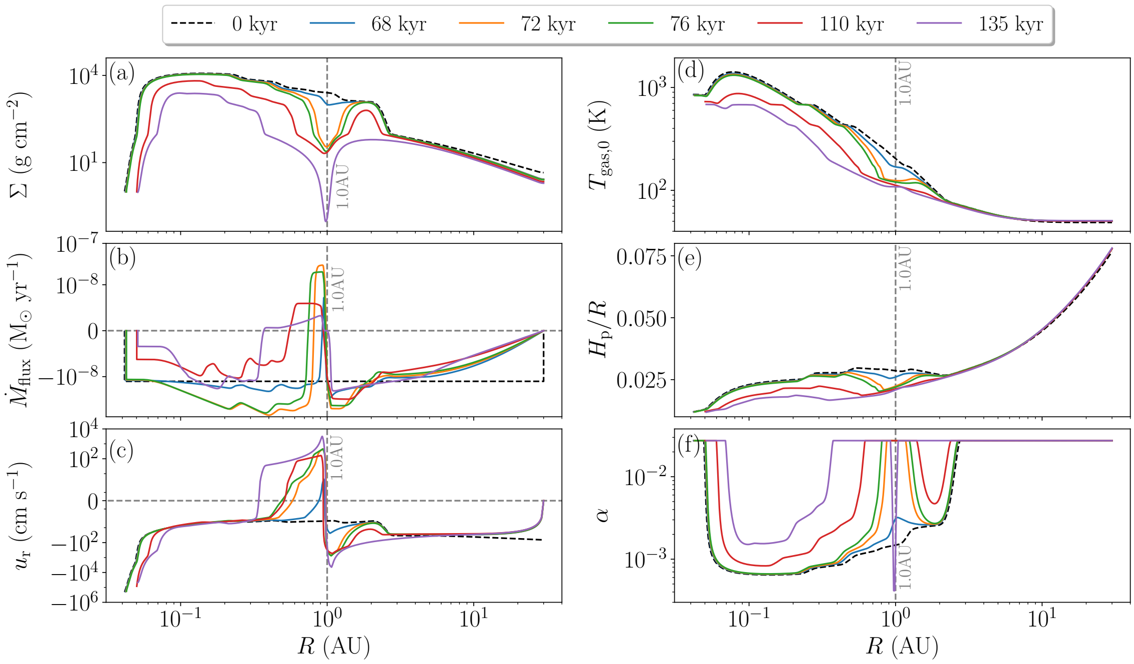

Figure 5.10: Snapshots during the formation of a gap caused by a planet of $M_{\mathrm{p,init}}$ =0.1M$_\oplus$ located at 1 AU. Panel (a) shows the gap in Σ, panel (b) shows the mass flux $\dot{M}_{\mathrm{flux}}$, panel (c) is the evolution of radial velocity u_{r}, and panel (d) pictures the gas temperature $T_{\mathrm{gas,0}}$, panel (e) is the scale height compared to radial extension H_{p}/R and panel (f) shows the viscosity parameter α. The same colour in each plot correspond to the same snapshot. The horizontal dashed line in panel (c) is $\dot{M}_{\mathrm{flux}} = 0$.

the growing pressure gradient, u_{r} and $\dot{M}_{\mathrm{flux}}$ increase over time until $\dot{M}_{\mathrm{flux}}$ outmatches $\dot{M}_{\mathrm{p}}$. Hence, a weak mass transport rate beyond the gap boundaries can be maintained, which limits the pressure gradient in this region and leads to a gap refill. This refill is an effect which works against the gap creation, as already implied in Sec. 5.1. This counteracting effect allows a more efficient angular momentum transport, which causes $\dot{M}_{\mathrm{flux}}$ to decrease in this area (compare green and red lines in panel (b)) and the radial point of the $\dot{M}_{\mathrm{flux}}$-sign change (which has been moving inward up until now) starts to move back outwards and decreases $\dot{M}_{\mathrm{flux}}$ in the gap region. As soon as $\dot{M}_{\mathrm{flux}}$ is low enough for $\dot{M}_{\mathrm{p}}$ to exceed the mass transport rate, the gap formation proceeds and the planet is able to resume draining the disk annuli in its surrounding until the pressure gradient again increases to a value at which it triggers a gap-refill. This alternating process off draining and refilling can take place several times during the gap formation

process and during disk evolution. It will be discussed further in Sec. 5.3.2. This effect can also occur for constant sink terms, but in a less distinct form.
The temperature in panel (d) shows a significant drop during the gap formation. This can be explained by a smaller viscous heating, which leads to a smaller gas temperature in the gap area, and this causes also a dip in the scale height, which is shown in panel (e). Compared to the fiducial model, where no change in $T_{\mathrm{gas},0}$ and H_{p}/R is visible, one can conclude that the higher the accretion rate, the bigger is the impact on all disk parameters. The planetary accretion rate of the fiducial model seems to be too small to have a distinct impact on $T_{\mathrm{gas},0}$ and H_{p}/R.
The α-parameter in panel (f) of Fig. 5.10 also shows signs of a significant impact due to the perturbation generated by the planet. In the gap region a higher viscosity is noticeable during the gap formation process, since the mass extraction leads to a removal of the dead zone at the gap's position. Therefore, the star's UV- and X-ray radiation is able to penetrate deeper into the disk at the planet's orbital distance. So, the dead zone vanishes there and the viscosity can be more effective, which increases the growth rate of the embedded planet. After the gap has fully developed, Σ gets to small for MRI activation in our model, thus the viscosity drops down again. Therefrom one can see that a planet which is massive enough to form a gap has a huge impact on the disk dynamics and the PPD's evolution and the properties of the time-dependent Bondi-accretion rate can lead to more distinct features and impacts on the disk characteristics, especially if the planet is located in the dead zone.

5.3 Layered viscosity

5.3.1 Impact of gap formation on the outburst behaviour

This section focuses on the influence of a planet embedded in a PPD, which develops recurring, episodic accretion outbursts.
Fig. 5.11 shows how a forming planet influences the number of bursts during the disk lifetime. In panel (a) the accretion rate onto the star $\dot{M}_\star$ of an unperturbed disk is plotted. It can be seen that the episodic high accretion events occur for the first ~200kyr of the disk's evolution. Panels (b) and (c) show the occurrence of bursts for disks with an embedded planet of $M_{\mathrm{p,init}} = 0.05\ \mathrm{M}_\oplus$ and $0.1\ \mathrm{M}_\oplus$, respectively, located at
$a = 1.0$ AU. Comparing the disk without a planet to the models in panels (b) and (c), it can be seen that the time period during which bursts occur, is significantly shorter for the disks with an embedded planet, which is caused by the formation of a gap. As discussed

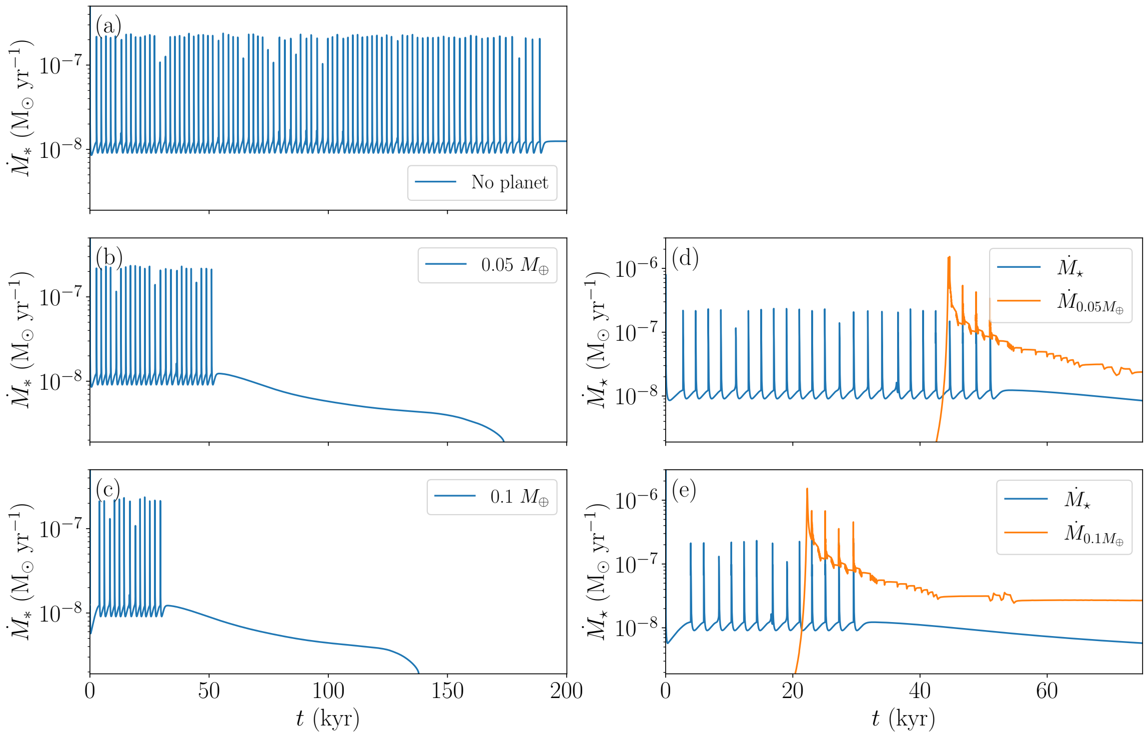

Figure 5.11: Behaviour of the accretion rate onto the star $\dot{M}_\star$ over time for disks without a planet (a) and with planets of $M_{\mathrm{p,init}} = 0.05$ M$_\oplus$ and 0.1 M$_\oplus$ at 1.0 AU are shown in panel (b) and (c), respectively. In plot (d) and (e) the accretion rates onto the planet are shown in orange.

in Sec. 5.2.2, the inner disk evolves unaffected like a PPD with an outer radius of r_{p} after its separation from the outer disk. The inner disk empties on a shorter timescale than it would without gap, due to the lack of mass supply from the outer disk. Therefore this disk does not fulfil the criterion for TI triggered bursts anymore in earlier evolutionary stages than the unperturbed PPD, which causes the occurrence of those episodic high accretion events to stop. A higher planetary accretion rate causes an earlier gap formation, which stops the occurrence of bursts earlier in the disk's lifetime. Hence, $\dot{M}_\star$ for $M_{\mathrm{p,init}}$ =0.1M$_\oplus$ (panel (c)) shows a significantly smaller number of bursts than the disk with the smaller planet $M_{\mathrm{p,init}} = 0.05$ M$_\oplus$, since the latter causes a smaller accretion rate and therefore a later evolving gap (panel (b)).

In panels (d) and (e) the accretion rates of the planets of $M_{\mathrm{p,init}} = 0.05$ M$_\oplus$ and 0.1 M$_\oplus$ (orange) are shown, respectively. The steep increase in $\dot{M}_{\mathrm{p}}$ indicates the run-away growth of the planet and the subsequent opening of a gap. As soon as the planet has emptied its

own orbit, the planetary accretion is limited by the mass transport rate through the gap, which is indicated by the sudden stop of the fast increasing $\dot{M}_{\rm p}$. After this sudden stop $\dot{M}_{\rm p}$ slowly decreases and is limited to the material support on the viscous timescale of the PPD. The inner disk then accretes its leftover material onto the star through episodic outbursts. A similar behaviour can be observed for sink terms located at different orbital distances from the star.
In Fig. 5.11 it can also be seen that the magnitude of $\dot{M}_\star$ is the same for all three simulations in panels (a)-(c). Hence, the gap should not affect the behaviour of a single outburst. Analogous to Sec. 4.3 the same disk properties as in Fig. 4.3 and Fig. 4.4 were investigated for a PPD with an embedded planet of $M_{\rm p,init} = 0.1\ {\rm M}_\oplus$ at 1.0 AU. Comparing the results of this simulation to the disk model without a planet, no differences in the burst behaviour can be found. The disk is still able to reach the activation temperature $T_{\rm active}$ which then leads to thermal instabilities. Also the parameter values are nearly the same as in the unperturbed model. Since a burst alters especially the innermost disk region and gaps in this work's simulations form in areas farther out, the TI is developing largely unaffected without any direct influence from the forming gap. So, the only impact on a burst, induced by a gap, is that the gap can regulate the mass transport towards the star and therefore the number of episodic accretion events.
These results support the statement that the inner disk evolves unaffected by the perturbations induced by a gap.

5.3.2 Impact of bursts on gap formation

The following section analyses the effect of episodic accretion events on the development of gap formation and on the gap itself. Fig. 5.12 shows the beginning of gap formation at an orbital distance of 1.0 AU, caused by a planet with $M_{\rm p,init} = 0.1\ {\rm M}_\oplus$. The time of each snapshot can be seen in the right panel, where the accretion rate onto the star is shown. Between two bursts the blue line starts to show a small perturbation in the surface density Σ at 1.0 AU, which indicates the starting moment of gap formation. This impact is also visible in $\dot{M}_{\rm flux}$, again depicted by the sign change of the blue line at 1.0AU in panel (b). Over time the planet extracts more mass, which causes the gap to deepen and widen (yellow line). In the meantime, the green line indicates the occurrence of another episodic accretion event. The ionisation fronts, generated by TI, alter the disk structure (as discussed in Sec. 4.3), which leads to a mass refill of the gap, discussed as in the following. In panel (b) the ionisation fronts at the inner disk rim develop at ~ 0.075 AU (green) and move in- and outward (red line). The additional heat, induced by the

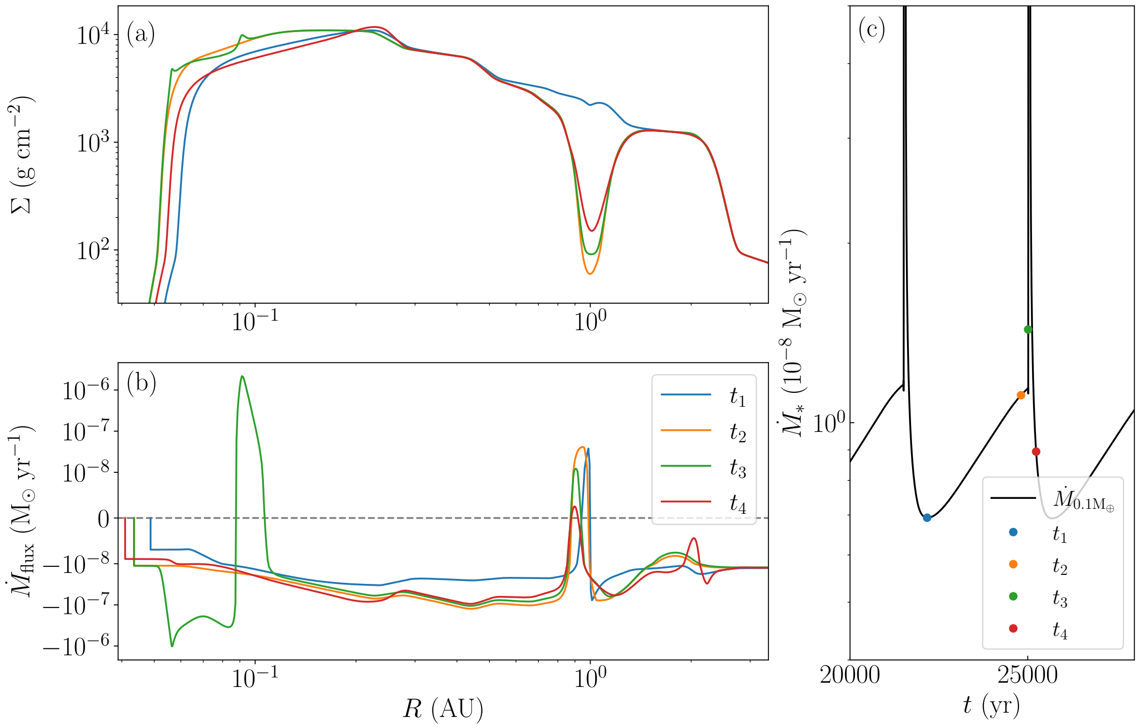

Figure 5.12: Surface density Σ (panel(a)) and mass transport rate $\dot{M}_{\rm flux}$ (panel(b)) during gap formation and the presence of outbursts. A gap is created by $M_{\rm p,init} = 0.1$ M$_\oplus$ at $a = 1.0$ AU. Each colour marks a certain point in time during an outburst. The snapshot moments are marked in panel(c) where $\dot{M}_\star$ is plotted.

outward moving ionisation front, increases the pressure gradient at the gap rim, therefore $\dot{M}_{\rm flux}$ increases at the inner gap edge. When $\dot{M}_{\rm flux}$ is high enough to outgo $\dot{M}_{\rm p}$, the gap is refilled with disk gas, hence Σ increases, which causes $\dot{M}_{\rm p}$ to increase too. Furthermore, the additional heat induced by the ionisation fronts and accretion luminosity coming from the accreting planet leads to an enhanced viscosity during the outburst phase. The filled-up gap is indicated by a higher Σ-value for the snapshot at t_4, indicated by the red line, at 1.0 AU than for the yellow one, although the former is at a later moment in the disk's lifetime. Hence, either a higher planet accretion rate $\dot{M}_{\rm p}$ is needed to form a gap in the same time span as in a quiescent PPD or the gap needs more time to form due to the

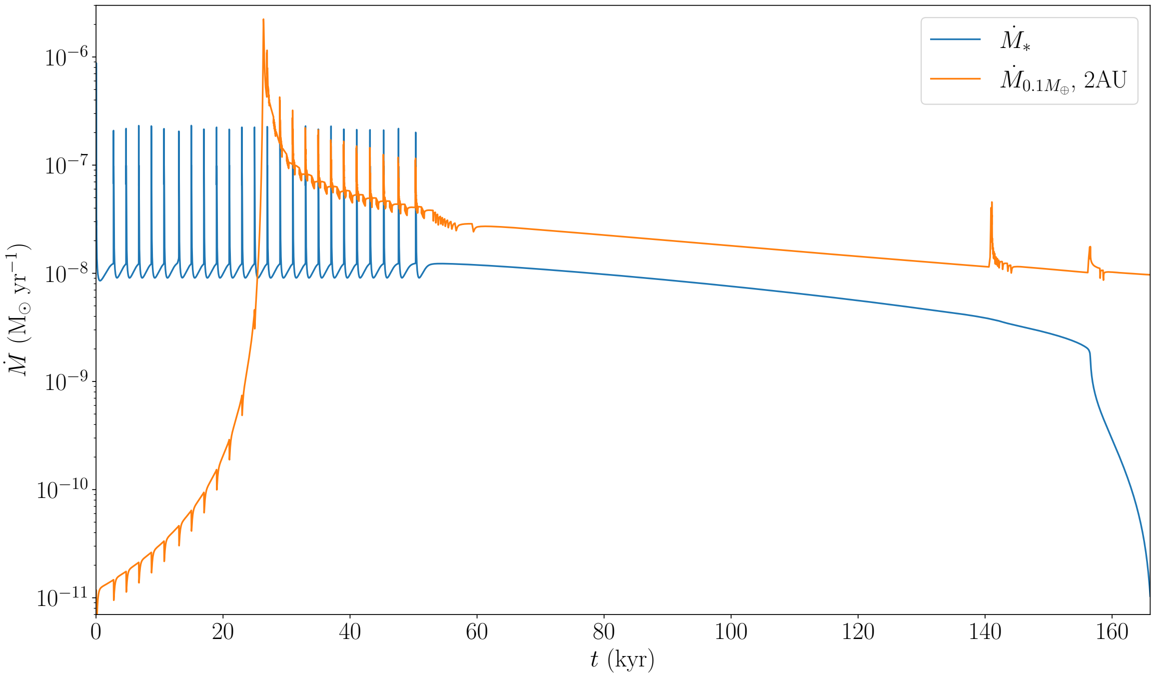

Figure 5.13: The accretion rate of a planet (orange) of $M_{\mathrm{p,init}} = 0.1\ \mathrm{M}_\oplus$ at 2.0 AU. The blue line is the accretion rate onto the star $\dot{M}_\star$ with occurring bursts.

gap refill. [3] This figure shows that the refill takes place during a burst and shortly after one, since the mass rearrangement takes place on the dynamical timescale and therefore the material needs some time to redistribute and fill up the forming gap.

5.3.3 Effect of bursts on the planet's mass accretion rate

A planet's accretion rate depends on the planet's parameters and on its surrounding conditions. Since a burst has a distinct impact on the gap formation it may also affect the planet's accretion rate. Fig. 5.13 shows the accretion rate onto the star $\dot{M}_\star$ (blue line) and the planet's accretion rate $\dot{M}_\mathrm{p}$ of a planet with $M_{\mathrm{p,init}} = 0.1\ \mathrm{M}_\oplus$ at 2.0 AU in orange. The simultaneity of episodic accretion events and occurring dips and peaks in $\dot{M}_\mathrm{p}$ indicate a correlation of these two quantities. Interestingly, bursts occurring during the run-away growth are counteracting planet accretion, whereas it is boosted by bursts during the phase where the gap refill rate limits planetary accretion. This can be explained by the dependency of the planet's accretion rate on the density ρ, the sound speed c_s and the

[3] In the following the reader will see that this refill also has an impact on the time dependent sink term which modifies $\dot{M}_\mathrm{p}$ and therefore can lead to an even faster gap formation.

planetary mass. $\dot{M}_\mathrm{p}$ is proportional to $\rho \cdot M_\mathrm{p}^2/c_\mathrm{s}^3$. M_p does not induce this effect since it cannot be decreased. Hence, it depends on the change of the relation ρ/c_s^3. Before the gap forms the density does not change much in this area but due to the outbursts the temperature and therefore also the sound speed increases. The indirect proportionality of c_s^3 causes the accretion rate to decrease. Though, beginning at that point in time where the gap develops, the alteration of the relation ρ/c_s^3 becomes bigger than 1 due to big changes in Σ, so the outburst increases $\dot{M}_\mathrm{p}$ as soon as a gap has formed. Additionally, as mentioned above, the gap can be refilled by bursts, which also enhances the planet's accretion rate, since more material is available in the disk annuli for the planet to accrete. The two peaks in $\dot{M}_\mathrm{p}$ at 140 and 160 kyr are caused by a refill of the gap, similar to the discussed gap-refill in the paragraph before.

5.4 Comparison of burst and non-burst models

In this section the findings of an in-depth comparison between a PPD experiencing episodic accretion and a quiescent disk are presented. The existence of episodic accretion events can have a significant impact on the planet's mass growth rate as can be seen in Fig. 5.14, where the mass gain of a planet with an initial mass of $M_\mathrm{p,init} = 0.1\ \mathrm{M}_\oplus$ placed at different locations of $a = 0.5$, 0.7, 1.0, 3.0, 5.0 and 7.0 AU for the panels (a)-(f), respectively, is plotted. The solid line shows the evolution of M_p in a PPD without outbursts, whereas the dashed line depicts the planetary mass gain in a disk with occurring outbursts. Note that for the models where the sink term lies in the dead zone (panel (a)-(c)) a distinct divergency of the mass evolution can be seen. The planets which are embedded in a disk with FU Ori-like outbursts are able to gain mass faster than those located in PPDs without outbursts. This can be explained by the processes described in Sec. 4.3 and Sec. 5.3.3, where it is claimed that the more dynamic mass transport rate throughout the whole disk is induced by the burst, therefore the planet is able to accrete slightly more mass during its earliest growing phase, which leads to a faster increasing M_p for planets in the dead zone of burst-active PPDs than in quiescence ones. Consequently, its mass accretion rate also increases faster than without bursts, since $\dot{M}_\mathrm{p} \propto M_\mathrm{p}^2$. So, despite to the refill of the gap and the more dynamic disk, the planet is able to clear out its annulus faster, since it is able to increase its mass in a shorter time-span.

For planets located outside the dead zone the impact of bursts on the planetary accretion rate evolution is similar to the already mentioned diminishing effect of the small ρ/c_s^3-relation, which leads to an overall smaller $\dot{M}_\mathrm{p}$ for those planetary cores. Panel (d) shows a planet placed at 3.0 AU, which is able to reach the run-away phase just barely and form

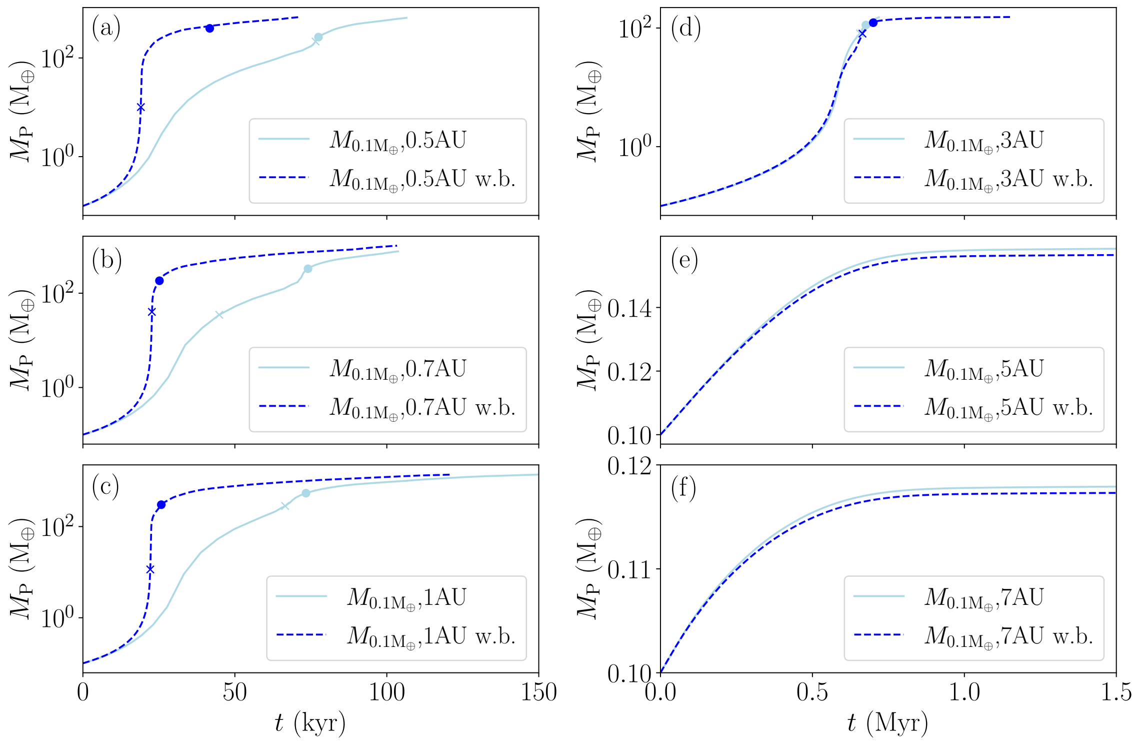

Figure 5.14: The temporal evolution of the planet's mass for planets with initial masses of $M_{\rm p,init} = 0.1$ M$_\oplus$ at different orbital distances of a =0.5, 0.7, 1.0, 3.0, 5.0 and 7.0 AU. The dashed lines are the simulations with an outbursting PPD, the solid ones are without outbursts. The markers ($\star$) and ($\bullet$) depict the moments of an emerging dip in Σ and a fully developed gap, respectively.

a gap. Contrary to the results of models with planets inside the dead zone, the formation of a gap for this planet is almost the same, if it is embedded either in a quiescent disk or in a disk with outbursts.

Panels (e) and (f) depict the mass evolution of planets at 5.0 AU and 7.0 AU, respectively. For neither a disk with nor a disk without bursts the planets at these orbital distances are able to open a gap. The mass for planets which do not reach the run-away phase in a quiescent disk are slightly higher, which indicates that disks with episodic accretion empties faster compared to a quiescent disk, and therefore less mass is available to form a planet over the whole disk lifetime, as mentioned in Sec. 4.3.

The more rapid growth of planets which are embedded in the dead zone can also be seen

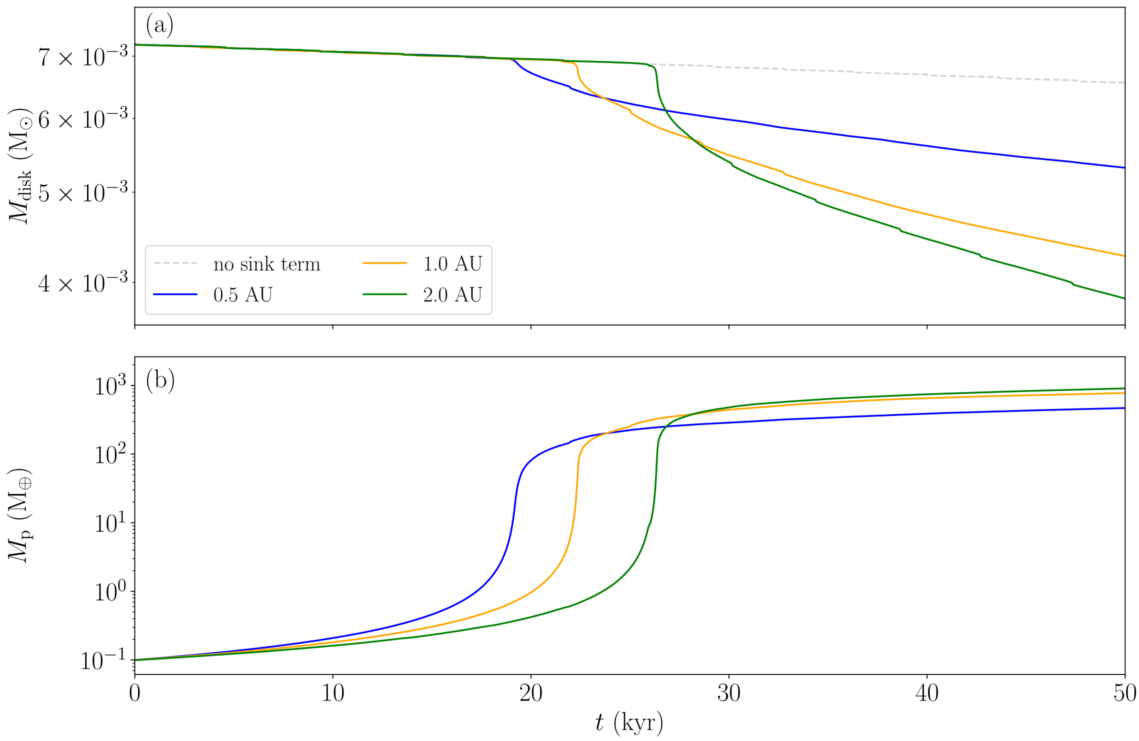

Figure 5.15: Panel (a) shows the total disk mass over time for embedded planets of $M_{\rm p,init} = 0.1\ \rm M_\oplus$ located at orbital distances of $a = 0.5$ AU (blue), 1.0 AU (yellow) and 2.0 AU (green). The grey dashed line depicts the evolution of a disk without a sink term. Panel (b) shows the evolution of the masses for these planets. Same colours correspond to the same model.

in the evolution of the disk mass as shown in Fig. 5.15, where the evolution of the total disk mass $M_{\rm disk}$ (panel (a)) and the mass of the growing planet $M_{\rm p}$ (panel (b)) are shown. The moment at which the planet reaches the run-away phase and a gap starts to form, the disk mass decreases significantly. Interestingly, whether the disk is quiescent or undergoes episodic accretion, has no notable influence on the final planetary mass $M_{\rm p}$ of cores which experienced a run-away growth. For all runs with the same orbital distance, $M_{\rm p,fin}$ reaches almost the same value, regardless of whether there are outbursts present or not for the planets in panels (a)-(d) in Fig. 5.14.

Another impact of bursts can be seen in Fig. 5.16 where the gap development for planets of $M_{\rm p,init} = 0.1\ \rm M_\oplus$ at different orbital distances of $a = 0.5$, 0.7, 1.0 and 2.0 AU is shown. The blue models correspond to planets lying in a non-bursting disk and the red ones are located in a PPD with occurring outbursts. The different markers characterise the

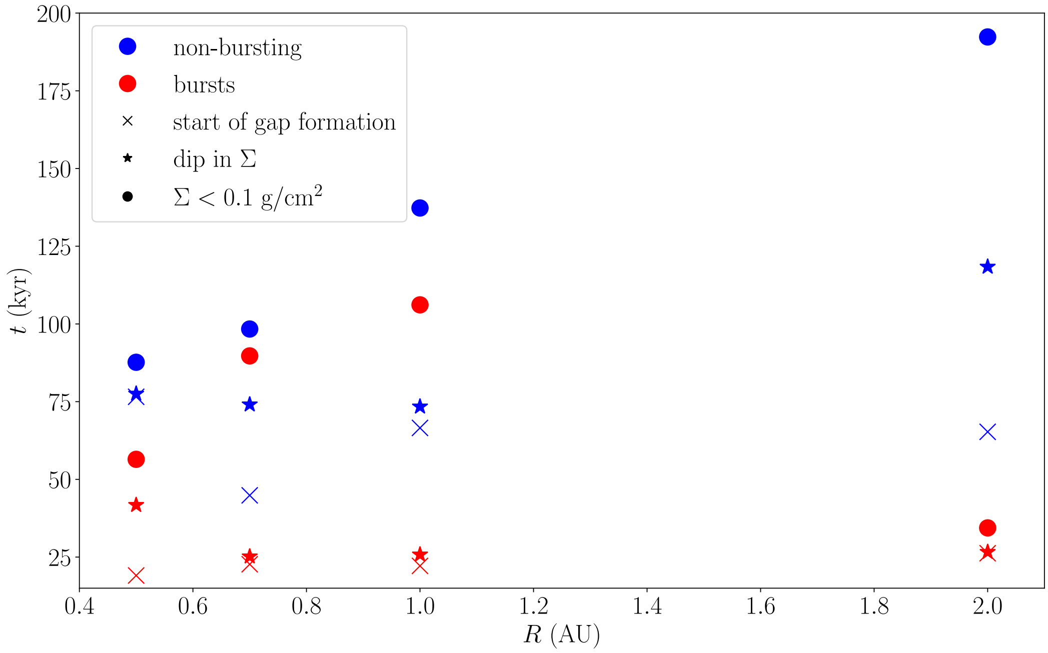

Figure 5.16: The moment of gap formation and development for planets of $M_{\mathrm{p,init}}$ =0.1M$_\oplus$ at orbital distances of a = 0.5, 0.7, 1.0 and 2.0 AU. The blue symbols correspond to planets embedded in PPDs without outbursts, the red symbols mark models with a planet in a disk with episodic accretion. The different markers correspond to ($\times$) a small deviation from the undisturbed Σ profile, ($\star$) a clearly visible diminution of Σ and ($\bullet$) a fully developed gap.

different stages of gap formation. Fig. 5.16 shows that the presence of outbursts impacts the temporal evolution of a gap distinctly. For a PPD with episodic accretion events an embedded growing planet is able to open a gap earlier and faster than for a quiescent disk, which is caused by the already described effect of a more efficient viscosity, since the planet is able to gain more mass in a shorter time-span, which leads to a rapidly increasing mass accretion rate and therefore an earlier gap formation.

A contrary effect can be seen for constant mass accretion rates in Fig. 5.17, where the gap formation induced by constant sink terms of $\dot{M}_{\mathrm{p}} = 5 \cdot 10^{-3}$ M$_\oplus$/yr (blue and red) and $\dot{M}_{\mathrm{p}} = 1 \cdot 10^{-3}$ M$_\oplus$/yr (cyan and pink) at various orbital distances are plotted. For these models the gap formation takes longer for planets in bursting disks (red, pink) than in quiescent ones (blue, cyan). This longer gap formation time is indicated by the distance between the markers ($\times$) and ($\bullet$) and shown by the black lines. The farther they

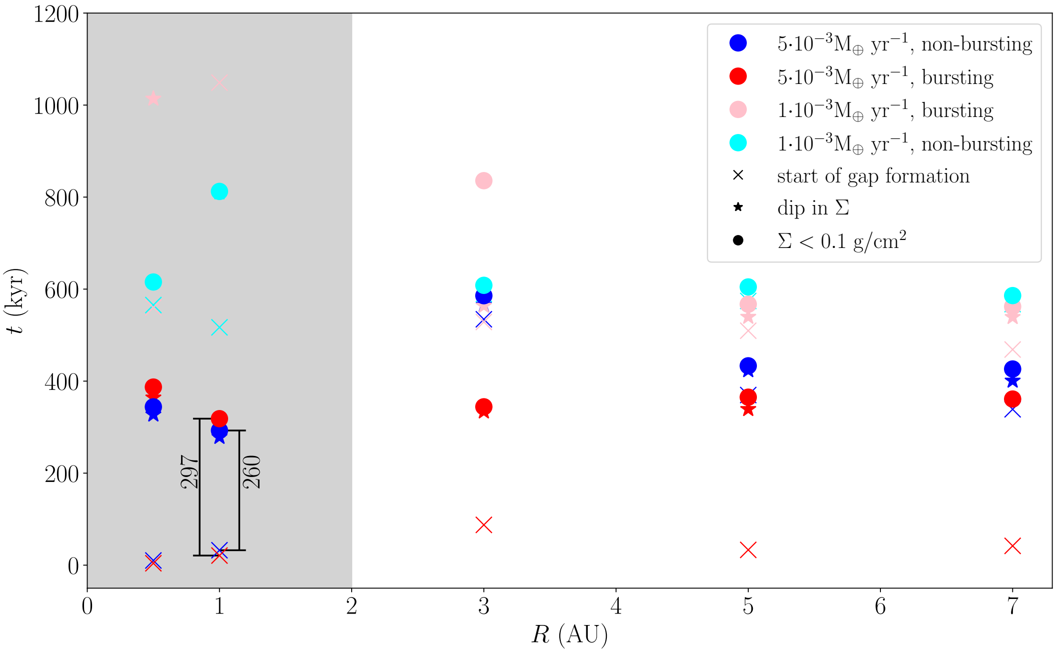

Figure 5.17: The point in time of gap formation and development for planets at orbital distances of a = 0.5, 1.0, 3.0, 5.0 and 7.0 AU. The blue and cyan ones correspond to planets embedded in PPDs without outbursts, the red and pink symbols mark models with a planet in a disk with episodic accretion. Red and blue are constant planetary accretion rates of $\dot{M}_\mathrm{p} = 5 \cdot 10^{-3}$ $\mathrm{M}_\oplus/\mathrm{yr}$ and pink and cyan are $\dot{M}_\mathrm{p} = 1 \cdot 10^{-3}$ $\mathrm{M}_\oplus/\mathrm{yr}$. The different markers ($\times$), ($\star$) and ($\bullet$) correspond to a small deviation from the unperturbed Σ-profile, a clearly visible dip in Σ and a fully developed gap, respectively. The grey area marks the dead zone.

are apart from each other for each simulation, the longer it takes to form a gap. The earlier gap formation in outer regions for the higher constant accretion rate in a bursting environment can be explained by the faster decreasing disk mass in bursting PPDs, since the mass transport rate also decreases faster, therefore $\dot{M}_\mathrm{p}$ is able to overcome $\dot{M}_\mathrm{flux}$ in younger disk ages.

To summarise, planets with a constant accretion rate form gaps easier in disk regions with lower $\dot{M}_\mathrm{flux}$, which corresponds to outer regions of quiescent PPDs and planets with a time-dependent accretion rate form gaps more likely in high density regions of burst-active disks due to their more efficient viscosity and angular momentum transport.

6 Discussion

This work presents the results of the impact of a sink cell on the evolution of a protoplanetary disk. In this section these results will be discussed and compared to results of other works.

The long-term evolution of gap formation induced by a mass extraction due to a growing planet on a fixed orbit and its impact on the evolution of the PPD has not been investigated by many other authors. Most papers examine 2D or 3D simulations for short-term evolution (e.g. Jin et al. (2016),Vorobyov and Elbakyan (2019), Kuwahara et al. (2022), Paardekooper et al. (2022)), spiral-arm or vortice evolution (e.g. Dong et al. (2015), Marr and Dong (2022)), planetesimal growth (e.g. Dipierro et al. (2015), Andama et al. (2022)), the gap structure itself (e.g. Kanagawa et al. (2015), Crida, Morbidelli and Masset (2006)). But the theoretical study of the long-term evolution of such PPD systems with sink terms is challenging to cover with numerical simulations and has therefore not been studied in detail yet. Consequently, due to the absence of appropriate similar work, it is difficult to verify the results of this work by comparing it to other publications.

A comparison can be done for this work's gap formation scenario to others. As mentioned in Sec. 2.3.1 there are different gap formation criteria. This paragraph will investigate these criteria with respect to the gap formation of this work's simulations. Fig. 6.1 shows the mass-evolution of planets with different initial masses of $M_{\mathrm{p,init}} = 0.01\ \mathrm{M}_\oplus$ (dashed), $0.05\ \mathrm{M}_\oplus$ (dash-dotted) and $0.1\ \mathrm{M}_\oplus$ (solid), where for each simulation one of these planets is embedded at an orbital distance of $a = 0.5$ AU (blue), 0.7 AU (yellow) and 1.0 AU (red), respectively. The different markers, which are listed below, indicate the time where the corresponding gap formation criterion from Sec. 2.3.1 is fulfilled. The criteria with the corresponding markers (in Fig. 6.1) beneath it are

$$\underset{(\curlywedge)}{\frac{R_\mathrm{H}}{H_\mathrm{p}} \geq 1} \quad , \quad \underset{(\blacklozenge)}{M_\mathrm{p} \geq \frac{81\pi\nu_\mathrm{p}M_*}{8\Omega_\mathrm{p}a^2}}, \quad \underset{(\boldsymbol{+})}{\frac{3H_\mathrm{p}}{4R_\mathrm{H}} + \frac{40\nu_\mathrm{p}M_\mathrm{p}}{M_*\Omega_\mathrm{p}a^2} < 1}, \qquad \underset{(|)}{\Sigma < 0.1.}$$

The last criterion is this work's definition of a gap. Additionally, the start of gap formation is marked with a cross ($\times$), similar to Fig. 5.16 or Fig. 5.17. In Fig. 6.2

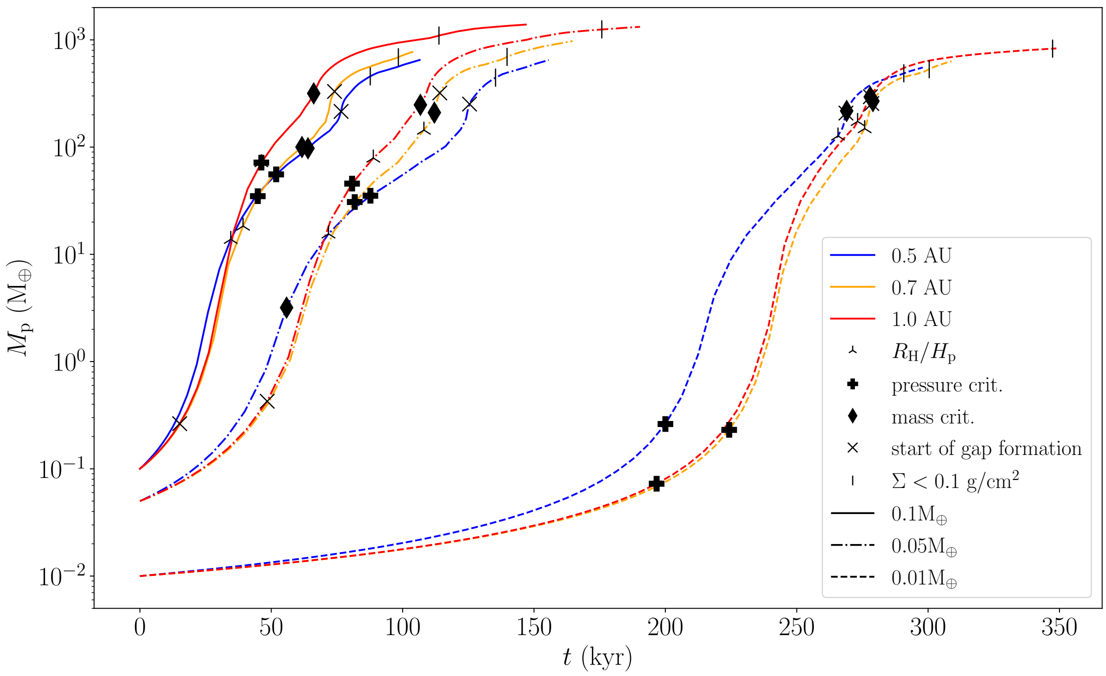

Figure 6.1: Evolution of the planet mass for planets with different initial masses of $M_{\mathrm{p,init}} = 0.01\ \mathrm{M}_\oplus$ (dashed), $0.05\ \mathrm{M}_\oplus$ (dash-dotted) and $0.1\ \mathrm{M}_\oplus$ (solid). These planets are located at different spots in the disk of $a = 0.5$ AU (blue), 0.7 AU (yellow) and 1.0 AU (red). The different markers indicate the moment at which a certain gap criterion is reached, i.e. the (⅄) marks the equality of R_H and H_p, (✚) is the pressure criterion, (♦) is the mass criterion and (|) is the moment where $\Sigma < 0.1$ g/cm^2.

the same properties are shown, but for planets with $M_{\mathrm{p,init}} = 0.1\ \mathrm{M}_\oplus$ (solid), $0.2\ \mathrm{M}_\oplus$ (dash-dotted) and $0.3\ \mathrm{M}_\oplus$ (dotted), all located at 3.0 AU. They are plotted separately, because these planets are not located in the dead zone. Therefore they need more time and higher initial masses to form gaps, which would reduce the meaningfulness of Fig. 6.1 by plotting them in the same figure.

As can be seen the moments of criterion fulfilment is different for each criterion and each planet. The time-span for fulfilling all criteria can vary from ∼60 kyr (solid yellow) up to over 350 kyr (dashed red in Fig. 6.1 or dotted green in Fig. 6.2). Also the order of criterion fulfilment differs for the diverse simulations. In most cases the pressure criterion (✚) is reached first. In the majority of the cases the criterion sequence is the same for

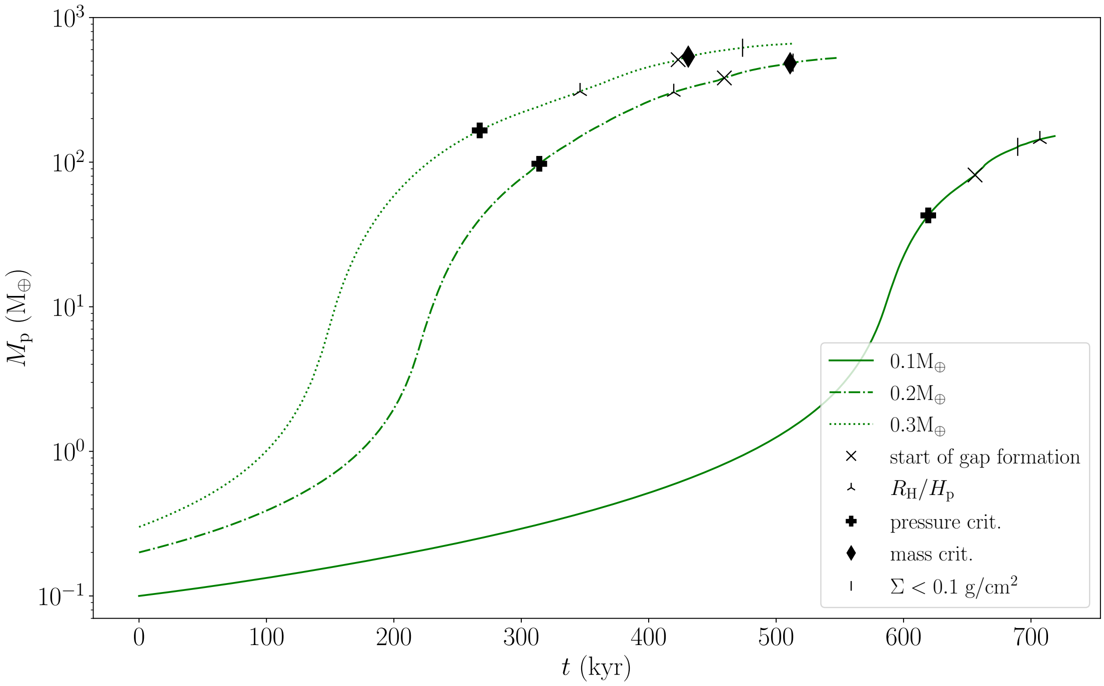

Figure 6.2: Similar plot to Fig. 6.1 but for planets of $M_{\mathrm{p,init}} = 0.1$ M$_\oplus$ (solid), 0.2 M$_\oplus$ (dash-dotted) and 0.3 M$_\oplus$ (dotted), all located at an orbital distance of 3.0 AU. The different markers characterise the same criteria as in the figure before.

the same initial planet mass, thus the order seems to depend strongly on $M_{\mathrm{p,init}}$. The criterion of $\Sigma < 0.1\mathrm{g/cm}^2$ is the last one to be fulfilled for almost all simulations and is reached clearly after the stop of an increasing mass accretion rate. The mass criterion (♦) is also reached late compared to the other criteria and therefore seems to be the closest criterion to this simulation's criterion of $\Sigma < 0.1\mathrm{g/cm}^2$. In Fig. 6.2 the planet with $M_{\mathrm{p,init}} = 0.1$ M$_\oplus$ (solid) is not able to fulfil this criterion. The planet is not massive enough to have an accretion rate, which is high enough to generate such a deep gap. For a planet with such a low $M_{\mathrm{p,init}}$ also the other criteria are reached quite late during the gap evolution. Hence, this case seems to be a special case, where the planet is just big enough to form a gap. If it would have just a slightly lower accretion rate it would not have been able to trigger the creation of a gap.

The final masses of the planets are in a range of a few $10^2 - 10^3$ M$_\oplus$. This coincides with the masses of exoplanets (gas giants) around solar like stars, which have been found by now (NASA, 2022) or were simulated by e.g. Stökl et al. (2016) or Ndugu, Bitsch and

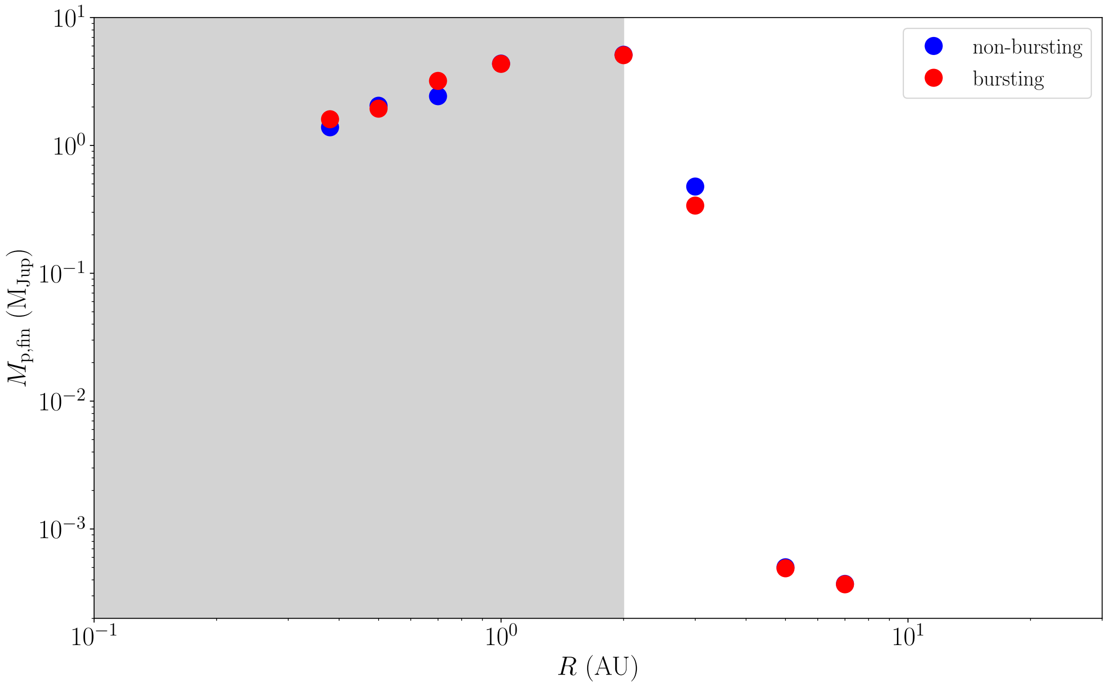

Figure 6.3: Final planet masses $M_{\mathrm{p,fin}}$ in units of Jupiter masses at diverse orbital distances in the range of a = 0.38-7.0 AU. Their initial masses are $M_{\mathrm{p,init}} = 0.1\ \mathrm{M}_\oplus$. Blue planets are embedded in non-bursting disks, whereas red ones evolve in out-bursting PPDs. The grey area marks the dead zone.

Jurua (2019). This shows that the amount of mass provided from the disk for planet growth in this work is realistic.

The final planet masses also depend on the orbital distance of the evolving planet, which is shown e.g. by Xiao and Jin (2015) (cf. Fig. 2.6). Their work concludes that the final mass of a giant planet growing within a PPD strongly depends on its semi major axis, besides the initial conditions of the star and disk forming molecular cloud core. Fig. 6.3 shows the dependency of $M_{\mathrm{p,fin}}$ on the orbital distance for the simulations of this work. The planets are located at diverse distances of a = 0.38-7.0 AU. Blue and red ones are embedded in quiescent and burst-active disks, respectively. One can see that no distinct differences between red and blue models are visible, but the dependency on a can be seen clearly. The innermost four planets lie inside the dead zone, whereas the two outermost are placed in in a low density region. The planets at 3.0 AU are located directly beyond the dead zone. Hence, similar to the mentioned paper, different growing

regimes can be observed and they strongly depend on a, especially in the transition zone from high to low density regions. Planets with $a \leq 2.0$ AU are able to gain mass fast enough to open a gap, whereas planets with $a > 3$ AU do not grow enough and therefore their accretion rate does not overrule $\dot{M}_{\mathrm{flux}}$, so a gap cannot evolve and their final mass decreases with increasing a. Compared to Xiao and Jin (2015), the sharp drop in $M_{\mathrm{p,fin}}$ for the innermost disk region is missing, which can be explained by the simple planetary growth model used in this work, which does not suit all orbital distances. The shift of the $M_{\mathrm{p,fin}}$-function in radial direction compared to the function calculated by Xiao and Jin (2015) can be explained by the differing PPD properties, including without limitation the greater expansion of the protoplanetary disk and a different viscosity in their work. The disk in their work is more expanded and has a more extended high-density region (∼0-10AU). The value of this work's final masses also approximately coincide with the ones in the cited paper which again shows that the simple Bondi-accretion approximation is suitable for most cases of this work.
By comparing the evolution of these planets (cf. Fig. 5.9) to other works, one can see that the simulated planetary mass growth is similar to other calculations, e.g. the simulations of Stökl et al. (2016). The results of panel (a) of Fig. 5.9 show similar evolutionary tracks as the planets in Fig. 6 of Stökl et al. (2016), as e.g. some of the planets are able to reach the run-away phase, whereas smaller ones do not. Analysing these tracks shows that this mainly depends on their initial mass and therefore their accretion rates. Note that the planets in the work of Stökl et al. (2016) have an infinite mass supply for their growth, hence if a planet reaches the run-away phase nothing stops it from accumulating mass and growing unnaturally big, whereas the planets of this work are restricted in their growth by the amount of mass available in the disk annuli due to gap formation. The values of the initial conditions do not exactly coincide for these two works, which leads to a different result for the same initial masses and their accomplishment of reaching the run-away phase. Stökl et al. (2016) use an unlimited mass reservoir of $\rho = 5 \cdot 10^{-10}\mathrm{g/cm^3}$ that corresponds to a value of $\Sigma \sim 200\ \mathrm{g/cm^2}$, which is the surface density of the minimum mass solar nebula at 1.0 AU, and differs from the value for Σ of this work's disk at the same distance by a factor of 10 ($\Sigma_{1\mathrm{AU}} \sim 2000\ \mathrm{g/cm^2}$) caused by the dead zone. The disk has an initial density of $\Sigma_{5\mathrm{AU}} \sim 90\ \mathrm{g/cm^2}$, which is more similar to Stökl et al. (2016)'s planetary environment than $\Sigma_{1\mathrm{AU}}$, therefore this work compares the evolutionary tracks of the planets located at 5.0 AU instead of 1.0 AU, and these simulations show similar information about the planet's run-away status compared to Stökl et al. (2016). These findings indicate that the results of this work can provide more realistic boundary conditions for the formation of giant planets due to the interaction of

the evolving planet with the disk.
Additionally, in Fig. 5.9 the correlated evolution of the total disk masses M_{disk} is shown, where the impact of a growing giant planet on the disk's mass can be seen. The bigger the planet is, the bigger is its impact for same orbital distances. If a planet does not reach the run-away phase and therefore is not able to open a gap, no effect on the M_{disk}-evolution is noticeable. The effect on the total disk mass induced by a growing planet cannot be observed yet and also simulations of this topic are quite rare.
Another effect of gaps on the disk structure is the mass accumulation on the outer edge of a gap and was found by diverse studies, e.g. by Paardekooper and Mellema (2006) or Kuwahara et al. (2022). As mentioned in 5.1 this effect can also be explained by the results of this work. By looking at the mass transport rate at the edges of a gap (e.g. Fig. 5.10) one can see that material is transported to the inner and outer gap rim, which can be explained by the increasing gas pressure gradient combined with the perturbed angular momentum transport as described in Sec. 5.2.
An effect which is not mentioned by other works is the gap refill process occurring multiple times. This effect could be investigated in more detail by including the azimuthal dimension in these simulations.
A 1D-Code published by Schib, Mordasini and Helled (2022), which also simulates a 1D disk with an embedded evolving planet modelled as a sink term, is aimed to investigate the interaction of a planet and a disk. They use a diffusion description of the disk and are therefore not able to include the role of steep pressure gradients in the vicinity of a gap or in the very inner disk regions (cf. Steiner et al. (2021)). Note that in their work, planetary migration as well as gravitational interaction between planet and disk are modelled, which limits the comparability with this work. Nevertheless, since the planet in both approaches serves as the sole mass sink term, the physics involved of forming a gap due to such a mass sink can be compared to each other. Schib, Mordasini and Helled (2022) locate a planet of $M_{\text{p,init}} = 5.0\ \text{M}_\oplus$ at 5.2 AU, let it accrete and migrate, under the assumption of axisymmetry, and analyse the evolution of the relation of Σ at the planets orbital distance and the initial value of the surface density at this position Σ_{init}. In panel (a) of Fig. 6.4 the evolution of the surface density at the planet's location Σ_{p} in units of the initial surface density Σ_0 is shown for planets of $M_{\text{p,init}} = 0.5\ \text{M}_\oplus$ (green) and $M_{\text{p,init}} = 5.0\ \text{M}_\oplus$ (orange). These planets are embedded in a quiescent PPD at 5.0 AU. Panel (b) depicts the corresponding mass evolution of the growing planets. Comparing Fig. 6.4 to the results of the work of Schib, Mordasini and Helled (2022) one is able to see that the Σ-evolution in their paper is much faster. Their planet reaches a mass of $10^{-3}\ \text{M}_\odot$ in about 10^3 orbits ($\sim 10^4$ yr), whereas in this work it takes about

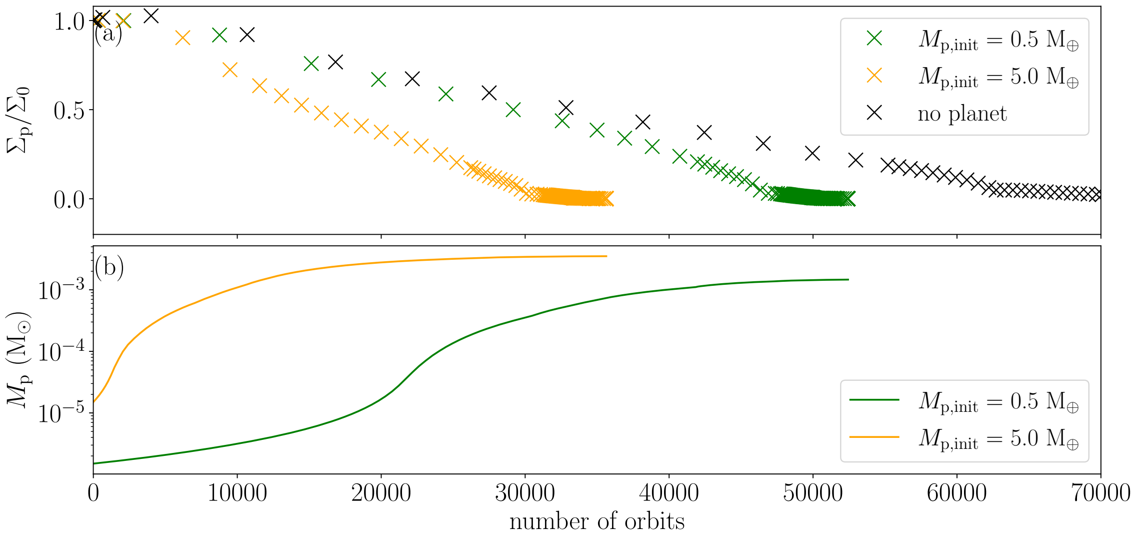

Figure 6.4: Panel (a) shows the surface density at the position of the planet Σ_p in units of the initial surface density Σ_0 for planets of $M_{p,init} = 0.5$ $M_\oplus$ (green) and $M_{p,init} = 5.0$ $M_\oplus$ (orange) at a= 5 AU. The black markers depict the evolution of Σ for an unperturbed model. Panel (b) shows the evolution of the corresponding planet masses.

10^4 orbits ($\sim 10^5$ yr) for the same planet to reach this mass, so these evolutionary tracks differ by a factor of 10. Also the evolution of the surface density at the position of the planet does not look exactly the same, since the slope of the Σ-evolution in their work is bigger. The differences appearing in these results can be traced back to the different initial conditions of the disk. The initial surface density in the cited paper is larger by a factor of 2, which influences the planetary accretion rate and therefore the depletion of Σ. The effect of using a higher Σ_0-value has a shortening impact on the evolution time-span for all simulations done in this work and the work of Schib, Mordasini and Helled (2022), hence the fact that planets with time-dependent accretion rates grow faster in the dead zone (cf. 5.2.2) can be verified by their embedment in a high density region as shown by the cited work. Slightly different results can be explained by the different model used by Schib et al. (2022), including migration, torques and a constant viscosity.
The results of this thesis' simulations are in good agreement to observational studies, e.g. Andrews et al. (2018), ALMA Partnership et al. (2015), Long et al. (2020), etc., where many gap structures were detected. Even the clearance of the inner disk after the formation of a gap, as discussed by Owen (2016), was observed, whereas other effects,

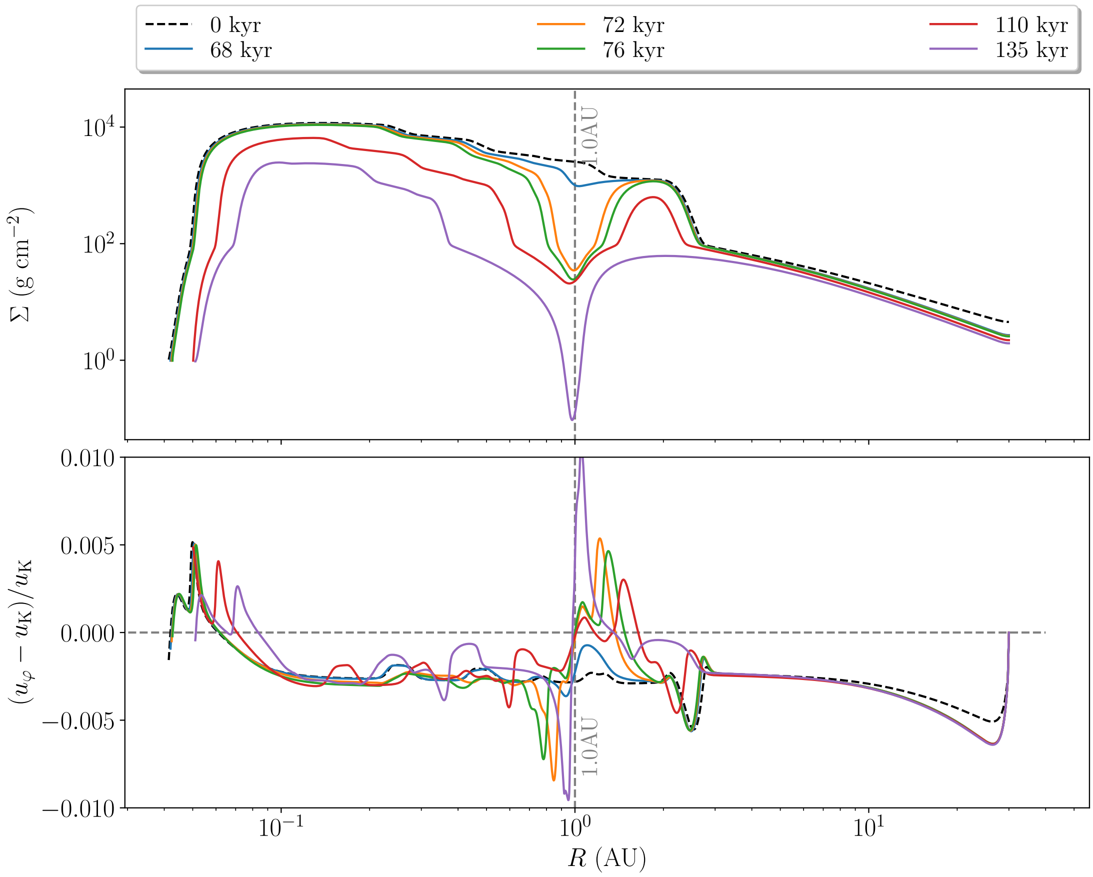

Figure 6.5: Evolution of the surface density Σ (upper panel) and the correlated deviation of u_φ from the Keplerian velocity (lower panel) with a planet of $M_{\mathrm{p,init}}$=0.1M$_\oplus$ present within the disk at 1 AU.

like the impact of outbursts on the planetary mass support behaviour or the gap refill events, have not been observed by now.

As discussed in Sec. 2.3.1, the gap formation can also be seen in u_φ (Teague et al., 2018; Pinte et al., 2018), which is visible in this work's simulations in e.g. Fig. 5.4 for constant sink terms. Zhang et al. (2018) did some theoretical work on this topic, where they located planets with different masses between 11 M$_\oplus$ and 3 M$_{\mathrm{Jup}}$ in a disk with different constant α of $10^{-4} - 10^{-2}$. Their surface density is calculated by the finite difference method, which is a much more simple approach than the method used in this work, and they only simulate the local surrounding of the planet whereas this work studies the entire PPD. Fig. 6.5 shows the deviation of u_φ from the Keplerian velocity during the formation of a gap. This gap is induced by a planet of $M_{\rm p,init}$= 0.1 $M_\oplus$ located at 1 AU. Compared to Zhang et al. (2018) similar effects can be observed. The inner gap edge is sub-keplerian, whereas at the outer gap rim the material is super-keplerian. The gap induced by the planet generates perturbations in the angular velocity component, similar to the results of the mentioned work. But the results of this work show the process and impact of this effect in more detail and more accurate since the code solves the hydrodynamic equations self-consistently.

6.1 Limitations to the model

This work's model is a simplification of the physical world. Since the technology is not developed for including all physical processes and resolving every little detail over long time-spans, the scientific world must be satisfied by the technical and numerical possibilities available today. Therefore following limitations had to be made:

- The model is a 1+1D axisymmetric code, so asymmetric effects and processes, like spiral arms, gravitational instabilities, etc. cannot be considered. But this 1D approximation still provides interesting results especially for the inner disk region where the disk can be treated self-consistently. For limitations of the disk model itself see Ragossnig et al. (2020) and Steiner et al. (2021).

- Due to the axisymmetric treatment of the PPD, the planet needs to be assumed to be smeared over the whole annulus to avoid asymmetric effects. The usage of a planet, which normally induces non-axisymmetric effects, in a 1D-axisymmetric code is applicable if the planet's orbiting time is smaller than the formation time-scale of the gap. The gap formation time, as e.g. Fig. 5.17 shows, is a few 10-10^2 kyr, which is definitely longer than the average Kepler time of a planet. Gravitational interactions like tidal arms are not included in these simulations. The planet is not modelled as a localised, orbiting mass sink, but merely as an axisymmetric ring-like mass sink at a certain radius. It just accretes mass from the disk and is implemented as a simple sink term and has no other impact parameters on the disk. The form of its accretion profile is artificially defined as a Gaussian profile extended over the Hill radius but coincides with the observed and theoretical Bondi-mass accretion rate for giant planets in the run-away phase.

- The sink term is set to a fixed orbit, hence it cannot react to forces working on its position. So migration and its effects are neglected in this work.

- Due to numerical restrictions a minimum surface density is required to have a positive finite value, $\Sigma > \Sigma_{\mathrm{min}}$. In this work this value has been chosen to be Σ_{min}=0.1g/cm^2, which is sufficiently small to consider the gap cleared and at the same time allows the simulation to evolve the disk further in time. The sink term is artificially restricted to a certain surface density value, so it cannot extract too much mass from an annulus. If Σ reached a value lower than 0.1 g/cm^2 then the accreted mass of the sink term would be restricted to accrete an maximal amount of mass, so that there still would be 0.1 g/cm^2 in the annulus left behind.

- Also due to some numerical difficulties the code was not able to calculate every model to the disk's end of lifetime since at the inner boundary Σ gets too low too soon and the time step shrinks to 10^3s. This does not allow to calculate up to a few million years.

- To include the change in viscosity caused by low surface density regions in the disk, the so called *MRI-flag* was introduced. If $\Sigma < 0.1$ g/cm^2,then the surface density is assumed to be too low for MRI-driven viscosity, since MRI needs a certain coupling of gas and magnetic field to work effectively, hence $\alpha = \alpha_{\mathrm{base}}$. For $\Sigma > 1.0$ g/cm^2 the MRI-flag is 1, hence, there is no effect on α, and if 0.1 g/cm^2 $< \Sigma <$ 1.0 g/cm^2 linear smoothing for the calculation of the MRI-flag value is applied to simulate a transition zone.

7 Conclusion and further work

This work presents the results of the simulations for the evolution of a protoplanetary disk impacted by an accreting growing planet which is embedded at a fixed orbit in the disk. The simulations where made with the implicit 1+1D radiation hydrodynamics code *TAPIR*. The planet is implemented as a sink term in the hydrodynamical equations.
The simulations with a constant sink term show that even a small mass extraction can have a huge impact on the disc structure, its dynamics and its evolution. The impact strongly depends on the location of the sink term. A planet located farther out can be smaller to able to form a gap than more inner lying sinks due to higher mass fluxes in the inner disk regions, since $\dot{M}_{\mathrm{p}}$ outreaches the mass transport rate $\dot{M}_{\mathrm{flux}}$ as soon as the gap formation starts. The formation time-span of such a gap caused by a constant $\dot{M}_{\mathrm{p}}$ is about $\sim$ 100 kyr. If the accretion rate of a sink term is too small, no gap formation can be observed and also no impact on the disk's evolution is noticeable. The critical value for a gap opening sink term strongly depends on the mass transport rate at the planet's location.
The formation of a gap causes the disk to split into two parts, and after that the inner disk evolves unopposed as an independent smaller accretion disk. The outer disk is hindered in its evolution due to the perturbed mass transport, therefore it cannot deplete in a normal undisturbed pattern. Instead it looses material to the sink cell and partially to the inner disk on the viscous timescale, therefore the outer disk remains longer than in a non-gap case. Those PPDs with a big inner hole have already been observed as mentioned in the discussion.
The simulations with a time depending sink term yield to slightly different results for the gap opening scenarios. The sink terms in regions with higher densities can increase their mass accretion rate fast, hence they can trigger gap formation faster than in lower density regions or in the constant sink term simulations. During gap formation an increased gas pressure gradient combined with a disturbed angular momentum transport, generated by the lower surface density in the gap, causes the relatively constant inward directed mass flow to be perturbed and this leads to an increasing $\dot{M}_{\mathrm{flux}}$. This allows $\dot{M}_{\mathrm{flux}}$ to exceed $\dot{M}_{\mathrm{p}}$ for a short time, hence the gap can be refilled with mass, which leads to a higher

surface density and subsequently to an increasing planetary accretion rate, therefore the gap will be deepened by $\dot{M}_{\rm p}$ again after some time. If $M_{\rm p,init}$ is too low at the beginning, the planet cannot reach the run-away phase and therefore it is not able to create a gap, which again leads to a unperturbed disk evolution.
The occurrence of bursts is affected by the formation of a gap, since the disk separation prohibits the mass support of the inner disk coming from regions beyond the gap. Therefore the burst criterion can not be fulfilled anymore earlier than in a disk without a gap, whereas the behaviour of the outburst itself is not affected. On the other hand the occurrence of thermal instabilities can impact the gap formation. Due to higher temperatures and more turbulent dynamics in the disk during the out-bursting phase the gap can be refilled or out-smoothed by those activities, which allows the time-dependent sink term to grow faster than in quiescent disks. Due to the more active disk a higher $\dot{M}_{\rm p}$ is needed to trigger gap formation. But despite these results, the simulations show that gaps are generated earlier in bursting disks with time-dependent sink terms than in non-bursting disks, since their accretion rate increases fast.
The comparison of these results to other works shows that with this 1D approach many already observed effects can be reproduced by these simulations, e.g. gap formation due to a sink term, inner disk clearance or giant planetary growth via run-away and their final masses. Some results differ from results of other works due to different initial conditions or diverse used models or methods.
But to conclude, this work shows that, as predicted, a sink cell can cause the emergence of a gap in a PPD and has a huge impact on the evolution and dynamics of a protoplanetary disk. Despite various necessary approximations and limitations, which had to be made, this work's results provide some new, interesting insights in the long-term evolution of an accretion disk with an embedded planet.

7.1 Further Outlook

To get more realistic results many things need to be included and developed in *TAPIR*. Some points for further works would be as follows:

- Varying disk parameters: this work examines the impact of different sink terms on the evolution of a PPD with fixed parameters. Investigating the effect of different disk quantities, e.g. higher/lower viscosity, more/less expanded disks, stronger/weaker magnetic field of the star, etc., would lead to more robust results.

- Including photoevaporation: the impact on the disk with a planet and additionally photoevaporation (already under development)

- Migration: allowing the already implemented planet to migrate, so the long-term evolution of a PPD with a migrating planet and gap formation can be simulated.
- Implement a more realistic planet model: combining the disk *TAPIR* code with the work of Stökl et al. (2016) and Ragossnig et al. (2018) about primordial planetary atmospheres and planet growth.

Bibliography

Alexander, R. et al. (2014). 'The Dispersal of Protoplanetary Disks'. In: *Protostars and Planets VI*. DOI: 10.2458/azu_uapress_9780816531240-ch021. URL: http://dx.doi.org/10.2458/azu_uapress_9780816531240-ch021.

ALMA Partnership et al. (July 2015). 'The 2014 ALMA Long Baseline Campaign: First Results from High Angular Resolution Observations toward the HL Tau Region'. In: *APJL* 808(1), L3, p. L3. DOI: 10.1088/2041-8205/808/1/L3. arXiv: 1503.02649 [astro-ph.SR].

Andama, G. et al. (Feb. 2022). 'Planetary core formation via multispecies pebble accretion'. In: *MNRAS* 510(1), pp. 1298–1314. DOI: 10.1093/mnras/stab3508. arXiv: 2111.15218 [astro-ph.EP].

Andrews, S. M. et al. (2018). 'ALMA Observations of the Epoch of Planet Formation'. In: *The Messenger*(174), pp. 19–23.

Andrews, Sean M. (2020). 'Observations of Protoplanetary Disk Structures'. In: *Annual Review of Astronomy and Astrophysics* 58(1), 483–528. ISSN: 1545-4282. DOI: 10.1146/annurev-astro-031220-010302. URL: http://dx.doi.org/10.1146/annurev-astro-031220-010302.

Andrews, Sean M. and Jonathan P. Williams (2005). 'Circumstellar Dust Disks in Taurus-Auriga: The Submillimeter Perspective'. In: *The Astrophysical Journal* 631(2), 1134–1160. ISSN: 1538-4357. DOI: 10.1086/432712. URL: http://dx.doi.org/10.1086/432712.

Armitage, Philip (2010). *Astrophysics of Planet Formation*. Cambridge.

Armitage, Philip J., Mario Livio and J. E. Pringle (June 2001). 'Episodic accretion in magnetically layered protoplanetary discs'. In: 324(3), pp. 705–711. DOI: 10.1046/j.1365-8711.2001.04356.x. arXiv: astro-ph/0101253 [astro-ph].

Armitage, P.J. (2011). 'Dynamics of Protoplanetary Disks'. In: *Annual Review of Astronomy and Astrophysics*, pp. 195–236.

Bai, Xue-Ning and James M. Stone (May 2013). 'Wind-driven Accretion in Protoplanetary Disks. I. Suppression of the Magnetorotational Instability and Launching of the Magnetocentrifugal Wind'. In: *The Astrophysical Journal* 769(1), 76, p. 76. DOI: 10.1088/0004-637X/769/1/76. arXiv: 1301.0318 [astro-ph.EP].

Balbus, Steven A. and John F. Hawley (1991). 'A powerful local shear instability in weakly magnetized disks'. In: *The Astrophysical Journal*, pp. 214–233.

Bell, K.R. and D.N.C. Lin (1994). 'Using FU Orionis outbursts to constrain self-regulated protostellar disk models'. In: *The Astrophysical Journal*, pp. 987–1004.

Bertout, C. and J. Bouvier (Sept. 1989). 'T Tauri disk models.' In: *European Southern Observatory Conference and Workshop Proceedings*. Vol. 33. European Southern Observatory Conference and Workshop Proceedings, pp. 215–232.

Bodenheimer, Peter and James B Pollack (1986). 'Calculations of the accretion and evolution of giant planets: The effects of solid cores'. In: *Icarus (New York, N.Y. 1962)* 67(3), pp. 391–408.

Bondi, Hermann (1952). 'On Spherically Symmetrical Accretion'. In: *Monthly Notices of the Royal Astronomical Society*, pp. 195–205.

Brogan, C.L. et al. (2015). 'First results from high angular resolution ALMA observations toward the HL Tau region'. In: *APJL*.

Cameron, A. G. W. (Oct. 1979). 'The Interaction between Giant Gaseous Protoplanets and the Primitive Solar Nebula'. In: *Moon and Planets* 21(2), pp. 173–183. DOI: 10.1007/BF00897086.

Crida, A., A. Morbidelli and F. Masset (2006). 'On the width and shape of gaps in protoplanetary disks'. In: *Icarus* 181(2), pp. 587–604. DOI: 10.1016/j.icarus.2005.10.007. URL: https://doi.org/10.1016\%2Fj.icarus.2005.10.007.

Dawson, Rebekah I. and John Asher Johnson (Sept. 2018). 'Origins of Hot Jupiters'. In: *Annual Review of Astronomy and Astrophysics* 56, pp. 175–221. DOI: 10.1146/annurev-astro-081817-051853. arXiv: 1801.06117 [astro-ph.EP].

Demtroder, Wolfgang (2017). *Experimentalphysik 1: Mechanik Und Warme*. eng. Springer-Lehrbuch. Springer. ISBN: 9783662548462.

Dipierro, Giovanni et al. (Aug. 2015). 'On planet formation in HL Tau'. In: *Monthly Notices of the Royal Astronomical Society: Letters* 453(1), pp. L73–L77. ISSN: 1745-3925. DOI: 10.1093/mnrasl/slv105. eprint: https://academic.oup.com/mnrasl/article-pdf/453/1/L73/3057747/slv105.pdf. URL: https://doi.org/10.1093/mnrasl/slv105.

Dong, Ruobing et al. (2015). 'Observational signatures of planets in protoplanetary disks: spiral arms observed in scattered light imaging can be induced by planets'. In: *The Astrophysical Journal* 809(1), p. L5. DOI: 10.1088/2041-8205/809/1/l5. URL: https://doi.org/10.1088/2041-8205/809/1/l5.

Dorfi, Ernst and Luke O'C. Drury (1987). 'Simple Adaptive Grids for 1-D Initial Value Problems'. In: *Journal of computational physics*, pp. 175–195.

Dullemond, C.P. and C. Dominik (2005). 'Dust coagulation in protoplanetary disks: a rapid depletion of small grains'. In: *Astronomy and Astrophysics*(434), pp. 971–986.

Edgar, Richard (Sept. 2004). 'A review of Bondi-Hoyle-Lyttleton accretion'. In: *New Astronomy Reviews* 48(10), pp. 843–859. DOI: 10.1016/j.newar.2004.06.001. arXiv: astro-ph/0406166 [astro-ph].

Gammie, C.F. (1995). 'Layered accretion in T Tauri disks'. In: *The Astrophysical Journal*, pp. 355–362.

Gammie, Charles F. (Jan. 1996). 'Layered Accretion in T Tauri Disks'. In: *The Astrophysical Journal* 457, p. 355. DOI: 10.1086/176735.

Gammie, Charles F. (Apr. 1999). 'Instabilities in Circumstellar Discs'. In: Astronomical Society of the Pacific Conference Series 160. Ed. by J. A. Sellwood and Jeremy Goodman, p. 122.

Goldreich, P. and S. Tremaine (1980). 'Disk-Satellite Interactions'. In: *The Astrophysical Journal* 241, pp. 425–441.

Goldreich, Peter and William R. Ward (1973). 'The Formation of Planetesimals'. In: *The Astrophysical Journal* 183, pp. 1051–1062.

Hartmann, L., G. Herczeg and N. Calvet (Sept. 2016). 'Accretion onto Pre-Main-Sequence Stars'. In: *Annual Review of Astronomy and Astrophysics* 54, pp. 135–180. DOI: 10.1146/annurev-astro-081915-023347.

Hartmann, Lee et al. (1998). 'Accretion and the Evolution of T Tauri Disks'. In: *The Astrophysical Journal*(495), pp. 385–400.

Henning, Thomas and Dmitry Semenov (2013). 'Chemistry in Protoplanetary Disks'. In: *Chemical Reviews* 113(12), pp. 9016–9042.

Hillenbrand, Lynne A. et al. (Dec. 2018). 'Gaia 17bpi: An FU Ori-type Outburst'. In: *The Astrophysical Journal* 869(2), 146, p. 146. DOI: 10.3847/1538-4357/aaf414. arXiv: 1812.06640 [astro-ph.SR].

Ida, S., D. N. C. Lin and M. Nagasawa (Sept. 2013). 'Toward a Deterministic Model of Planetary Formation. VII. Eccentricity Distribution of Gas Giants'. In: *The Astrophysical Journal* 775(1), p. 42. DOI: 10.1088/0004-637X/775/1/42.

Jin, Sheng et al. (Feb. 2016). 'Modeling Dust Emission of HL Tau Disk Based on Planet-Disk Interactions'. In: *The Astrophysical Journal* 818(1), 76, p. 76. DOI: 10.3847/0004-637X/818/1/76. arXiv: 1601.00358 [astro-ph.EP].

Johansen, Anders and Michiel Lambrechts (Aug. 2017). 'Forming Planets via Pebble Accretion'. In: *Annual Review of Earth and Planetary Sciences* 45(1), pp. 359–387. DOI: 10.1146/annurev-earth-063016-020226.

Kanagawa, Kazuhiro D. et al. (2015). 'Mass estimates of a giant planet in a protoplanetary disk from the gap structures'. In: *The Astrophysical Journal* 806(1), p. L15. DOI: 10.1088/2041-8205/806/1/l15. URL: https://doi.org/10.1088/2041-8205/806/1/l15.

Keppler, M. et al. (Sept. 2018). 'Discovery of a planetary-mass companion within the gap of the transition disk around PDS 70'. In: *Astronomy and Astrophysics* 617, A44, A44. DOI: 10.1051/0004-6361/201832957. arXiv: 1806.11568 [astro-ph.EP].

Kóspál, Á. et al. (Nov. 2016). 'Multiwavelength study of the low-luminosity outbursting young star HBC 722'. In: *Astronomy and Astrophysics* 596, A52, A52. DOI: 10.1051/0004-6361/201528061. arXiv: 1607.05925 [astro-ph.SR].

Kretke, K. A. et al. (Jan. 2009). 'Assembling the Building Blocks of Giant Planets Around Intermediate-Mass Stars'. In: *The Astrophysical Journal* 690(1), pp. 407–415. DOI: 10.1088/0004-637X/690/1/407.

Kuwahara, Ayumu et al. (June 2022). 'Dust ring and gap formation by gas flow induced by low-mass planets embedded in protoplanetary disks. I. Steady-state model'. In: *Astronomy and Astrophysics*, arXiv:2206.13453, arXiv:2206.13453. arXiv: 2206.13453 [astro-ph.EP].

Lambrechts, M. and A. Johansen (Aug. 2012). 'Rapid growth of gas-giant cores by pebble accretion'. In: *Astronomy and Astrophysics* 544, A32, A32. DOI: 10.1051/0004-6361/201219127. arXiv: 1205.3030 [astro-ph.EP].

LeVeque, R.J. (2002). *Finite Volume Methods for Hyperbolic Equations*. Cambridge.

LeVeque, R.J. et al. (1997). *Computational Methods for Astrophysical Fluid Flow*. Springer.

Lin, D. N. C., P. Bodenheimer and D. C. Richardson (1996). 'Orbital migration of the planetary companion of 51 Pegasi to its present location'. In: *Nature* 380(6575), p. 606. URL: https://uaccess.univie.ac.at/login?url=https://www.proquest.com/scholarly-journals/orbital-migration-planetary-companion-51-pegasi/docview/204474130/se-2?accountid=14682.

Lin, D. N. C. and J. C. B. Papaloizou (Jan. 1993). 'On the Tidal Interaction Between Protostellar Disks and Companions'. In: *Protostars and Planets III*. Ed. by Eugene H. Levy and Jonathan I. Lunine, p. 749.

Lin, D. N. C. and John Papaloizou (Oct. 1986). 'On the Tidal Interaction between Protoplanets and the Protoplanetary Disk. III. Orbital Migration of Protoplanets'. In: *The Astrophysical Journal* 309, p. 846. DOI: 10.1086/164653.

Lin, D. N. C. and J. E. Pringle (Jan. 1976). 'Numerical Simulation of Mass Transfer and Accretion Disc Flow in Binary Systems'. In: *Structure and Evolution of Close Binary Systems*. Ed. by Peter Eggleton, Simon Mitton and John Whelan. Vol. 73, p. 237.

Long, Feng et al. (July 2020). 'Dual-wavelength ALMA Observations of Dust Rings in Protoplanetary Disks'. English (US). In: *The Astrophysical Journal* 898(1). Publisher Copyright: © 2020. The American Astronomical Society. All rights reserved. ISSN: 0004-637X. DOI: 10.3847/1538-4357/ab9a54.

Lubow, S. and S. Ida (2010). 'Planet migration'. In: *University of Arizona Press* 241, pp. 347–371.

Lubow, S. H. and G. D'Angelo (Apr. 2006). 'Gas Flow across Gaps in Protoplanetary Disks'. In: *The Astrophysical Journal* 641(1), pp. 526–533. DOI: 10.1086/500356. arXiv: astro-ph/0512292 [astro-ph].

Lynden-Bell, D. and J. E. Pringle (Sept. 1974). 'The Evolution of Viscous Discs and the Origin of the Nebular Variables'. In: *Monthly Notices of the Royal Astronomical Society* 168(3), pp. 603–637. ISSN: 0035-8711. DOI: 10.1093/mnras/168.3.603. eprint: https://academic.oup.com/mnras/article-pdf/168/3/603/18325229/mnras168-0603.pdf. URL: https://doi.org/10.1093/mnras/168.3.603.

Marr, Metea and Ruobing Dong (May 2022). 'The Appearance of Vortices in Protoplanetary Disks in Near-infrared Scattered Light'. In: *The Astrophysical Journal* 930(1), 80, p. 80. DOI: 10.3847/1538-4357/ac63ab. arXiv: 2203.11953 [astro-ph.SR].

Mayor, Michel and Didier Queloz (Nov. 1995). 'A Jupiter-mass companion to a solar-type star'. In: *Nature* 378(6555), pp. 355–359. DOI: 10.1038/378355a0.

Mayor, Michel and Didier Queloz (1995). 'A Jupiter-mass companion to a solar-type star'. In: *Nature* 378(6555), p. 355. URL: https://uaccess.univie.ac.at/login?url=https://www.proquest.com/scholarly-journals/jupiter-mass-companion-solar-type-star/docview/204462023/se-2?accountid=14682.

Morishima, R. (Mar. 2012). 'Gap opening beyond dead zones by photoevaporation'. In: *MNRAS* 420(4), pp. 2851–2858. DOI: 10.1111/j.1365-2966.2011.19940.x. arXiv: 1110.2250 [astro-ph.EP].

Mulders, G.D. (2013). 'Radiative transfer models of protoplanetary disks: Theory vs. observations'. MA thesis. University of Amsterdam.

NASA (2022). *Exoplanet Catalog - Discovery*. https://exoplanets.nasa.gov/discovery/exoplanet-catalog/. Accessed: 2022-06-22.

Ndugu, N., B. Bitsch and E. Jurua (Sept. 2019). 'Are the observed gaps in protoplanetary discs caused by growing planets?' In: *MNRAS* 488(3), pp. 3625–3633. DOI: 10.1093/mnras/stz1862. arXiv: 1906.11491 [astro-ph.EP].

Owen, James E. (Feb. 2016). 'The Origin and Evolution of Transition Discs: Successes, Problems, and Open Questions'. In: *PASA* 33, e005, e005. DOI: `10.1017/pasa.2016.2`. arXiv: `1512.06873 [astro-ph.SR]`.

Paardekooper, S.-J. and G. Mellema (2006). 'Dust flow in gas disks in the presence of embedded planets'. In: *Astronomy and Astrophysics* 453(3), 1129–1140. ISSN: 1432-0746. DOI: `10.1051/0004-6361:20054449`. URL: `http://dx.doi.org/10.1051/0004-6361:20054449`.

Paardekooper, Sijme-Jan et al. (Mar. 2022). 'Planet-Disk Interactions'. In: *arXiv e-prints*, arXiv:2203.09595, arXiv:2203.09595. arXiv: `2203.09595 [astro-ph.EP]`.

Pinte, C. et al. (2018). 'Kinematic Evidence for an Embedded Protoplanet in a Circumstellar Disk'. In: 860(1), p. L13. DOI: `10.3847/2041-8213/aac6dc`. URL: `https://doi.org/10.3847/2041-8213/aac6dc`.

Pringle, J.E. (1981). 'Accretion disks in astrophysics'. In: *Annual Reviews of astronomy and astrophysics* 19, pp. 137–162.

Ragossnig, Florian et al. (Oct. 2018). 'Interaction of infalling solid bodies with primordial atmospheres of disk-embedded planets'. In: *Astronomy and Astrophysics* 618, A19, A19. DOI: `10.1051/0004-6361/201832681`. arXiv: `1809.05307 [astro-ph.EP]`.

Ragossnig, Florian et al. (Nov. 2020). '1+1D implicit disk computations'. In: *Computer Physics Communications* 256, 107437, p. 107437. DOI: `10.1016/j.cpc.2020.107437`. arXiv: `2006.12939 [physics.comp-ph]`.

Ratschiner, Bernhard (2020). 'Episodic Accretion on T-Tauri Stars'. MA thesis. University of Vienna.

Reipurth, Bo (Jan. 1990). 'Fu-Orionis Eruptions and Early Stellar Evolution'. In: *Flare Stars in Star Clusters, Associations and the Solar Vicinity*. Ed. by L. V. Mirzoian, B. R. Pettersen and M. K. Tsvetkov. Vol. 137, p. 229.

Sano, T. and J.M. Stone (2002). 'The Effect of the Hall Term on the Nonlinear Evolution of the Magnetorotational Instability: I. Local Axisymmetric Simulations'. In: *The Astrophysical Journal*, pp. 534–576.

Schib, Oliver, Christoph Mordasini and Ravit Helled (May 2022). 'Calibrated Gas Accretion and Orbital Migration of Protoplanets in 1D Disc Models'. In: *arXiv e-prints*, arXiv:2205.02858, arXiv:2205.02858. arXiv: `2205.02858 [astro-ph.EP]`.

Shakura, N.I. and R.A. Sunyaev (1973). 'Black Holes in Binary Systems. Observational Appearance'. In: *Astronomy and Astrophysics*(24), pp. 337–355.

Shu, F.H. et al. (2007). 'Mean-Field Magnetohydrodynamics of Accretion Disks'. In: *The Astrophysical Journal*.

Simon, J.B. et al. (2018). 'Turbulence in the outer regions of protoplanetary disks. I. Weak accretion with no vertical magnetic flux'. In: *The Astrophysical Journal.*

Smith, B. A. and R. J. Terrile (June 1984). 'Optical Searches for Protoplanetary Disks'. In: *Bulletin of the American Astronomical Society.* Vol. 16, p. 702.

Steiner, D. et al. (Nov. 2021). 'Time-dependent, long-term hydrodynamic simulations of the inner protoplanetary disk. I. The importance of stellar magnetic torques'. In: *Astronomy and Astrophysics* 655, A110. DOI: 10.1051/0004-6361/202140447. arXiv: 2109.08919 [astro-ph.SR].

Steiner, Daniel (2012). 'Time-dependent galactic winds'. MA thesis. University of Vienna.

Stoekl, A. et al. (2016). 'Dynamical accretion of primordial atmospheres around planets with masses between 0.1 and 5 $M_{\oplus}$ in the habitable zone'. In: *The Astrophysical Journal.*

Stökl, Alexander et al. (July 2016). 'Dynamical Accretion of Primordial Atmospheres around Planets with Masses between 0.1 and 5 M $_{\oplus}$ in the Habitable Zone'. In: *The Astrophysical Journal* 825(2), 86, p. 86. DOI: 10.3847/0004-637X/825/2/86.

Takeuchi, Taku, Shoken M. Miyama and D. N. C. Lin (Apr. 1996). 'Gap Formation in Protoplanetary Disks'. In: *The Astrophysical Journal* 460, p. 832. DOI: 10.1086/177013.

Teague, Richard et al. (2018). 'A Kinematical Detection of Two Embedded Jupiter-mass Planets in HD 163296'. In: *The Astrophysical Journal* 860(1), p. L12. DOI: 10.3847/2041-8213/aac6d7. URL: https://doi.org/10.3847/2041-8213/aac6d7.

Unsöld, Albrecht and Bodo Baschek (2005). *Der neue Kosmos.* 7th. Springer.

Urpin, V. and A. Brandenburg (Mar. 1998). 'Magnetic and vertical shear instabilities in accretion discs'. In: *MNRAS* 294(3), pp. 399–406. DOI: 10.1046/j.1365-8711.1998.01118.x.

Vorobyov, E. I. and Shantanu Basu (2005). 'The Origin of Episodic Accretion Bursts in the Early Stages of Star Formation'. In: *The Astrophysical Journal* 633(2), pp. L137–L140. DOI: 10.1086/498303. URL: https://doi.org/10.1086/498303.

Vorobyov, Eduard I. and Vardan G. Elbakyan (Nov. 2019). 'Gravitoviscous protoplanetary disks with a dust component. II. Spatial distribution and growth of dust in a clumpy disk'. In: *Astronomy and Astrophysics* 631, A1, A1. DOI: 10.1051/0004-6361/201936132. arXiv: 1908.10589 [astro-ph.SR].

Weidenschilling, S.J. (1977). 'Aerodynamics of solid bodies in the solar nebula'. In: *Monthly Notices of the Royal Astronomical Society* 180, pp. 57–70.

Weinberger, Alycia (July 2004). *Imaging of Ices in Circumstellar Disks.* HST Proposal ID 10167. Cycle 13.

Xiao, Lin and Liping Jin (2015). 'Diversity of extrasolar planets and diversity of molecular cloud cores. II. Masses of gas giant planets'. In: *The Astrophysical Journal* 802(2),

p. 79. DOI: 10.1088/0004-637x/802/2/79. URL: https://doi.org/10.1088/0004-637x/802/2/79.

Yorke, Harold W., Peter Bodenheimer and G. Laughlin (Apr. 1995). 'The Formation of Protostellar Disks. II. Disks around Intermediate-Mass Stars'. In: *The Astrophysical Journal* 443, p. 199. DOI: 10.1086/175514.

Zhang, S. et al. (2018). 'The Disk Substructures at High Angular Resolution Project(DSHARP). VII. The Planet–Disk Interactions Interpretation'. In: *The Astrophysical Journal Letters*.

Zhang, Shangjia et al. (Dec. 2018). 'The Disk Substructures at High Angular Resolution Project (DSHARP). VII. The Planet-Disk Interactions Interpretation'. In: *The Astrophysical Journal* 869(2), L47, p. L47. DOI: 10.3847/2041-8213/aaf744. arXiv: 1812.04045 [astro-ph.EP].